

# Surveying the Bright Stars by Optical Interferometry I: A Search for Multiplicity Among Stars of Spectral Types F–K

D. J. Hutter,<sup>1</sup> R. T. Zavala,<sup>1</sup> C. Tycner,<sup>2</sup> J. A. Benson,<sup>1</sup> C. A. Hummel,<sup>3</sup> J. Sanborn,<sup>4</sup> O. G. Franz,<sup>4</sup> and K. J. Johnston<sup>5,6</sup>

Received \_\_\_\_\_; accepted \_\_\_\_\_

Submitted to the ApJ Supplement Series 2016-03-29; accepted 2016-09-12

---

<sup>1</sup>U.S. Naval Observatory, Flagstaff Station, 10391 West Naval Observatory Road, Flagstaff, AZ 86005-8521; djh@nobs.navy.mil

<sup>2</sup>Central Michigan University, Department of Physics, Mount Pleasant, MI 48859

<sup>3</sup>European Southern Observatory, Karl-Schwarzschild-Str. 2, Garching, 85748, Germany

<sup>4</sup>Lowell Observatory, 1400 West Mars Hill Road, Flagstaff, AZ 86001-4499

<sup>5</sup>U.S. Naval Observatory, 3450 Massachusetts Avenue, NW, Washington, DC 20392-5420

<sup>6</sup>Retired

## ABSTRACT

We present the first results from an ongoing survey for multiplicity among the bright stars using the Navy Precision Optical Interferometer (NPOI). We first present a summary of NPOI observations of known multiple systems, including the first detection of the companion of  $\beta$  Scuti with precise relative astrometry, to illustrate the instrument’s detection sensitivity for binaries at magnitude differences  $\Delta m \lesssim 3$  over the range of angular separation 3 - 860 milliarcseconds (mas). A limiting  $\Delta m_{700} \sim 3.5$  is likely for binaries where the component spectral types differ by less than two. Model fits to these data show good agreement with published orbits, and we additionally present a new orbit solution for one of these stars,  $\sigma$  Her. We then discuss early results of the survey of bright stars at  $\delta \geq -20^\circ$ . This survey, which complements previous surveys of the bright stars by speckle interferometry, initially emphasizes bright stars of spectral types F0 through K2. We report observations of 41 stars of apparent visual magnitude  $m_V \leq 4.30$ , all having been observed on multiple nights. Analysis of these data produces fitted angular separations, position angles, and component magnitude differences for six previously known visual binaries. Three additional systems were examined as possible binaries, but no conclusive detection could be made. No evidence of close stellar companions within our detection limit of  $\Delta m \approx 3$  was found for the remaining 32 stars observed; however, uniform-disk angular diameters are reported for 11 of the resolved stars in this last group.

*Subject headings:* astrometry — binaries: spectroscopic — binaries: visual — instrumentation: interferometers — techniques: high angular resolution — techniques: interferometric

## 1. Introduction

Knowledge of the frequency of multiplicity among stars is fundamental to furthering our understanding of many areas of astrophysics and has direct impact on the design of future experiments to detect and image extrasolar planets. However, multiplicity surveys of even the brightest stars using modern techniques were surprisingly incomplete until the 1990s (Hartkopf 2000). Early surveys of the bright stars by speckle interferometry (McAlister et al. 1987, 1993), although themselves incomplete, revealed that the frequency of visual binaries in the range of angular separations accessible to that technique was several times that previously known, including substantial numbers of wider binaries missed by classical visual observers. These imaging surveys, combined with radial velocity observations and other techniques, contributed to bright star multiplicity catalogs. Eggleton & Tokovinin (2008) present a catalog of bright, multiple (two or more components) star systems and discuss the implications of multiplicity upon several topics in astrophysics. Their catalog is derived from a number of input catalogs and observational techniques and consists of more than 4,500 stars. A catalog consisting of bright systems with three or more stars, the *Multiple Star Catalog* (MSC, Tokovinin 1997), also draws its sources from different observational techniques. The MSC is available online <sup>1</sup> and was updated in 2010.

As noted by Raghavan et al. (2010), continued multiplicity survey efforts using speckle interferometry (e.g., Mason et al. 1998; Horch et al. 2008) have now resulted in nearly complete coverage, at least for bright, solar-type stars, down to the diffraction limit of large telescopes ( $\sim 30$  mas). These surveys, along with systematic, higher-precision radial velocity observations have also largely closed the historical gap in orbital period coverage between these techniques (Raghavan et al. 2012). McAlister (1992) points out, however, that only long-baseline optical interferometry, using multiple-telescope arrays with baseline

---

<sup>1</sup>Catalog J/A+AS/124/75 in the VizieR catalog access tool (Ochsenbein et al. 2000).

lengths of hundreds of meters, offers a single technique for multiplicity detection throughout the angular-separation/period range from classical visual doubles to interacting binaries (Schmitt et al. 2009; Zavala et al. 2010) and contact binaries. Optical interferometry not only provides the data products of speckle interferometry with improved precision, but at the narrower angular separations not accessible to speckle where most spectroscopic binaries reside, offers sensitivity for binary detection in a range of orbital inclinations complementary to spectroscopy. The combination of visual orbits from interferometry with spectroscopic orbits for SB2 systems can yield stellar masses and orbital parallax and, if one or more of the components are resolved, stellar angular and potentially linear diameters (Hummel et al. 1994). High precision mass determinations are potentially possible for SB1 systems as well should GAIA parallaxes become available for such bright stars. Improving our knowledge of stellar multiplicity for both physical and *optical* systems of small angular separation also has important implications for precision navigation, where the presence of stellar companions and their relative motions can affect the determination of the “center of light” by relatively low-resolution star trackers (Hartkopf 2000).

We report here the first results of what is anticipated to be an ongoing survey of the brighter stars using the Navy Precision Optical Interferometer (NPOI). We first describe the capabilities of the NPOI for such a survey in § 2. Based on these capabilities (*c.* 2004), we next discuss the selection of the targets for the initial survey in § 3. The standard observing procedures and data reduction are described in § 4.1, including the selection and observation of calibration stars, and use of the resulting data to produce the accurately calibrated fringe visibility data for the program stars upon which all subsequent source modeling depends. The remainder of § 4, followed by § 5, present the results of models in three areas; first, the systematic examination of the calibrated data for evidence of binary systems among the program stars (§ 5.2) and subsequent detailed astrometric and photometric modeling of the detected systems (§ 5.3, 5.4); second, the observation and

modeling of previously known binary systems (§ 4.2, 5.1), plus detected binaries among the program stars (§ 5.2, 5.3), to determine the maximum detected magnitude difference ( $\Delta m$ ) of binary star pairs in our survey as a function of their angular separation (§ 5.5); and, third, the subsidiary result of accurate angular diameters for the resolved, single stars among the program sample (§ 5.6). Plans for future stages of this survey are also discussed (§ 6).

## 2. The NPOI

The NPOI (Armstrong et al. 1998) located on Anderson Mesa, AZ, is a joint project of the U. S. Naval Observatory and the Naval Research Laboratory in cooperation with Lowell Observatory. A brief description of the instrument and the specific configuration used in the observations reported in this paper are as follows.

### 2.1. Instrumentation

#### 2.1.1. *Siderostat Arrays*

The NPOI includes arrays for both imaging and astrometry. The four stations of the astrometric array (AC, AE, AN, and AW) are fixed and feature a laser metrology system for monitoring the siderostat pivot (Hutter & Elias 2002). Six additional imaging siderostats are operational at the E03, E06, E07, N03, W04, and W07 stations. The resulting baselines range from 9.8 m (AC-W04) to 97.6 m (E07-W07). Recently constructed shelters at the E10, N06, N07, and W10 piers will allow the commissioning of additional baselines of up to 432 m (E10-W10) in the near future through reconfiguration of the six imaging siderostats. The unvignetted aperture is the same for all siderostats (35 cm), but is stopped down to a 12.5 cm diameter by the feed-system optics. All stations are equipped with wave-front

tip-tilt correctors. The light feed system to the beam combining lab is evacuated and contains remotely actuated mirrors that allow the configuration of light paths from each of up to six siderostats to a corresponding delay line. The NPOI has six fast vacuum delay lines (FDLs) that can add up to 35 m of optical path. These delay lines are used to track the atmospheric and sidereal motion of the fringes. Long delay lines (LDLs, Clark et al. 1998), which use pop-up mirrors to switch in and out additional path, are being integrated into the feed paths and will enable observations on all baselines in the original NPOI design, to a maximum baseline of 437 m (E10-N10).

### 2.1.2. Beam Combination and Fringe Detection

The beam combiner used for all the observations reported here is a pupil-plane, free-space, bulk-optics system (Figure 1). The original three-beam combiner used for all observations prior to 2002 was subsequently expanded into a six-beam combiner simply by adding a mirror, M3B, which injects the next three beams at the back of the first beam splitter (BS) to combine with the original three beams. After interferometric combination at BC, the three combined beams each contain light from up to four stations. (The three complimentary output beams from the other side of BC are discarded.) Thus, our beam combiner can be considered a *hybrid* design intermediate between an all-in-one combiner, which places all beams onto a single detector, and a pairwise combiner, which puts single pairs of beams on separate detectors (Mozurkewich 1994, 2000).

The combined beams, after spatial filtering using pinholes, pass through prism spectrometers and are then collimated onto lenslet arrays and detected by three banks of photon-counting avalanche photodiodes (APDs). The spectral range covered is from 450 to 860 nm in 32 channels, equally-spaced in wave number. In addition to tracking the fringe motions, each FDL also imposes on its beam a 500 Hz triangle-wave modulation. The

resulting delay modulation on a baseline is the difference between two FDL modulations. The modulation sweeps the fringe pattern of that baseline across the detectors, causing an intensity that varies sinusoidally with time. Changing the amplitude of the modulations (also called *strokes*) changes the frequencies at which the fringes pass over the detectors. Since the three output beams of our hybrid six-beam combiner contain contributions from up to four input beams, there are a maximum of six baselines present on each. There are many stroke amplitude solutions that will place the baselines at separate frequencies. As long as no two baselines on the same detector have the same fringe frequency, the fringes can be cleanly separated (Mozurkewich 1994). The NPOI fringe detection algorithms grew out of the work pioneered by the Mark III stellar interferometer (Shao et al. 1988). The path length modulation and stroke pattern used to separate the fringes were initially laid out in Shao & Staelin (1977).

Custom electronics and software, described in greater detail elsewhere (Benson et al. 1998, 2003; Hummel et al. 2003), are required to bin the detected photons in synchrony with the delay modulation and compute real-time fringe tracking error signals. A binner board generates timing signals for 64 bins for up to 32 different wavelength channels. Custom APD processor boards use the timing signals to accumulate the incoming photons into the bins. Digital signal processors (DSPs) on the APD boards calculate the real and imaginary components of the Fourier transforms along the bin direction at eight frequencies. In addition, the real and imaginary components of the Fourier transform along the wavelength direction at each of the eight frequencies are also computed to produce the group delay, which in turn is used to calculate the fringe tracking error signals. Our implementation of group-delay fringe tracking is described in Benson et al. (1998).

Observations taken before 2002 used the original pairwise beam combiner. For observations after 2002 presented here, only the binner board and one 32-channel APD

processor board were integrated into our fringe engine. In order to detect and process six beams with this less-than-complete hardware implementation, we feed the output from two spectrometers to our single APD processor board. Sixteen wavelength channels (550 - 860 nm) from each spectrometer are sent to separate channels on the 32-channel APD board. This arrangement enables us to observe 11 of the 15 baselines that are available with six stations. One of the 11 baselines appears on both spectrometers. The beam combinations entering any two spectrometers are sufficient to phase the array. The sixteen detected wavelength channels are centered near 700 nm, approximating the original Johnson *R* band (Johnson 1966; Hindsley et al. 2011).

### 2.1.3. Array Phasing and Control

Until recently, our array-phasing algorithm was very simple. A reference FDL station (AC for most of the observations reported here) and the five baselines connecting the reference station to the other five FDL stations are designated as *tracking baselines*. The fringe tracker then looks only at the frequencies of the designated tracking baselines to calculate and apply its fringe tracking error signal. The error signal is always applied to the non-reference FDL. The beam-combiner design, the thermal stability of the beam-combining room, and the judicious choice of tracking baselines ensure that once all five tracking baselines are locked on, the array is truly phased up, that is, fringes on all 15 baselines provided by the six beams are present and constrained by the tracking baselines.

The NPOI control system includes a high degree of operational automation. The observer-level control system is based on a graphical user interface that provides control of the various subsystems, such as the tip-tilt star tracking system, the FDLs, and the fringe tracking system. After system set up and alignment, selection of a target causes the control system to acquire the star simultaneously with all specified stations. Once this is



accomplished, fringe search begins on all tracking baselines. The observer can specify a threshold corresponding to the minimum fringe amplitude signal-to-noise ratio required before the control system switches from the fringe-search mode to the fringe-tracking mode. After all required fringe data are acquired, a sequence of 2 ms fringe frames is sent to a data recorder. The NPOI currently averages  $\approx 120$  multi-baseline observations (§ 4.1) per night to a limiting visual magnitude  $m_V \approx 5.5$  under typical observing conditions and to  $m_V \gtrsim 6.0$  during periods of excellent seeing. The NPOI was the world’s first long-baseline optical interferometer to simultaneously co-phase six elements (Hummel et al. 2003). The wide detection bandwidth and rapid observing duty cycle of the NPOI make rapid surveys (§ 4) and snapshot imaging (Zavala et al. 2007) practical.

#### 2.1.4. *Wavelength Calibration*

Both binary star models (§ 5.1, 5.3) and single-star angular diameter models (§ 5.6) are fit to calibrated squared visibility amplitude ( $V^2$ ) data as a function of  $u$  and  $v$ , or  $uv$ -radius for circularly-symmetric diameters. Since  $u$  and  $v$  are expressed as a spatial frequency, which is the baseline length divided by the wavelength, uncertainties in our knowledge of the wavelength scale of our observations translate linearly into errors in the fitted angular separations of binary star components, the scale (e.g., semimajor axis) of binary orbits, and errors in fitted stellar diameters. The NPOI has had the capability to operate in a Fourier transform spectrometer (FTS) mode since 2005 March that allows very accurate, simultaneous measurement of the central wavelengths of all spectrometer channels. FTS observations are currently made on a regular basis, mostly on cloudy nights or after the APD lenslet arrays are translated with respect to the output of the spectrometers for specialized, spectral line observations (e.g.,  $H\alpha$ ).

Repeated FTS measurements, made during a single night, have shown that the lenslet

arrays can each be positioned to a desired translation with a  $1\sigma$  accuracy of  $\approx 0.7$  nm (0.1% at 656 nm). Repeated FTS measurements made when the lenslet arrays have not been actively translated for long periods (intervals of weeks to months, spanning 2012 - 2016) show slow drifts in the wavelength scale on individual spectrometers of  $\approx 0.6$  nm RMS, again  $\approx 0.1\%$  at 656 nm. This latter result is of particular significance because the great majority of the observations reported here were made prior to the start of regular FTS measurements. Prior to 2005 May an assumed wavelength scale (Mozurkewich 2005), calculated using the as-designed geometry of the spectrometers and the index of refraction of the glass (BK7) used in the manufacture of the spectrometer prisms, was used in the modelling of NPOI data. Measurements of the wavelength scale made in 1998 (prior to the upgrade of the beam combiner to 6-beam operation) using a prototype FTS system, along with those made in 2005 March using the current system, both agreed with the older, calculated scale to within 2 - 3 nm ( $\approx 0.4\%$  at 700 nm). Since there were no significant changes made to any of the spectrometer optics or mechanics between the epochs of the observations reported here and the present, we assume that the FTS measurements made after early 2005 are characteristic of the level of wavelength scale stability at prior times, and that the 1998 and 2005 measurements are representative of our knowledge of the wavelength scale pre-2005 as well. Therefore, we assume that the systematic errors in our wavelength scale are likely of order  $\pm 0.5\%$ .

### 2.1.5. *Interferometric Field of View*

As discussed in § 2.1.2, the beam combiner used for the observations reported here is a free-space, bulk-optics combiner. Thus, single-mode optical fibers are not used in the beam combination process. Single-mode fibers are likewise not used for spatial filtering. [The 50  $\mu$ m diameter pinholes used as spatial filters in the spectrometers (§ 2.1.2) serve only to

restrict the *photometric* field of view to a radius of  $\approx 1.5$  arcseconds (Mozurkewich 2005).] Therefore, our beam combiner does not suffer from the various effects (Guyon 2003; Absil et al. 2011) that effectively limit the interferometric field of view of combiners employing single-mode fibers to typically  $\leq 50 - 100$  mas. One of the most important of these effects derives from the coupling of the input telescope pupils with the fibers (Dyer & Christensen 1999).

However, the finite bandwidth of our beam combiner’s 16 spectral channels reduces visibility contrast and, as is well known from radio interferometry, will produce radial smearing over a large interferometric field of view (Bridle & Schwab 1999; Thompson, Moran & Swenson 2001). In the context of our survey, this is seen as a reduction in the  $V^2$  of stellar companions at large angular separations from the primary star. The magnitude of this effect can be estimated, for example, from Eq. 6.76 of Thompson, Moran & Swenson (2001). Using typical values of  $\lambda_0 = 700$  nm (channel wavelength),  $\Delta\lambda = 21$  nm (channel width), and  $D = 18.9$  m (baseline length, § 2.2), the reduction in the  $V^2$  of a secondary star at 30 mas separation would be  $\approx 1\%$ , but grows to  $\approx 10\%$  at 100 mas, and to  $\approx 90\%$  at 860 mas, the extreme limit of detection with the NPOI (§ 5.3.4, Figure 14). The effects of bandwidth smearing are explicitly accounted for in the modelling software used to search for stellar companions in our survey data (GRIDFIT, § 5.1) and for detailed modelling of detected binary systems (OYSTER, § 5.1). A monochromatic formula for a binary observed with an optical interferometer was presented in Eq. 17 of Hanbury Brown et al. (1967b). Formulae for model fitting to visibility data for relative astrometry and magnitude differences of binary stars observed with rectangular bandpasses are provided in Eqs. 5, 6, and 7 of Pan et al. (1992). In practice, our modelling software computes complex visibilities on a fine grid of wavelengths and then averages these over each spectral channel (Figures 9, 14).

## 2.2. System Configuration

In anticipation of the very large number of observations and subsequent data reduction effort required in the initial (§ 4.2) and subsequent installments of this survey, we chose one of the simplest configurations of the NPOI, having the advantages of maximum sky coverage, simple and robust operation of the instrument (ensuring the maximum number of observations each night), and relatively easy fringe visibility calibration.

First, while as noted above (§ 2.1.2), the NPOI is capable of coherently combining light from as many as six stations, we chose to use a subset of the available stations for our initial survey. Unless otherwise noted (§ 4.2), all observations were made utilizing the Center (AC), East (AE), and West (AW) stations of the astrometric array corresponding to baselines of lengths 18.9 m (AC-AE), and 22.2 m (AC-AW), with azimuths of  $113^\circ$  and  $244^\circ$ , respectively, for the East and West stations relative to the Center station. Figure 2 shows the sky coverage for this array, while plots of the typical  $uv$ -plane coverage for a night’s observation of program stars (§ 3) are shown in Figure 3 for the AC-AE and AC-AW baselines.

Second, unless otherwise noted (§ 4.2), the transport optics of the starlight feed system were configured to place each of the beams from the AC, AE, and AW stations at a separate input to the beam combiner (§ 2.1.2) such that the interferometric combination of the light for each of the three baselines appeared uniquely and simultaneously at each of the three beam combiner outputs. Due to the limited fringe processing electronics available at the epoch of most of the observations reported in this paper (2004, § 2.1.2), only two of the outputs, corresponding to the AC-AE and AC-AW baselines, respectively, were utilized for the great majority of the observations. This arrangement significantly simplifies the calibration of the raw fringe data relative to other configurations that produce multiple superimposed fringe patterns at one or more beam combiner outputs. (The third beam

combiner output, typically containing the AE-AW baseline, was utilized for observations in 1997 through 2001 § 5.1.1.)

### 3. Program Star Selection

For the purposes of our initial survey, the target list (“Program Stars,” see Table 1) was limited to a small subset of the stars in the *Hipparcos Catalogue* (Perryman et al. 1997). Specifically, a spreadsheet chartered by the Terrestrial Planet Finder Interferometer Science Working Group (TPF-I SWG; Lawson et al. 2007; Turnbull 2004), was used as a basis for our source selection. This list includes all *Hipparcos* stars within 30 pc [2,350 sources, per the original *Hipparcos* reduction (ESA 1997)], augmented with data on age indicators, kinematics, and spectral type, plus data from the *Washington Double Star* (WDS; Mason et al. 2001), *2MASS* (Skrutskie et al. 2006), and *IRAS* (Neugebauer et al. 1984) catalogs. This list was systematically culled using four criteria designed to down-select a modest list of sources that could be practically observed given the capabilities of the NPOI in 2004:

1) The list was first culled to eliminate stars that were too faint for practical observation with the NPOI in 2004. The stars selected (148 sources) were required to have an apparent visual magnitude in the Johnson system [550 nm effective wavelength (Johnson 1966)]  $m_V \leq 4.30$  (Table 1, Col. 5).

2) Next, the list was culled to include only stars with  $B - V \geq 0.30$  (Table 1, Col. 6; 98 sources). This eliminated all stars with spectral types earlier than approximately F0. This criterion was originally adopted in consistency with the TPF-I SWG, but also eliminated overlap with other current NPOI multiplicity studies of A and B stars (Patience et al. 2012; De Rosa et al. 2014).

3) The third cut was made to include only stars with declinations  $\delta \geq -20^\circ$  (61 sources).

This declination cutoff limits the sample to only those stars for which NPOI observations over a reasonable range of hour angles can be obtained during a single night ( $\approx 2$  hours, Figure 2) using the array configuration described in § 2.2.

4) Lastly, the two reddest stars in the remaining list [HR 5340,  $\alpha$  Boötis;  $B-V = 1.24$  (Mozurkewich et al. 2003), and HR 1457,  $\alpha$  Tauri;  $B-V = 1.54$  (White & Feerman 1987)] were dropped since their angular diameters ( $\approx 20$  mas) are too *large* for practical observation with the baselines available in 2004, due to very low interferometric fringe contrast. This last cull has the effect of setting a red cutoff to the list at  $B-V = 1.20$  (mid-K spectral type).

Thus, the final program star list (Table 1) consists of 59 stars. HR (Hoffleit & Warren 1991) and FK5 (Fricke et al. 1988) designations are included in this and subsequent tables for consistency with the NPOI observation planning and data archiving software. A color-magnitude diagram for these sources is given in Figure 4. Per Raghavan et al. (2010), we adopt absolute magnitude limits of -2 and +1.5 with respect to the Schmidt-Kaler (1982) Main Sequence as the nominal range of Main Sequence stars. We will next discuss some statistical properties of various subsets of our sample, referencing Figure 4.

First, assuming that the line at -2 mag above the nominal Main Sequence in Figure 4 is the threshold above which stars are significantly evolved, there are 19 giants and sub-giants in our sample. By comparison, if one were to apply the same color and declination selection criteria as used in selecting our sample but increased the apparent magnitude cutoff to  $m_V = 7.3$ , the limit to which the *Hipparcos Catalogue* is complete for all spectral types and galactic latitudes (Raghavan et al. 2010), the resulting list would contain 24 stars above the Main Sequence limit. Of these, 13 are within 22 pc, the distance at which  $m_V = 7.3$  corresponds to the upper demarcation of the Main Sequence at  $B-V = 1.20$  ( $M_V = 5.6$ ; Figure 4). Of the 19 giants/sub-giants in our sample, 12 are within the same distance

cutoff. Therefore, even with the modest apparent magnitude limit of our initial program star list, we are capturing  $\sim 90\%$  (12/13) of all the (same) evolved stars in a complete, volume limited sample within 22 pc.

Next, we considered the stars in our sample within the Main Sequence bounds of Figure 4. Given the modest magnitude limit of our initial sample, it is not surprising that a similar analysis shows we sample a much lower percentage of the Main Sequence stars. This analysis proceeds in two parts.

First, examination of Figure 4 shows that a substantial fraction of our sample (35 stars) lie within our adopted Main Sequence boundaries at  $B-V \leq 0.60$ . Of these stars, 34 lie within 25 pc, the distance to which Raghavan et al. (2010) demonstrated the completeness of the *Hipparcos Catalogue* for Main Sequence stars in an overlapping color range. There are 122 stars in the *Hipparcos Catalogue* within the same color, Main Sequence, declination, and distance bounds, and within the completeness limits in apparent magnitude ( $m_V = 7.3$ ). Therefore, we are likely sampling only  $34/122 \approx 28\%$  of the complete, volume-limited *Hipparcos* sample in this part of the Main Sequence.

Second, our sample contains only five stars within our Main Sequence bounds at  $B-V > 0.6$ , and none redder than  $B-V = 0.9$ . The corresponding number of stars in the *Hipparcos Catalogue* to  $m_V = 7.3$ , within the same color, Main Sequence, declination, and distance range is 153, or 18 to the distance (10.5 pc) of the most distant of our five stars. Therefore, we are sampling less than a third of the *Hipparcos* sources to 10.5 pc and only  $\approx 3\%$  of the complete, volume-limited *Hipparcos* sample of Main Sequence stars in this color range.

## 4. Observations and Data Reduction

Here we describe the observing sequence and aspects of the data reduction (§ 4.1), and summarize the log of observations (§ 4.2).

### 4.1. Observation Sequence and Reduction

Each observation of a program star consisted of 30 seconds of continuous (or nearly continuous) coherent fringe measurements, sampled at 500 Hz (hereafter, an *observation*). Each coherent observation of a star was immediately followed by an *incoherent* observation where the delay lines were deliberately moved so as to collect the total flux on each baseline outside the fringe packet. *Background* observations were also obtained while pointing the siderostats off-target. The incoherent and background observations are both utilized in the data reduction process to perform the photon noise bias correction in the calculation of the squared visibility amplitude  $V^2$  (e.g., Hummel et al. 2003). After subtraction of the bias using the incoherent observations, we would expect the incoherent  $V^2$  to have a mean of zero. Examination of the incoherent observations after the bias correction confirms this expectation (Figure 5).

Because the raw visibility amplitudes are degraded by atmospheric turbulence and instrumental effects, observations of calibrator stars, weakly resolved or unresolved stars, were interleaved with those of the program stars. Since the theoretical response of an interferometer to an unresolved source is known, the observed visibilities of the calibrator stars can be used to normalize the visibilities of the program stars. Once normalized, the program star visibilities can be reliably compared to single or multiple source models. Basic data on each of the calibrator stars are listed in Table 2. All calibrators were chosen to be within  $15^\circ$  of their respective program stars and similar in magnitude, where possible.



Frequently, several program stars shared a common calibrator. In most cases, the adopted limb darkened angular diameters ( $\theta_{LD}$ ) for the calibrator stars (Table 2, Col. 8) were estimated from the photometric properties of the stars ( $m_V$  and  $V - K$ ; Cols. 5 and 6, respectively) using Eqs. 5 and 7 of Mozurkewich et al. (2003), while for five stars (Table 2, note “b”) diameters estimated from the infrared flux method (Blackwell et al. 1991) were used. For one star (HIP 26311,  $\epsilon$  Orionis; Table 2, note “a”), a measured uniform disk diameter ( $\theta_{UD}$ ; Mozurkewich et al. 1991), corrected to a  $\theta_{LD}$  via Eq. 5 of Hanbury Brown et al. (1974), was used. The methodology for the determination of the limb-darkening coefficients is discussed below.

To estimate the uncertainty of our estimated calibrator diameters, we compared the values in Table 2 with those found in the literature from the *JMMC Stellar Diameters Catalogue* (JSDC; Lafrasse et al. 2010, 26 stars in common) and with the *PTI Calibrator Catalog* (van Belle et al. 2008, 14 stars in common). In the former case, estimated  $\theta_{LD}$  were also computed from  $m_V$  and  $V - K$  using Eqs. 9 and 10 of Bonneau et al. (2006), while in the latter case, spectral energy distribution (SED) fitting was used.

In the case of the comparison with the JSDC angular diameters (average quoted errors of 7% for the 26 in-common stars), our values are systematically *larger* with the exception of two stars, the average difference being  $0.067 \pm 0.049$  mas (approximately 11% at the mean JSDC diameter of 0.606 mas). However, this discrepancy can be accounted for by the difference in the surface brightness *vs*  $V - K$  relations of Mozurkewich et al. (2003) and Bonneau et al. (2006). If, for example, one calculates the predicted angular diameters over the range of  $V - K$  of the 26 stars common with the JSDC (approximately -0.7 to 1.2), assuming their average  $m_V = 3.83$ , using both the Mozurkewich et al. (2003) and Bonneau et al. (2006) equations, one finds that Bonneau et al. (2006) predicts progressively smaller angular diameters (as  $V - K$  is decreased) with respect to Mozurkewich et al. (2003) for

$V - K \lesssim 0.5$ , the range of  $V - K$  that includes 23 of the 26 stars common with the JSDC.

In the case of the comparison with the PTI angular diameters (average quoted error of 9% for the 14 in-common stars), our values are again systematically larger, but the average difference is only  $0.037 \pm 0.081$  mas (approximately 6% at the mean PTI diameter of 0.593 mas). Given the different methodology used in the estimation of the PTI angular diameters, the somewhat better agreement with our estimates is reassuring.

Based on these comparisons, we conservatively estimate our calibrator angular diameters to be good to  $\pm 10\%$  for purposes of estimating the effects of visibility calibration uncertainty in our later analysis (e.g., § 5.6).

The calibration of NPOI visibility data utilizes the calibrator stars as follows: The spectral types from the *The Bright Star Catalogue* (Hoffleit & Warren 1991, Table 2, Col. 7) are utilized to obtain  $T_{\text{eff}}$  and  $\log g$  for each calibrator from the appropriate tables of Schmidt-Kaler (1982) and Straižys (1992), respectively. These quantities are then used with the tables of monochromatic limb-darkening coefficients of Van Hamme (1993), via a quadratic interpolation in the range 450 - 860 nm, to determine the value of the linear limb-darkening coefficient at the center wavelength of each NPOI spectral channel. The expected value for the squared visibility amplitude of the calibrator at the time of each observation is then calculated via Eq. 4 of Hanbury Brown et al. (1974). Comparison of the expected and observed squared visibility amplitudes for the calibrator were used to generate the multiplicative correction for the instrumental and atmospheric reduction of  $V^2$  for the program star.

Additional details of the reduction of the visibility data are described in Hummel et al. (1998). As noted there, the seeing conditions and the squared visibility amplitudes of the calibrators vary significantly during a night, often on the time scale of an hour or less. Standard reduction procedure of NPOI data includes smoothing the systematic

variations in the squared visibilities with time in the calibrator for each program star with a Gaussian weighting function, whose FWHM, the “weighting interval,” is expressed in minutes. However, the exact value of the weighting interval to use is not obvious and the choice can significantly affect the results of subsequent modeling of the calibrated squared visibilities (e.g., § 5.6). Extensive empirical experimentation was performed to determine the best overall value for the weighting interval: The data for each of eight resolved program stars of various angular diameters were repeatedly calibrated for a number of values of the weighting function on each of several nights. The calibrated data for each star, on each night, were then fit with a uniform angular disk model. The values of the fitted diameters and the goodness of fit ( $\chi^2$ ) were seen to change significantly with choice of the weighting interval (e.g., Figure 6). However, comparison of such results for the various stars and nights showed a weighting interval of approximately 80 minutes to be an optimal overall value in terms of producing the smallest variation in the fitted diameters relative to those individually optimized with respect to weighting interval on a nightly basis. Adopting a standard value for the calibration weighting interval significantly reduced the labor involved in visibility calibration for all the nights at the expense of introducing a systematic error of perhaps  $\pm 1\%$  in the angular diameter fits for resolved stars (§ 5.6).

## 4.2. Observation Logs

The observations of the program stars discussed here were obtained at the NPOI over 46 nights from 2004 March 10 UT through 2004 October 08 UT (Table 3, with stars listed in the same order as in Table 1). A total of 1,389 coherent, multi-baseline observations were obtained for 41 of the 59 program stars (Figure 7). Program stars were typically each observed on five nights, with all the stars reported here having at least two nights of observations. Table 3 lists the UT dates of the observations, the number of multi-baseline

observations on each night, the total number of  $V^2$  measurements on each night, and the calibrator star observed.

Additionally, known, *non – program* binary systems (§ 5.1) covering a wide range of component  $\Delta m$  and angular separation were observed on most nights. These systems were observed as “test” binaries in the sense that their observations were to be reduced and analyzed in the same manner as the program stars to determine the maximum  $\Delta m$  detectible by NPOI observations at various component angular separations. A total of 705 multi-baseline observations of 15 such binaries was obtained (including observations obtained on additional nights during 1997 May - 2001 May, 2004 June - August, 2009 November - December, and 2013 March - May). Basic data for these systems are presented in Table 4, and a summary of the nights of observation and observation totals are presented in Tables 5 & 8.

## 5. Data Modeling

After the data reduction procedures were completed, we systematically examined all of the calibrated visibility data for both our program stars (§ 3, Table 3) and the  $\Delta m$  test binaries that were not part of the program sample (§ 4.2, Table 4) for the possible sinusoidal signature of a binary star (Brown 1974, § 5.1, 5.2). For those systems where a statistically significant binary detection was obtained, we proceeded to detailed modeling of the separation ( $\rho$ ), position angle ( $\theta$ ), and magnitude difference ( $\Delta m$ ) of the binary components (§ 5.1, § 5.3). Lastly, we also performed uniform-disk, angular diameter model fits to those resolved program stars that proved to have no detectable stellar companions (§ 5.6).

### 5.1. Modeling of $\Delta m$ Test Binaries

When embarking on a survey of stellar multiplicity one naturally would want to know the expected detection limits of that survey in angular separation and  $\Delta m$ . An empirical assessment of the NPOI’s capabilities was performed by observing a number of known binary systems, including program stars, with estimated  $\Delta m$  values  $\lesssim 4$  in  $m_V$  (hereafter  $\Delta m_V$ ) over a range of angular separations between 3 mas and 860 mas (§ 4.2). Once the reduction of the observations to calibrated  $V^2$  data was completed (§ 4.1), we next proceeded to systematically examine the calibrated visibility data for all of the sources observed to date (Tables 3 & 5) for statistically significant evidence of a stellar companion using the software GRIDFIT, written by R. T. Zavala. This procedure performs a gridded search of the  $\Delta m$ ,  $\rho$ ,  $\theta$  space for evidence of a stellar companion by locating the values of these parameters for which a binary star model, fit to all the calibrated  $V^2$  data for a source on a given night, produces a minimum in the reduced  $\chi^2$  ( $\chi_\nu^2$ ). Beginning at a fixed  $\Delta m = 0$ , GRIDFIT calculates the value of  $\chi_\nu^2$  for a binary model fit to the  $V^2$  data at each point of a semicircular grid of radius 500 mas in increments of 0.1 mas in both RA and Dec. The lowest resulting value of  $\chi_\nu^2$  was then saved, the  $\Delta m$  value incremented by 0.1 mag, and the process repeated up through  $\Delta m = 4.0$ . Figure 8 illustrates the results of this process for one star ( $\chi$  Dra) on a single night: The top panel shows the minimum value of  $\chi_\nu^2$  over the position-grid search at each  $\Delta m$  value, as a function of  $\Delta m$ . The second and third panels display the corresponding values of the component separation and position angle, respectively, for the best-fit model at each  $\Delta m$  value.

The plots analogous to Figure 8 for each star, on each night, were examined for evidence of a *significant*  $\chi_\nu^2$  minimum [ $\chi_\nu^2(\text{min})$ ], here defined as a minimum with a corresponding 99% confidence interval ( $\chi_\nu^2(\text{min}) + 11.3$  for a three-parameter  $\Delta m$ ,  $\rho$ ,  $\theta$  fit; Avni 1976; Wall 1996) with a half-width of  $\pm 1$  or less in  $\Delta m$  (i.e., relatively small with respect to the

whole  $\Delta m$  search range).

Thus, the GRIDFIT search is a brute force method that searches all possible locations and  $\Delta m$  within designated limits and produces an initial estimate of possible binary parameters for use in later fitting. While computationally intensive, the global minimum is found using a very fine grid spacing. The 500 mas limit of the GRIDFIT searches was chosen partly for a reasonable computational and analysis effort and to avoid an extensive overlap with other techniques of courser resolution such as speckle interferometry and adaptive optics (AO). As was noted in § 1, previous well documented work has been published for speckle or in some cases AO observations at separations of 500 mas and greater.

For those sources for which GRIDFIT demonstrated significant, global  $\chi_\nu^2(\text{min})$ , we next proceeded to detailed modeling. All binary modeling was performed using C. A. Hummel’s OYSTER software package ([www.eso.org/~chummel/oyster/oyster.html](http://www.eso.org/~chummel/oyster/oyster.html)), which has been the standard for displaying, editing, averaging, calibrating, and modelling interferometry data from the NPOI for many years (e.g., Hummel et al. 2003). OYSTER was used to fit binary models on a night-by-night basis to the  $V^2$  as a function of  $u$  and  $v$  using a Levenberg-Marquardt nonlinear least-squares technique. Experience has shown that the most efficient path to fully optimized models is a three-step iterative process: first, fitting the astrometric parameters  $\rho$  and  $\theta$  while holding  $\Delta m$  fixed at an estimated value, second, fitting  $\Delta m$  while holding  $\rho$  and  $\theta$  fixed at the values determined in the first stage, and third, performing a final, simultaneous fit for all three parameters.

To begin the modeling process, estimates of  $\rho$  and  $\theta$  for each night, the  $\Delta m$  of the system, and the angular diameters of the individual stars are required. In the case of the  $\Delta m$  test binaries, initial estimates for  $\rho$  and  $\theta$  were derived in most cases from published orbital elements, as verified using the GRIDFIT results. However, where the GRIDFIT results differed by  $> 2$  mas from the position predicted from the orbital elements, or if no

orbital elements existed, the GRIDFIT values were used.

Initial estimates for  $\Delta m$  were taken from the literature in most cases, or from the GRIDFIT results where there were no published values in the visible. For the primary star angular diameters, we used values from the literature or estimates from the NPOI data reduction software (§ 4.1). Secondary star angular diameters were either taken from the literature, estimated from either the relative colors, spectral types, or known masses of the primary and secondary stars, or set to small values. Unless otherwise noted, we subsequently held the component angular diameters fixed in all three fitting stages outlined above since the baselines we used were not long enough to reliably determine the component diameters in the case of these stars.

The results of the fitting process for the  $\Delta m$  test binaries are presented in Tables 6, 9 & 11. Table 6 lists the fitted angular separations and position angles for each system (with the exception of  $\sigma$  Her; Table 9, § 5.1.1), on each night, along with the parameters of the fit error ellipse. The uncertainty ellipses correspond to one-seventh of the synthesized beam, which has been shown to give realistic estimates of the astrometric accuracy of NPOI multi-baseline observations (Hummel et al. 2003, 2013). In some cases, the fitted position angles for a system were adjusted by  $180^\circ$  for consistency with those listed in the *Fourth catalog of interferometric measurements of binary stars* (INT4, Hartkopf et al. 2001b) at similar epochs or with the predictions of the published orbits cited above. The lack of closure phase in our single-baseline data leads to a  $\pm 180^\circ$  ambiguity in the fitted position angles. However, in the case of  $\alpha$  Dra and V1334 Cyg, where data from additional baselines were available, closure phase data were used to independently determine the position angles. For seven of the sources in Table 6, where published orbits based on observations from long-baseline optical interferometers exist (PTI:  $\kappa$  UMa and  $\beta$  CrB; NPOI/Mark III/PTI: o Leo; NPOI:  $\zeta$  UMa A and  $\eta$  Peg; Mark III: 113 Her, and

CHARA: V1334 Cyg), the agreement of our nightly fits with the positions calculated from the orbits is excellent, the typical observed minus calculated (O-C) values being  $\sim 0.5$  mas. For 59 Cyg, where the orbit of Mason (2011) was based mostly on speckle interferometry observations through 2008, the agreement is  $\lesssim 4$  mas. For  $\zeta$  Ori A (Hummel et al. 2013) and  $\phi$  Her (Zavala et al. 2007) binary model fits to the observations listed in Table 5 have been published, and so were not again fitted, the literature values being reproduced in Table 6. Columns 3 and 5 of Table 11 contain the mean of the nightly fitted  $\rho$  values from Table 6 and the log thereof, with the exception of  $\alpha$  Dra and  $\sigma$  Her (Table 9), where the values at the minimum and maximum angular separations are listed.

Table 11, Col. 6 contains the mean of the nightly fitted  $\Delta m$  values at 700 nm ( $\Delta m_{700}$ , § 2.1.2) for each star, while Col. 7 contains the standard deviation of the nightly fitted  $\Delta m_{700}$  values. We conservatively quote standard deviations rather than the uncertainty of the mean ( $\sigma/\sqrt{N}$ , where  $N$  is the number of nights) to compensate for the fact that the systematic errors in the  $V^2$  calibration (§ 4.1) are not explicitly accounted for in the modeling. Once again, the modeling process for  $\zeta$  Ori A and  $\phi$  Her was not repeated, so the mean  $\Delta m_{700}$  values ( $\langle \Delta m_{700} \rangle$ ) and error estimates in Table 11 for these systems are taken from the literature. In the case of  $\zeta$  UMa A, where our  $\Delta m$  fit was of lesser quality, we have substituted the published values of Hummel et al. (1998).

Figure 9 shows an example (for a binary of relatively large  $\rho$  and  $\Delta m$ ) of the  $uv$ -plane sampling for a night’s observations, and model  $V^2$  values resulting from the best-fit binary parameters from Tables 6 & 11 overlayed on the calibrated  $V^2$  data. Lastly, Figure 10 displays the  $\langle \Delta m_{700} \rangle$  value for each  $\Delta m$  test binary plotted against the log of its mean  $\rho$ , values taken from Table 11.

Notes pertaining to the modeling of each  $\Delta m$  test binary (except  $\sigma$  Her; § 5.1.1,  $\beta$  Sct; § 5.1.2, and V1334 Cyg; § 5.1.3) are as follows:



$\zeta$  Ori A (HR 1948, HD 37742, WDS J05407-0157Aa,Ab): Binary model fits to the observations listed in Table 5 have been published by Hummel et al. (2013), and so were not again fitted. The values of Hummel et al. (2013) are reproduced in Table 6.

$\kappa$  UMa (FK5 341, HR 3594, HIP 44471, HD 77327, WDS J09036+4709AB): An estimated primary star angular diameter  $\theta_P = 0.746$  mas was provided by the NPOI data reduction software (§ 4.1). A secondary star angular diameter  $\theta_S = 0.5$  mas was assumed. An initial  $\Delta m_V = 0.38$  was taken from the *Sixth catalog of orbits of visual binary stars* (ORB6, Hartkopf et al. 2001a). Initial estimates for  $\rho$  and  $\theta$  were derived using the orbital elements of Muterspaugh et al. (2010a). These estimates agree with the global minima from GRIDFIT to  $\leq 0.4$  mas on two of the three nights, the GRIDFIT result on the third night being highly divergent and likely spurious. The O-C values of the fits listed in Table 6 with respect to the Muterspaugh et al. (2010a) orbit are all  $\leq 0.5$  mas.

o Leo (FK5 365, HR 3852, HIP 47508, HD 83809, WDS J09412+0954Aa,Ab): An estimated primary star angular diameter  $\theta_P = 1.273$  mas was provided by the NPOI data reduction software (§ 4.1). A secondary star angular diameter  $\theta_S = 0.5$  mas and an initial  $\Delta m_{700} = 1.05$  were taken from Hummel et al. (2001). Initial estimates for  $\rho$  and  $\theta$  were derived using the orbital elements of Hummel et al. (2001). These estimates agree with the global minima from GRIDFIT to  $\leq 0.5$  mas on all three nights. The O-C values of the fits listed in Table 6 with respect to the Hummel et al. (2001) orbit are all  $\leq 0.3$  mas.

$\zeta$  UMa A (FK5 497, HR 5054, HD 116656, WDS J13239+5456Aa,Ab): Estimates for the primary star angular diameter  $\theta_P = 0.8$  mas, the secondary star angular diameter  $\theta_S = 0.8$  mas, and an initial  $\Delta m_{800} = 0$  were taken from Hummel et al. (1998). Initial estimates for  $\rho$  and  $\theta$  were derived using the orbital elements of Hummel et al. (1998). These estimates agree with the global minima from GRIDFIT to  $\leq 0.3$  mas on all three nights. The O-C values of the fits listed in Table 6 with respect to the Hummel et al. (1998) orbit are all  $\leq$

0.2 mas.

$\alpha$  Dra (FK5 521, HR 5291, HIP 68756, HD 123299): Estimates for the primary star angular diameter  $\theta_P = 0.6$  mas, secondary star angular diameter  $\theta_S = 0.3$  mas, an initial  $\Delta m_V = 1.8$ , and initial  $\rho$  and  $\theta$  values were all provided by Hummel (private communication). For consistency, only data from the AC-AE and AC-AW baselines were modeled.

$\beta$  CrB (FK5 572, HR 5747, HIP 75695, HD 137909, WDS J15278+2906AB): A primary star angular diameter  $\theta_P = 0.721$  mas and a secondary star angular diameter  $\theta_S = 0.361$  mas were estimated as per § 4.1 using the  $m_V$  value from Table 4 (3.68),  $m_K = 3.28$  (Ducati 2002), and assuming the same  $V - K = 0.4$  value for both components, along with an initial  $\Delta m_V = 1.5$  from the ORB6. Initial estimates for  $\rho$  and  $\theta$  were derived using the orbital elements of Muterspaugh et al. (2010a). These estimates agree with the global minima from GRIDFIT ( $> 99\%$  confidence detections on all three nights) to  $\leq 0.7$  mas on all three nights. The O-C values of the fits listed in Table 6 with respect to the Muterspaugh et al. (2010a) orbit are all  $\leq 0.5$  mas.

$\phi$  Her (FK5 601, HR 6023, HIP 79101, HD 145389, WDS J16088+4456AB): Binary model fits to the observations listed in Table 5 have been published by Zavala et al. (2007), and so were not again fitted. The values of Zavala et al. (2007) are reproduced in Table 6.

113 Her (FK5 3508, HR 7133, HIP 92818, HD 175492, WDS J18547+2239Aa,Ab): An estimated primary star angular diameter  $\theta_P = 1.4$  mas, an estimated secondary star angular diameter  $\theta_S = 0.2$  mas, and an initial  $\Delta m_{800} = 3.00$  were all taken from Hummel et al. (1995). Initial estimates for  $\rho$  and  $\theta$  were derived using the orbital elements of Hummel et al. (1995). These estimates agree with the global minima from GRIDFIT ( $\geq 99\%$  confidence detections on two of three nights) to  $\leq 1.2$  mas on all three nights. The O-C values of the fits listed in Table 6 with respect to the Hummel et al. (1995) orbit are all  $\leq 0.9$  mas.

32 Cyg (HR 7751, HIP 99848, HD 192910, WDS J20155+4743A): An estimated primary star angular diameter  $\theta_P = 5.361$  mas was provided by the NPOI data reduction software (§ 4.1). A secondary star angular diameter  $\theta_S = 0.3$  mas was assumed. An initial  $\Delta m_V = 3.8$  was taken from Parsons & Ake (1998). Orbital elements from Ren & Fu (2013), and references therein, were used to estimate  $\rho$  and  $\theta$ . Using these values in the OYSTER modelling procedures produced better quality (lower  $\chi_\nu^2$ ) models than the alternative single star model on two nights, equal quality fits on two nights, and a marginally lower quality fit compared to the single star model on one night. The application of GRIDFIT likewise produced no convincing evidence for a binary, with a  $\sim 99\%$  confidence detection on only one night, wildly divergent minimum in position angle between the various nights, and separations smaller than the estimated primary star angular diameter on three of the five nights. We therefore conclude that we have failed to detect the secondary star in this system.

59 Cyg (FK5 1551, HR 8047, HIP 103632, HD 200120, WDS J20598+4731Aa,Ab): An estimated primary star angular diameter  $\theta_P = 0.492$  mas was provided by the NPOI data reduction software (§ 4.1). A secondary star angular diameter  $\theta_S = 0.2$  mas was assumed. An initial  $\Delta m_V = 2.8$  was taken from the ORB6. Initial estimates for  $\rho$  and  $\theta$  were derived using the orbital elements of Mason (2011). These estimates, for this wide, slowly moving binary ( $P = 161.5$  yr), agree with the GRIDFIT results to  $\approx 2.2$  mas. The O-C values of the fits listed in Table 6 with respect to the Mason (2011) orbit are all  $\leq 3.8$  mas.

5 Lac (FK5 3799, HR 8572, HIP 111022, HD 213310, WDS J22295+4742AB): An estimated primary star angular diameter  $\theta_P = 5.290$  mas was provided by the NPOI data reduction software (§ 4.1). A secondary star angular diameter  $\theta_S = 0.5$  mas was assumed. An initial  $\Delta m_V = 3.6$  was taken from Parsons & Ake (1998). The most closely contemporaneous speckle interferometry measurement ( $\rho = 82$  mas,  $\theta = 43.1$  Hartkopf et

al. 1997) was used for the initial values of  $\rho$  and  $\theta$ . Using these values in the OYSTER modelling procedures produced good quality binary fits on five of the six nights, but the alternative single star models were essentially equal in quality ( $\chi_\nu^2$ ) on these nights and significantly better on the sixth night (2004 August 02 UT). The application of GRIDFIT likewise produced no convincing evidence for a binary, with wildly divergent minima in position angle and separation between the various nights, and angular separations smaller than the estimated primary star angular diameter on half the nights. We therefore conclude that we have failed to detect the secondary star in this system.

$\eta$  Peg (FK5 857, HR 8650, HIP 112158, HD 215182, WDS J22430+3013Aa,Ab): An estimated primary star angular diameter  $\theta_P = 3.045$  mas was provided by the NPOI data reduction software (§ 4.1). An estimated secondary star angular diameter  $\theta_S = 0.5$  mas was assumed. An initial  $\Delta m_{800} = 3.61$  was taken from Hummel et al. (1998). Initial estimates for  $\rho$  and  $\theta$  were derived using the orbital elements of Hummel et al. (1998). These estimates agree with the global minima from GRIDFIT ( $\gtrsim 99\%$  confidence detections on five of six three nights) to  $\leq 0.4$  mas. The O-C values of the fits listed in Table 6 with respect to the Hummel et al. (1998) orbit are all  $\leq 0.9$  mas.

### 5.1.1. $\sigma$ Her

For  $\sigma$  Her (FK5 621, HR 6168, HIP 81126, HD 149630, WDS J16341+4226AB) Tables 7 & 8 list the calibrator stars used and the log of observations, respectively. Multiple calibrator stars were used for the calibration of the  $\sigma$  Her visibility data on each night. The calibrator star data were time weighted as per § 4.1, but the calibrator stars were not necessarily within  $15^\circ$  of  $\sigma$  Her.

A primary star angular diameter  $\theta_P = 0.52$  mas and a secondary star angular diameter

$\theta_S = 0.16$  mas were estimated as per § 4.1 using the  $m_V$  value from Table 4 (4.20),  $m_K = 4.05$  (Cutri et al. 2003), and assuming the same  $V - K$  value for both components, along with an initial  $\Delta m_V = 2.6$  estimated from the values listed in the INT4. Initial estimates for  $\rho$  and  $\theta$  were derived using the orbital elements of Balega & Balega (1988). A program within OYSTER, similar to GRIDFIT, was also used to search a grid of 80 mas by 80 mas at 0.2 mas spacings, centered on the predicted position of the secondary star, to verify these estimates.

Columns 1 through 8 of Table 9 list the fitted angular separations and position angles, and their errors, for this system on each night, in a format similar to Table 6. For the earlier 1997 through 2001 observations listed in Table 8, data were obtained simultaneously on the three baselines formed by the AC, AE, and AW (or E02) stations, so closure phase data were available for inclusion in the fitting process. The magnitude differences were fitted at three wavelengths (550 nm, 700 nm, and 850 nm), the resulting mean values being  $\Delta m_{550} = 2.70 \pm 0.05$ ,  $\Delta m_{700} = 2.34 \pm 0.05$ , and  $\Delta m_{850} = 2.28 \pm 0.05$ . The minimum and maximum values of  $\rho$  from Table 9 (14.06 mas, 115.13 mas), the log of these values, and the mean  $\Delta m_{700}$  are listed in Cols. 3, 5, and 6 of Table 11.

Given the more than seven-year timespan of the observations of  $\sigma$  Her listed in Table 8, it was also possible to obtain a high-quality orbit fit using *only* NPOI data. The resulting orbital elements are listed in Table 10, with the corresponding apparent orbit overplotted on the nightly  $\rho$ ,  $\theta$  fits from Table 9 in the left panel of Figure 11. The  $O - C$  values in  $\rho$  and  $\theta$  of the nightly fits with respect to this orbit are listed in Cols. 9 and 10 of Table 9, respectively. For purposes of comparison, archival observations from the INT4 ( $\theta$  adjusted by  $180^\circ$  in some cases) are added in the right panel of Figure 11.

### 5.1.2. $\beta$ Sct

For  $\beta$  Sct (FK5 1489, HR 7063, HIP 92175, HD 173764) the application of GRIDFIT to our eight nights of data (Table 5) indicates marginal,  $\leq 68\%$  confidence interval (Avni 1976; Wall 1996), detections on two nights (2004 August 06 UT and 2004 August 27 UT) at  $\Delta m = 3.8$  to 4.0. For purposes of comparison, we also applied the CANDID algorithm (Gallenne et al. 2015)<sup>2</sup> to our 2004 August 06 UT data. CANDID reported a significant detection at a position (modulo  $180^\circ$ ) within 2 mas of the GRIDFIT result. We subsequently used the GRIDFIT position for this night ( $\rho = 15.57$  mas,  $\theta = 162^\circ 28'$ ) as initial values in the modelling of the data from all eight nights using OYSTER. We also used an estimated primary star angular diameter  $\theta_P = 2.212$  mas, as provided by the NPOI data reduction software (§ 4.1). A secondary star angular diameter  $\theta_S = 0.1$  mas was estimated from the ratio of the stellar radii, derived using the adopted  $\theta_P$  value and the parallax of Parsons et al. (2005) to estimate the radius of the primary, then using the spectral type and mass (Parsons et al. 2005) and the tables of masses and radii of Drilling & Landolt (1999) to estimate the radius of the secondary. An initial  $\Delta m_V = 3.8$  was estimated from the GRIDFIT results.

In all cases, the binary models (Table 6) were a better, lower  $\chi^2$ , fit than a single-star model. However, the nightly fits for the  $\Delta m_{700}$  of this binary varied widely. Given that our best nightly model fit (2004 August 06 UT) reports an essentially identical result ( $3.59 \pm 0.06$ ) as that found by CANDID, but in consideration of the other nightly OYSTER and GRIDFIT results that report larger values, we adopt a tentative value of  $\Delta m_{700} = 3.6 +0.2/-0.1$  for the binary.

The results reported here represent the first detection of the secondary star in this

---

<sup>2</sup><https://github.com/amerand/CANDID>

system at precisely measured separations and position angles<sup>3</sup>. Given the limited time span of our observations ( $\approx 21$  days, Table 5) relative to the orbital period of  $\approx 833$  days (e.g., Parsons et al. 2005), we did not attempt an orbital solution using the combination of our astrometric data with those from spectroscopy (e.g., Griffin 2008). However, it is likely that our detection does correspond to the secondary star detected by spectroscopy. One can use the orbital elements of Griffin (2008), along with the largest likely value of the system semimajor axis from Parsons et al. (2005) ( $\sim 18$  mas) to predict separations and position angles on the dates of our observations that are  $\leq 4$  mas in separation and  $\leq 30^\circ$  in position angle of our measured positions (Table 6).

### 5.1.3. *V1334 Cyg*

For V1334 Cyg (HR 8157, HIP 105269, HD 203156, WDS J21194+3814Aa,Ab) an estimated primary star angular diameter  $\theta_P = 0.50$  mas was provided by averaging the values cited by Gallenne et al. (2013), and references therein. A secondary star angular diameter  $\theta_S = 0.2$  mas was assumed. An initial  $\Delta m_{700} = 2.7$  was derived using GRIDFIT (below). Initial estimates for  $\rho$  and  $\theta$  were derived using the orbital elements of Gallenne et al. (2013).

We also performed a systematic search for the intermittently detected third (B) component in this system (Gallenne et al. 2013, and references therein), using our three nights of data (Table 5). GRIDFIT and the similar program within OYSTER were each used to search a region of 500 mas radius around this system at a resolution of 0.1 mas.

---

<sup>3</sup>Parsons et al. (2005) reported TRANS mode observations from the HST Fine Guidance Sensor that demonstrated duplicity in the signal but failed to provide reliable relative astrometry.

Neither program provided any evidence of a third component in this system, but both recovered the Ab component at positions within 0.6 mas in separation and  $4^\circ$  in position angle of those predicted by the Gallenne et al. (2013) orbit in the data from our first two night nights of observation. We also made use of the CANDID algorithm (Gallenne et al. 2015) to search a region within 50 mas of the primary. In this case, the Ab component was again recovered within 0.2 mas in separation and  $2^\circ$  in position angle on the first two nights, but another  $3\sigma$  detection at  $\rho = 20$  mas and  $\text{PA} = 40^\circ$  was also reported for 2009 December 01 UT. Given that this result was not repeated on our other two nights, we assume it to be spurious.

Both CANDID and GRIDFIT produced highly discrepant position angles for the Ab component for our third night of observations (2009 December 18 UT), producing values of approximately  $45^\circ$  and  $136^\circ$ , respectively, from that predicted by the (Gallenne et al. 2013) orbit. Given the lesser quantity and the relatively poor qualitative appearance of the calibrated  $V^2$  on this night, these results may not be surprising. Given all these indications, we chose to down-weight our model fit for this night in determining a value of  $\Delta m_{700} = 2.69 \pm 0.27$  for this system (Table 11), weighting the model fits for the individual nights by the number of  $V^2$  measures on each night (Table 5).

#### 5.1.4. *Nondetections*

As per § 5.1, two sources (HR 7751 = 32 Cyg and HR 8572 = 5 Lac) listed in Tables 4 & 5 do not appear in Table 6 since it was not possible to fit a statistically significant, low reduced  $\chi^2$  binary model to the  $V^2$  data. For each of these sources, a single-star model of angular diameter similar to the initial primary star diameter estimate provided an equal or better model fit. This leads to the conclusion that for these large- $\Delta m$  stars, we have failed to detect the secondary component. However, for purposes of comparison, we have added



*estimates* of likely angular separations and  $\Delta m$  values for these sources at the mean epoch of our observations to Table 11 and Figure 10.

Examining Figure 10, it initially appears curious that 32 Cyg and 5 Lac were not detected by our observations given the close proximity of their plotted  $\Delta m$  *vs*  $\log \rho$  values to those of  $\beta$  Sct and  $\eta$  Peg, respectively. However, on further examination, it may not have been surprising that these systems were not detected as binaries by our observations. They, along with  $\beta$  Sct were originally chosen for observation to test the limits of large  $\Delta m$  binary detection based on their very large ( $\geq 3$ ) *estimated*  $\Delta m$  values (Parsons & Ake 1998). Each of these systems consists of a luminous cool primary and a hot companion for which Parsons & Ake (1998) utilized IUE observations and the total UV-optical energy distribution to determine the spectral class of the hot secondary star along with an estimated  $\Delta m_V$  of the binary. Given that the wavelength of the “crossover point” at which the dominance of the total flux in the spectral fits transitions from the hot to cool components given by Parsons & Ake (1998) is quite blue ( $\leq 380$  nm), one would expect that the observed  $\Delta m$  would steadily increase as the effective wavelength of the observations increases. Such is demonstratively the case for 113 Her and  $\eta$  Peg, where the measured  $\Delta m$  varies as 1.61 (500 nm), 2.01 (550 nm), and 3.00 (800 nm) for 113 Her (Hummel et al. 1995), and 2.01 (450 nm), 2.76 (550 nm), and 3.61 (800 nm) for  $\eta$  Peg (Hummel et al. 1998). Given that the primary-secondary spectral type differences are most extreme for 32 Cyg (K3Ib + B3V) and 5 Lac (M0II + B8V), large for  $\beta$  Sct (G4IIa + B9V), and relatively moderate for 113 Her (G4III + A6V) and  $\eta$  Peg (G2II-III + A5V), it is likely that the variation in  $\Delta m$  from the  $V$  band to the  $\sim R$  band of our observations is even larger for 32 Cyg and 5 Lac, making their  $\Delta m_{700}$  values considerably larger than their estimated  $\Delta m_{550}$  values plotted in Figure 10, thus accounting for their nondetection as binaries in the current NPOI observations. Likewise, the wavelength dependence of  $\Delta m$  can explain why, for 5 Lac, historical speckle interferometry observations (INT4) made at effective wavelengths  $<$

500 nm consistently detect the secondary in this system, while observations at  $> 550$  nm consistently fail to do so<sup>4</sup>.

#### 5.1.5. $\Delta m$ Limit

Figure 10 and the discussion of § 5.1.4 thus indicate that the NPOI is sensitive to binary companions to  $\Delta m_{700} \approx 3$  at angular separations  $\gtrsim 6$  mas (e.g., V1334 Cyg) and to  $\Delta m_{700} \approx 2$  down to 3 mas (e.g.,  $\alpha$  Dra). Our  $\Delta m_{700}$  limit is perhaps somewhat larger ( $\sim 3.5$ ) for binaries where there is not more than a difference of about two full spectral types between the components (e.g.,  $\eta$  Peg and  $\beta$  Sct).

### 5.2. Detecting Binaries among the Program Stars

We next proceeded to systematically examine the calibrated visibility data for all of the program sources observed to date (Table 3) for statistically significant evidence (99% confidence, § 5.1) of a stellar companion using GRIDFIT. Based on this examination, the observed sources can be placed into several groups.

The first group ( $\alpha$  Aur, 10 UMa,  $\gamma$  Vir,  $\zeta$  Her,  $\chi$  Dra, and  $\beta$  Del) all display obvious,

---

<sup>4</sup>An alternative interpretation of this system is that of a binary in a highly inclined orbit that occasionally closes to a separation less than the angular resolution of our observations. The INT4 records indicate an average position angle  $\approx 44^\circ$ , with a general trend toward decreasing separation. Hartkopf (private communication) notes that many of the observations reported the INT4 were made using *photographic* speckle interferometry whose  $\Delta m$  sensitivity is likely  $< 3$  magnitudes, implying the secondary should be detectable by the NPOI when more widely separated.

deep  $\chi_\nu^2$  minima in the GRIDFIT plots on all nights, similar to the example of Figure 8. These are all well known binary systems for which we then proceed to detailed modeling of the separation, position angle, and magnitude difference of the binary components in § 5.3. For four of these six sources (10 UMa,  $\gamma$  Vir,  $\zeta$  Her, and  $\beta$  Del) the  $\chi_\nu^2(\text{min})$  occur at angular separations at or very close to the 500 mas outer edge of the grid search. Subsequent detailed fitting in § 5.3 shows the actual separations of the binary components to range up to  $\sim 860$  mas and the implications of these results are discussed in § 5.5.

A second group of sources ( $\alpha$  Ari,  $\beta$  Gem,  $\theta$  UMa,  $\alpha$  Ser, and  $\eta$  Dra) all have significant  $\chi_\nu^2(\text{min})$  on one or more nights each, but these minima correspond to  $\rho$  values  $\lesssim$  (usually  $\ll$ ) the known or estimated (per the methods of § 4.1) angular diameters of the primary stars. We made no further attempt to model these sources as binaries, rather proceeding to accurate single-star model fitting of all of these sources (§ 5.6), with the exception of  $\theta$  UMa, where the estimated primary diameter ( $\sim 1.7$  mas) is marginally too small to allow accurate angular-diameter modeling from our data. See § 5.6 for a quantitative assessment of our ability to fit angular diameters  $< 2$  mas. Conversely, in § 5.6 we fit single-star angular diameters to an additional six sources ( $\beta$  Cas, 46 LMi,  $\kappa$  Oph,  $\beta$  Oph,  $\eta$  Ser, and  $\gamma$  Cep<sup>5</sup>) that had no significant  $\chi_\nu^2(\text{min})$  in any GRIDFIT output on any night of observation, but had estimated angular diameters  $\geq 2$  mas.

A third group of two sources ( $\eta$  Cep and  $\iota$  Peg) may be considered *marginal* detections in that GRIDFIT outputs for these stars show significant  $\chi_\nu^2(\text{min})$  on only one night each (2004 October 05 UT for  $\eta$  Cep, and 2004 September 30 UT for  $\iota$  Peg, respectively). For  $\eta$  Cep, we attempt both binary- and single-star models in § 5.4.1 and § 5.6, respectively, while a binary model for  $\iota$  Peg is attempted in § 5.4.2.

---

<sup>5</sup>Neuhäuser et al. (2007) reported the detection of  $\gamma$  Cep B at  $\rho \sim 890$  mas and  $\Delta m_K \sim 6.3$

None of the remaining sources observed show any indication of significant  $\chi^2_{\nu}(\text{min})$  in the GRIDFIT output plots. An example of such a plot is presented in Figure 12. However, to lend further confidence as to the completeness of the GRIDFIT search results, we additionally conducted an extensive search of the literature for references to multiplicity among our observed sources (Table 3). We searched the *Hipparcos Catalogue Double and Multiple Systems Annex* (ESA 1997), the *SIMBAD* database (Wenger et al. 2000), the *Seventh catalogue of the orbital elements of spectroscopic binary systems* (Batten et al. 1978), *The ninth catalogue of spectroscopic binary orbits* (Pourbaix et al. 2004), the WDS, the ORB6, the INT4, the *Third photometric magnitude difference catalog* (Mason 2008), and papers 1 through 233 of Griffin (e.g., Griffin 2013) for references to binary companions, particularly at  $\rho \leq 1''$  and  $\Delta m \leq 4$ . This search revealed seven systems of possible interest. Five of these ( $\beta$  Cas,  $\eta$  Cas,  $\alpha$  Tri,  $\rho$  Gem, and  $\theta$  Dra) contain known or suspected spectroscopic binaries. However, given the reported spectroscopic orbital solutions and the known parallaxes (Table 1), the likely angular separations of these binaries are all  $\leq 1$  mas, significantly below the resolution of the array configuration used for our observations ( $\lambda/(2*B) \approx 2.6$  mas, where  $\lambda = 550$  nm (§ 2.1) and  $B = 22.2$  m (§ 2.2); Traub 2000)<sup>6</sup>. Therefore, it is not surprising that these systems produce no evidence of binarity in the GRIDFIT searches. The remaining two sources ( $\beta$  CVn, and  $\delta$  Aql) each have one measurement of a companion made by speckle interferometry (Bonneau & Foy 1980; Bonneau et al. 1980) but numerous nondetections as well (INT4). Given that Bonneau & Foy (1980) found the  $\Delta m$  for  $\beta$  CVn to be large (“about 3 mag”), it could be that this companion, if it exists, lies beyond the  $\Delta m$  detection limit of our current observations (§ 5.1.5), but this source will be observed again with the more capable current

---

<sup>6</sup>In the case of  $\beta$  Cas, the notes to the WDS list a  $P = 27$  d spectroscopic binary (Aitken 1932), but Abt (1965) concluded there was no convincing evidence of binary motion.

NPOI array. For  $\delta$  Aql, Kamper et al. (1989) concluded, based on an orbit derived from astrometric and spectroscopic measurements, that the  $\Delta m$  is also large (and the Bonneau et al. 1980, observation likely spurious), so once again the lack of a detection from the current data does not necessarily reduce confidence in the completeness of the GRIDFIT search results and our claim of a  $\Delta m = 3.0$  detection limit. However, given the Kamper et al. (1989) and later *Hipparcos* orbital solutions (ESA 1997), we attempt a binary model of our  $\delta$  Aql data in § 5.4.3.

Thus, our search of the literature for references to multiplicity among our observed sources does not immediately contradict the GRIDFIT search results. In the following two sections we then proceed to the detailed modeling of the six detected binaries and the three possible binary detections ( $\eta$  Cep,  $\iota$  Peg, and  $\delta$  Aql) discussed above.

### 5.3. Binaries Among the Program Stars

The detailed modeling of the six detected binaries among the program sources observed to date (§ 5.2) closely followed the procedures used for the  $\Delta m$  test binaries described in § 5.1; fits for  $\rho$  and  $\theta$  on individual nights were first performed, the component angular diameters and  $\Delta m$  held fixed, after which fits for  $\Delta m$  were performed, followed by a final, simultaneous fit for  $\rho$ ,  $\theta$ , and  $\Delta m$ . As in § 5.1, the fitted position angles were adjusted by  $180^\circ$  as needed for consistency with those listed in the INT4 and with the predictions of published orbits. The results are tabulated in Tables 12 & 13, which follow the same format as Tables 6 & 11, respectively. Notes for individual systems follow.

### 5.3.1. $\alpha$ Aur

For  $\alpha$  Aur (FK5 193, HR 1708, HIP 24608, HD 34029, WDS J05167+4600 Aa,Ab), the orbital elements and component angular diameters (6.4 mas and 8.5 mas, respectively) of Hummel et al. (1994), along with  $\Delta m = 0$ , were used as inputs to the binary models. The grid fitting procedure within OYSTER was used to verify the initial estimates of  $\rho$  and  $\theta$ . The grid search was performed in 0.5 mas steps over a range of 50 mas in RA and DEC, centered on the position predicted by the Hummel et al. (1994) orbit. The results of this search show excellent agreement ( $< 0.5$  mas) with the orbit predictions on the first two nights, and for the position angle on the third night, but with a discrepancy of  $\sim 10$  mas in separation, evidently due to the poor quality of the  $V^2$  calibration on this night. The final OYSTER model fitting produced nightly  $\rho$ ,  $\theta$  fits (Table 12) showing excellent agreement with the Hummel et al. (1994) orbit (nightly O-C values ranging from 0.2 mas to 0.3 mas.), albeit with a large error in the fit for  $\rho$  on the third night. The fitted  $\Delta m_{700} = 0.0 \pm 0.1$  (Table 13) is consistent with values of both Hummel et al. (1994,  $\Delta m_{800} = -0.05 \pm 0.05$ ) and Baldwin et al. (1996), determined at similar effective wavelengths.

### 5.3.2. 10 UMa

For 10 UMa (FK5 339, HR 3579, HIP 44248, HD 76943, WDS J09006+4147 AB), the orbital elements of Muterspaugh et al. (2010a), an estimated primary star angular diameter  $\theta_P = 1.004$  mas provided by the NPOI data reduction software § 4.1, an assumed secondary star angular diameter  $\theta_S = 0.1$  mas, and  $\Delta m = 2.3$  (ORB6) were used as inputs to the binary models. The initial estimates of  $\rho$  and  $\theta$  were verified using the OYSTER ‘gridfit’ procedure.

The O-C values of the final nightly  $\rho$ ,  $\theta$  fits from OYSTER with respect to the

Muterspaugh et al. (2010a) orbit show good agreement ( $\leq 5$  mas), while the fitted  $\Delta m_{700} = 2.19 \pm 0.29$  is consistent with several measurements at similar effective wavelengths reported in the INT4.

### 5.3.3. $\gamma$ Vir

$\gamma$  Vir (HR 4825/6, HIP 61941, HD 110379, WDS J12417-0127 AB) is a visual binary with over 200 years of relative astrometric measures listed in the INT4 catalog. It is one of the first pairs of stars presented by Sir William Herschel (Herschel 1803) that conclusively demonstrated orbital motion. This was significant as previously most of these double stars were presumed to be coincident optical pairs as orbital motion had not been conclusively observed. The recent periastron passage in 2005 was key to a revision of some imprecisely known orbital elements (Scardia et al. 2007). Most magnitude differences recorded in the INT4 for the pair are  $\sim 0.0$ . A nearly equal brightness ratio is expected as the spectral types of the two stars are the same (Abt & Morrell 1995, Table 1). Interestingly, some magnitude differences for measurements within the 21st century are decidedly non-zero. These include a  $\Delta m = 0.69$  with the RYTSI speckle camera (Horch et al. 2010) and as large as 0.9 at 745 nm with the Robo-AO system (Riddle et al. 2015). This motivates use of the NPOI visibility data to provide a precise  $\Delta m$  to investigate the significance of a non-zero brightness ratio for these two stars.

For  $\gamma$  Vir, the orbital elements of Scardia et al. (2007), primary and secondary star angular diameters of 1.59 mas (Richichi et al. 2005), and a  $\Delta m = 0.1$  resulting from the GRIDFIT search (§ 5.2), were used as inputs to the binary model. The initial estimates of  $\rho$  and  $\theta$  were verified using the OYSTER ‘gridfit’ procedure. As the raw  $V^2$  on the AC-AW baseline are very low, varying from  $\sim 10\%$  in the red to  $\sim 3\%$  in the blue, and because the predicted period of the  $V^2$  oscillations as a function of wavelength is *much* less than the

widths of our spectral channels, calibrating and modelling these data proved very difficult. Therefore, these data were not used in the final modelling process. Our results (Table 12) are nicely bracketed in position angle by the contemporaneous observations of Hartkopf et al. (2008) and Scardia et al. (2005), and the O-C values of the nightly  $\rho$ ,  $\theta$  fits with respect to the Scardia et al. (2007) orbit (Figure 13) show reasonably good agreement (2 mas to 9 mas) considering the relatively poor north-south resolution of the single-baseline data used in our astrometric fits. Our fitted  $\Delta m_{700} = 0.0 \pm 0.10$  (Table 13) is smaller than most INT4 values, but is consistent with the identical spectral types for the components of  $\gamma$  Vir listed in Table 1.

#### 5.3.4. $\zeta$ Her

For  $\zeta$  Her (HR 6212, HIP 81693, HD 150680, WDS J16413+3136 AB), the orbital elements of Söderhjelm (1999), a primary star angular diameter  $\theta_P = 2.367$  mas (Mozurkewich et al. 2003), an estimated secondary star angular diameter  $\theta_S = 0.77$  mas, and  $\Delta m = 1.54$  (below) were initially used.  $\theta_S$  was estimated from the spectral type (G7V) and parallax (92.63 mas) listed in Table 1 using the tables of  $R/R_\odot$  of Drilling & Landolt (1999).

We next endeavored to improve our estimates for several of these parameters: First, the OYSTER gridfit procedure was used to improve the initial estimates of  $\rho$  and  $\theta$ . This grid search was performed in 0.5 mas steps over a range of 150 mas in RA and DEC, centered on the position predicted by the Söderhjelm (1999) orbit. As there was no evidence ( $V^2$  oscillations with wavelength/channel) for the wide companion in any of the observations on the AC-AW baseline, these data were not used in the grid search. However, such oscillations are often present for AC-AE observations (Figure 14). Next, the improved  $\rho$  and  $\theta$  values, along with the initial  $\theta_S$  and  $\Delta m$  values (all held fixed), were used to improve the  $\theta_P$  value



through a simultaneous fit of a binary model to all the data from both baselines on the seven nights of observation (Table 3). The value thus obtained  $\theta_P = 2.359$  mas is only slightly different from that of (Mozurkewich et al. 2003).

Lastly, final, nightly fits for  $\rho$ ,  $\theta$ , and  $\Delta m$ , using only the AC-AE baseline data were performed. The results are presented in Tables 12 & 13. Our position results are all quite similar and are bracketed in position angle by contemporaneous results at 2004.3031 (Hartkopf et al. 2008) and 2004.659 (Scardia et al. 2006). The average separation is about 1.8 mas less than the Söderhjelm (1999) orbit, while the average position angle is  $\approx 1^\circ 6'$  more, corresponding to  $\approx 25$  mas in a northwesterly direction. The average of the nightly fits for  $\Delta m$  ( $\Delta m_{700} = 1.52 \pm 0.04$ ) is much smaller than the values typically quoted in the INT4 for observations made at similar effective wavelengths ( $\sim 2.6$ ; e.g., Horch et al. 2004, 2008; Drummond 2014), but is clearly consistent with our data for observations where the period of the observed  $V^2$  oscillations with wavelength is large with respect to the width of the NPOI spectral channels (e.g., panel “a” of Figure 14).

### 5.3.5. $\chi$ Dra

For  $\chi$  Dra (FK5 695, HR 6927, HIP 89937, HD 170153, WDS J18211+7244 Aa,Ab), the orbital elements of Farrington et al. (2010), an estimated primary star angular diameter  $\theta_P = 1.531$  mas provided by the NPOI data reduction software (§ 4.1), an assumed secondary star angular diameter  $\theta_S = 0.1$  mas, and  $\Delta m = 2.13$  (ORB6) were used as inputs to the binary models. OYSTER’s gridfit procedure was used to improve the initial estimates of  $\rho$  and  $\theta$ . This grid search was performed in 0.5 mas steps over a range of 50 mas in RA and DEC, centered on the position predicted by the Farrington et al. (2010) orbit. The O-C values of the nightly  $\rho$ ,  $\theta$  fits from OYSTER (Table 12) with respect to the Farrington et al. (2010) orbit range from 2 - 11 mas. The fitted  $\Delta m_{700} = 2.12 \pm 0.02$  (Table 13) is consistent

with the values of both Schoeller et al. (1998) [ $\Delta m_{656} = 2.10 \pm 0.15$ ;  $\Delta m_{755} = 2.08 \pm 0.15$ ] and Horch et al. (2008) [ $\Delta m_{698} = 2.03 \pm 0.10$ ;  $\Delta m_{754} = 2.09 \pm 0.10$ ], determined at similar effective wavelengths.

### 5.3.6. $\beta$ Del

For  $\beta$  Del (HR 7882, HIP 101769, HD 196524, WDS J20375+1436 AB), the orbital elements of Muterspaugh et al. (2010b), an estimated primary star angular diameter  $\theta_P = 1.188$  mas provided by the NPOI data reduction software (§ 4.1), an assumed secondary star angular diameter  $\theta_S = 0.5$  mas, and  $\Delta m = 0.91$  (ORB6) were used as inputs to the binary models. OYSTER’s gridfit procedure was used to verify the initial estimates of  $\rho$  and  $\theta$  calculated from the Muterspaugh et al. (2010b) orbit. This grid search was performed in 0.5 mas steps over a range of 50 mas in RA and DEC, centered on the positions predicted by the Muterspaugh et al. (2010b) orbit. The O-C values of the nightly  $\rho$ ,  $\theta$  model fits from OYSTER (Table 12) with respect to the Muterspaugh et al. (2010b) orbit are all  $\leq 1.2$  mas. The fitted  $\Delta m_{700} = 1.08 \pm 0.14$  (Table 13) is consistent with the mean ( $\approx 1.1 \pm 0.1$ ) of the numerous measurements at  $\approx 700$  nm reported in the INT4.

## 5.4. Marginal Detections

Lastly, we attempted to model the three binaries ( $\eta$  Cep,  $\iota$  Peg, and  $\delta$  Aql) possibly resolved by our observations (§ 5.2).

#### 5.4.1. $\eta$ Cep

For  $\eta$  Cep (FK5 783, HR 7957, HIP 102422, HD 198149, WDS J20453+6150 A), we used the position and  $\Delta m$  values from the GRIDFIT output for 2004 October 05 UT (99% confidence detection, at  $\rho = 7.51$  mas,  $\theta = 25^\circ 30'$ , and  $\Delta m = 3.70$ ), an estimated primary star angular diameter  $\theta_P = 2.85$  mas provided by the NPOI data reduction software (§ 4.1), and an assumed secondary star angular diameter  $\theta_S = 0.5$  mas as initial values in binary model fits to the  $V^2$  data from the three nights of observations listed in Table 3.

We also applied CANDID to the identical data set from 2004 October 05 UT, producing very similar results ( $\rho = 7.50$  mas,  $\theta = 26^\circ 70'$ ,  $\Delta m = 3.65$ , and  $\theta_P = 2.58$ ). These values were likewise used as inputs to models of the data from all three nights.

We also fit an alternative model of a single star with an initial diameter of 2.85 mas or 2.58 mas to the data from all three nights, producing identical results for each night.

The binary models, starting with either the GRIDFIT or CANDID values, proved to be the best (much lower  $\chi_\nu^2$ ) fits to the data of 2004 October 05 UT, and marginally better fits for 2004 October 01 UT, while the single star model was a slightly better fit for 2004 September 30 UT. Thus, we are left with a rather inconclusive situation where the detection of a new stellar companion remains a possibility. (The literature search of § 5.2 produced no references to any likely companions in the detection range of our observations.) New NPOI observations are clearly indicated.

#### 5.4.2. $\iota$ Peg

For the very well studied binary  $\iota$  Peg (FK5 831, HR 8430, HIP 109176, HD 210027, WDS J22070+2521A; Boden et al. 1999; Morel et al. 2000; Konacki et al. 2010), we fit both binary and single-star models to the calibrated  $V^2$  data resulting from the two nights of

observations listed in Table 3.

We fit two different binary models using the orbital parameters of the “Primary Data Set” of Boden et al. (1999), then those of Konacki et al. (2010). In the first model, we also used an estimated primary star angular diameter  $\theta_P = 1.273$  mas provided by the NPOI data reduction software (§ 4.1), a secondary star angular diameter  $\theta_S = 0.71$  (Boden et al. 1999), and a component magnitude difference  $\Delta m = 2$  based on values at various bandpasses, cited in the previous references. In the second model, we used the primary and secondary star angular diameters of Konacki et al. (2010),  $\theta_P = 1.06$  mas and  $\theta_S = 0.6$ , respectively, along with a component magnitude difference  $\Delta m = 2$ . For the single-star model, an estimated angular diameter 1.06 mas was used as the initial input.

The resulting optimized models on each night show those based on the Boden et al. (1999) orbit to be marginally the best fit, followed by those based on the Konacki et al. (2010) orbit, then the single star model, but the  $\chi_\nu^2$  values do not differ widely and are all relatively large (2.9 to 5.9). Thus, we conclude that our observations have failed to resolve the secondary component in this system. This result is not surprising given that the angular separations of the secondary predicted by the Boden et al. (1999) and Konacki et al. (2010) orbits for these dates ( $\rho \approx 1.1$  mas to 1.3 mas) are well below the angular resolution of the observations (§ 5.2), the secondary star lying on portions of the highly inclined orbit ( $i = 95^\circ 83$ , Boden et al. 1999) close to the points of minimum projected separation.

We also independently examined the calibrated  $V^2$  data from both nights using GRIDFIT, and those from 2004 October 05 UT using CANDID. GRIDFIT indicated a 99% confidence detection at  $\rho = 9.39$  mas,  $\theta = 26^\circ 65$ , and  $\Delta m = 3.20$  on 2004 September 30 UT, and a  $\sim 68\%$  confidence detection at  $\rho = 24.80$  mas,  $\theta = 7^\circ 44$ , and  $\Delta m = 4.00$  on 2004 October 05 UT. CANDID also produced a weak detection at very similar values ( $\rho = 24.33$  mas,  $\theta = 7^\circ 34$ , and  $\Delta m = 3.76$ ) on 2004 October 05 UT. Given that these  $\rho$  and  $\theta$

values are widely divergent from the predictions of the Boden et al. (1999) and Konacki et al. (2010) orbits, and that a binary model based on the GRIFIT/CANDID results for the second night produces a fit no better than those cited above, we again conclude we have not detected the secondary star with our current observations. The NPOI currently has operational baselines to  $\approx 100$  m, which should make future observations that resolve this binary eminently practical.

#### 5.4.3. $\delta$ Aql

For  $\delta$  Aql (FK5 730, HR 7377, HIP 95501, HD 182640, WDS J19255+0307 A), we fit four different models to the calibrated  $V^2$  data resulting from the four nights of observations listed in Table 3:

- 1) First, using the parameters of the *Hipparcos* orbital solution (ESA 1997), with an estimated primary star angular diameter of 1.288 mas from the NPOI data reduction software (§ 4.1), an assumed secondary star angular diameter of 0.5 mas, and an assumed component magnitude difference of  $\Delta m = 2$ .
- 2) Second, using the parameters  $\rho = 16.8$  mas,  $\theta = 147^\circ.6$ , and  $\Delta m = 3.9$  corresponding to the very marginal ( $< 1 \sigma$ )  $\chi_\nu^2(\text{min})$  seen in the GRIDFIT output for 2004 September 23 UT as an initial model guess, along with the same component angular diameters. (CANDID was also applied to the data from this night, producing very similar results:  $\rho = 17.2$  mas,  $\theta = 148^\circ.3$ , and  $\Delta m = 4.1$ ).
- 3) Third, using the epoch 1979.4615 speckle observation of Bonneau et al. (1980) ( $\rho = 132$  mas,  $\theta = 130^\circ$ ) as an initial model guess, with  $\Delta m = 3.9$  and the same assumed component angular diameters.
- 4) Lastly, a model of a single star of an estimated angular diameter of 1.288 mas as an

initial model guess.

The results of these efforts were that the best-fit optimized model for the first night and marginally best fit to the data from the third night were derived using the second starting model, while the single-star model was clearly the best fit to the data for the second and fourth nights. These results, along with the significantly different final  $\rho$  and  $\theta$  values for the binary models for the first and third nights (16.9 mas and  $147^\circ.8$  *vs* 10.8 mas and  $125^\circ.6$ , respectively), lead to little confidence of a definite detection of a second star. Once again, additional observations are needed.

### 5.5. Limits of Binary Detection

The generally excellent agreement in the results of applying GRIDFIT and CANDID to our data on five stars ( $\beta$  Sct: § 5.1.2, V1334 Cyg: § 5.1.3,  $\eta$  Cep: § 5.4.1,  $\iota$  Peg: § 5.4.2, and  $\delta$  Aql: § 5.4.3) and our successful recovery of 13 of the 15  $\Delta m$  Test Binaries (§ 5.1) using GRIDFIT lend confidence to our claim of a limiting  $\Delta m_{700}$  sensitivity of  $\approx 3.0$ , and to perhaps  $\Delta m_{700} \sim 3.5$  for binaries where there is not more than a difference of two full spectral types between the components (§ 5.1.5, Figure 10, and Table 4). These results, along with the fact that the effects of bandwidth smearing are explicitly accounted for in GRIDFIT (§ 2.1.5), also lend confidence in the completeness of our survey out to its originally intended 500 mas angular separation limit (§ 1, 5.1).

Having completed the detailed modeling of the six detected binaries among the program sources observed to date, we added the log of the mean of the nightly  $\rho$  values, and the mean  $\Delta m_{700}$  values for each star from Tables 12 & 13 to Figure 10. The inclusion of the four very wide binaries (10 UMa,  $\gamma$  Vir,  $\zeta$  Her, and  $\beta$  Del) in this group greatly extends the range of angular separations over which we have fitted  $\Delta m_{700}$  values to  $\sim 860$  mas

( $\zeta$  Her), and appears likely consistent with the  $\Delta m_{700} \approx 3.0$  limit at smaller separations. However, can we claim completeness in our search for new binaries in the region  $> 500$  mas in Figure 10 without performing finely sampled GRIDFIT searches (§ 5.2) out to such large angular separations? As an alternative to extending the computationally intensive GRIDFIT process, we generated simulated  $V^2$  vs wavelength plots using the actual  $uv$ -plane coverage on typical nights for  $\gamma$  Vir and  $\zeta$  Her ( $\rho \approx 620$  mas and  $\approx 860$  mas, respectively) at various binary position angles and  $\Delta m$  values. These simulations show that for the full range of position angles up to  $\pm 90^\circ$  from the observed  $\theta$  values for these stars, one or more observations would have shown  $\pm 5\%$  -  $10\%$   $V^2$  oscillations so long as  $\Delta m \leq 2.6$ . While, as noted in § 5.3.4, the model fitting process for  $\zeta$  Her was not straightforward, the facts that good-quality fits were still possible and that the simulations predict similar  $V^2$  oscillations regardless of binary position angle indicate that similarly sampled NPOI observations would have detected (via the GRIDFIT process) all binaries out to the same range of angular separation and  $\Delta m$ . We also direct the reader to our plots of typical  $uv$  coverage in Figures 3 & 9. Taken together, these demonstrate how difficult it is for a binary to remain undetected within our limits. Just a few scans are needed to show a binary oscillation and deviation from a single star assumption.

Conversely, it can be shown that near the narrow-separation end of our search range ( $\approx 3$  mas) our search is reasonably complete with respect to the limited time span of the observations (average of 8 nights per source) occurring at times when companions in eccentric apparent orbits might lie at angular separations below our resolution limit. For the example of the Main Sequence primary stars in our sample, a limiting detectable magnitude difference of  $\Delta m_R \approx 3$  implies primary/secondary spectral type pairings of  $\sim$  F0V/K0V at the blue limit of our sample and  $\sim$  K2V/M2V at the red limit, respectively (Drilling & Landolt 1999). These in turn imply mass sums  $M_P + M_S$  of  $\approx 2.4 M_\odot$  and  $1.1 M_\odot$ , respectively. Examples of such systems with apparent semi-major axes near the 3

mas resolution limit and at the distance limit of our sample (30 pc) would have physical semi-major axes of  $\approx 0.1$  AU and orbital periods of  $\sim 7 - 11$  days. Since it is known that almost all binaries with periods this short have circular orbits as a result of tidal dissipation (Raghavan et al. 2010; Duchêne & Kraus 2013), it is likely that they would have been detectable unless viewed at inclinations  $i \gtrsim 60^\circ$ . A similar analysis pertains to the systems in our sample with giant primaries or of smaller  $\Delta m_R$  (greater mass sum), or at distances  $< 30$  pc (smaller physical semi-major axes at our angular resolution limit), where the resulting orbital periods would be even shorter.

## 5.6. Angular Diameters of Program Stars

For those sources where the results of § 5.2 and § 5.3 indicated the lack of detectable stellar companions, we next fit a circular, uniform intensity disk model (Eq. 9, Hanbury Brown et al. 1967a) to all the calibrated, squared visibility measurements on the nights listed in Table 3. The resulting uniform disk angular diameters  $\theta_{UD}$ , with assigned errors  $\sigma_{UD}$ , for 11 sources with  $\theta_{UD} \geq 2.0$  mas are listed in Table 14. Two contributing factors were combined in quadrature to determine the errors.

First, a bootstrap Monte Carlo technique (Tycner et al. 2010) was used to estimate the likely effects on the fitted diameters of quasi-random atmospheric variations on timescales shorter than the cadence between the program star - calibrator pairs, as well as the systematic effects of the choice of a standard calibration weighting interval (§ 4.1). In this technique, synthetic data sets (here 5,000 per source) are created using the actual observed data points picked at random, with the total number of points in each set being the same. The distribution of the best-fit model diameter fitted to the bootstrapped data sets was then used to estimate the uncertainty associated with the diameter fitted to the actual data. The resulting errors range from 0.2% to 2.3% of the fitted diameters for the stars in



Table 14. (Note that the star with the largest quoted error,  $\eta$  Cep, was also examined as a possible binary in § 5.4.1.) Fits to other program sources with angular diameters even marginally smaller than 2 mas had rapidly increasing uncertainties with decreasing angular diameter; therefore we decided to limit the stars included in Table 14 to  $\theta_{UD} \geq 2.0$  mas, where the errors of  $\lesssim 2\%$  meet the generally recognized minimal standard of accuracy for astrophysically useful stellar angular diameter measurements (Booth 1997; Holmberg et al. 2009).

The second factor used in estimating the total error in  $\theta_{UD}$  for each star is that due to the estimated 10% uncertainty in the angular diameters of our calibration stars (§ 4.1). The effect of the uncertainty of the calibrator diameter on the fitted program star diameter was estimated for each source by applying a  $\pm 10\%$  offset to the estimated calibrator angular diameter, recalculating its expected visibility at the time observation, then recalibrating and refitting the source visibilities. The resulting changes in the fitted  $\theta_{UD}$  for the sources in Table 14 ranged from 0.1% to 2.4%, depending on the relative size of the source and its calibrator. This result is not surprising given the small angular diameters of the calibrator stars observed for each of these 11 sources ( $\leq 1.0$  mas, Tables 2 & 3) and the relatively short baselines used (see e.g., Cruzalèbes et al. 2010).

After combining in quadrature the above error estimates, the final estimated errors for our fitted diameters in Table 14 range from 0.2% to 3%. As a further check on their accuracy, we compared these results with other high precision measurements only available in publications since *c.* 1999 for these sources. In Figure 15 we plot the diameter difference (literature minus the Table 14  $\theta_{UD}$  value) *vs* our  $\theta_{UD}$  values for the eight of the 11 stars for which published results exist (all from the NPOI or Mark III interferometers; Nordgren et al. 1999, 2001; Mozurkewich et al. 2003). The overall agreement with these previous results is good, the weighted mean of the differences being only  $-0.023 \pm 0.016$  mas. The most

discordant point in Figure 15 is a Mark III measurement for  $\eta$  Draconis (Mozurkewich et al. 2003). We can find no obvious explanation for this difference, but note that the previous NPOI measurement of this star plotted in Figure 15 (Nordgren et al. 2001), and results from the infrared flux method (see discussion of Figure 16, below) show good agreement.

A second comparison can be made between our results, converted to equivalent limb darkened angular diameters ( $\theta_{LD}$ ), and those from the literature. We converted our  $\theta_{UD}$  using the limb darkening correction (LDC) factors of Nordgren et al. (1999) for the same stars, or stars of the same spectral types (Table 14, Col. 5). The resulting equivalent  $\theta_{LD}$  values are listed in Table 14, Col. 6, with the estimated errors listed in Col. 7. These latter errors were derived by scaling our  $\theta_{UD}$  errors by the LDC factor for each star, then combining the result with the estimated error in the LDC (0.5% of the derived  $\theta_{LD}$ ; Nordgren et al. 1999). In Figure 16 we plot the differences between our equivalent  $\theta_{LD}$  values and those from the literature *vs* our  $\theta_{LD}$  values, for all 11 stars from Table 14. The  $\theta_{LD}$  from the literature were derived either by radiometric methods (Cohen et al. 1999), SED fits (Baines et al. 2009; van Belle & von Braun 2009), the infrared flux method (Alonso et al. 2000; Blackwell et al. 1991; Blackwell & Lynas-Gray 1994; Ramírez & Meléndez 2005), or the infrared surface brightness method (Di Benedetto 2005). The overall agreement with the literature is again excellent, the weighted mean of the differences being  $0.007 \pm 0.019$  mas. The largest outlier in Figure 16 is one of three diameter estimates for  $\gamma$  Cephei (Ramírez & Meléndez 2005).

## 6. Discussion

Our survey efforts to date have yielded a significant number of separation and position angle measurements for six binary systems from our program sample (§ 5.3), as well as for 13 additional systems observed to assist in establishing the NPOI’s range of

sensitivity to binary detection in  $\Delta m$  and angular separation (§ 5.1). We have also obtained astrophysically useful angular diameter measurements of 11 stars (§ 5.6). However, while we have obtained the first visual detection of the secondary star in the  $\beta$  Sct system, one of our test binaries, we have failed to unambiguously detect any new binary systems among our program stars (§ 5.2), with the possible exception of  $\eta$  Cep (§ 5.4.1). This null result might be tentatively construed as consistent with the results of Raghavan et al. (2012) in support of the conclusion of Raghavan et al. (2010) that the once presumed gap between the angular sensitivity ranges of spectroscopic and visual techniques for the detection of stellar companions to nearby solar-type stars has been largely filled by systematic surveys utilizing radial-velocity and interferometric techniques. However, while our survey has an order-of-magnitude greater range of angular separation sensitivity for binary detection (3 - 860 mas) as compared to that of Raghavan et al. (2012, 8 - 80 mas), and perhaps greater  $\Delta m$  sensitivity ( $\Delta m_{700} = 3.0$  *vs*  $\Delta m_K \lesssim 1.5$ ), the size of our sample to date [41 stars, only 27 of which are Main Sequence stars by our common definition (§ 3)] is small compared to that of Raghavan et al. (2012, 186 stars).

On the other hand, many more stars are potentially available for observation with the NPOI. As Figure 7 shows, there are still a significant number (13) of Main Sequence stars from our original sample yet to be observed as compared to only five evolved stars not observed. Additionally, the sensitivity of the NPOI has been significantly improved over the past decade. As noted in § 2.1 and § 3, respectively, the practical limit for NPOI observations was  $m_V \approx 4.3$  *c.* 2004, but is now (2016) routinely  $m_V = 5.5$ , and  $m_V = 6.0$  under good observing conditions. This opens the opportunity to greatly expand observational coverage of Main Sequence stars. For example, in the range  $0.30 \leq B-V \leq 0.70$  (spectral types F0 through G5), to a limiting magnitude  $m_V = 6.0$ , it is possible to define a complete, volume-limited sample of  $\sim 50$  stars within  $\approx 17$  pc, with parallax errors  $\leq 5\%$  (van Leeuwen 2007) and  $\delta \geq -20^\circ$ . The combination of a greater  $m_V$  limit with a

smaller distance limit for this sample results in proportionately many more intrinsically fainter stars in the range  $0.57 \lesssim B-V \leq 0.70$  (spectral types G0 - G5) relative to our current program sample (Figure 4). Observations of this list would provide a more robust comparison with the results of other surveys of solar-type stars (e.g., Raghavan et al. 2012) using a complementary wavelength bandpass, coupled with a capability for binary detection over a wide range of angular separations. Observing a sample of  $\sim 50$  stars in a reasonable length of time with the NPOI is also eminently practical. Based on the experience of the work reported here, approximately five nights of multiple observations of each star under reasonable observing conditions should be adequate to detect binary companion(s) in the  $\Delta m$  - angular separation range demonstrated in this paper. Given the known weather and seeing statistics at the NPOI, and a reasonably-sized nightly observing list (5 - 7 sources, plus calibrators), the survey of a 50-star sample could be completed within  $\sim 1$  year utilizing  $\approx 20\%$  -  $25\%$  of all scheduled NPOI observing time. Also, the substitution of siderostat stations more recently commissioned than those used in the present study could increase the angular resolution of future NPOI multiplicity surveys by up to a factor of three while maintaining the same simple fringe detection configuration described in § 2.2. This increase in angular resolution would provide obvious benefits in terms of resolving far more of the known or suspected spectroscopic binaries (§ 5.2), and possible, as yet unknown, stellar companions at similar angular separations. The bandpass of NPOI observations is also expected to be extended towards the blue (to 450 - 860 nm in 32 channels) in the near future, making the detection of binaries with components of widely differing spectral types (§ 5.1.4) more likely.

## 7. Conclusions

We have presented the first results from an ongoing survey for multiplicity among the bright stars using the NPOI. The initial source sample emphasized bright stars of spectral types F0 through K2. We report observations of 41 stars ( $m_V \leq 4.30$ ), all having been observed on multiple nights. Observations of known binary systems among the program star sample, combined with additional observations of other known binaries, including the first “visual” detection of the secondary star in the  $\beta$  Sct system at precisely measured separations and position angles, demonstrate the NPOI’s sensitivity for binary detection over a wide range of angular separations (3 - 860 mas) at component magnitude differences  $\Delta m_{700} \lesssim 3$ , and to perhaps  $\Delta m_{700} \sim 3.5$  for binaries where the component spectral types differ by less than two. Fitted angular separations, position angles, and component magnitude differences for six previously known binaries from the program sample are presented, along with angular diameters for 11 resolved stars from the sample that have no detected stellar companions. In the light of the significant improvements made to the limiting sensitivity of NPOI observations ( $m_V \approx 6.0$ ) in recent years, plans are being drafted to extend the initial survey to a complete, volume-limited sample of stars of spectral types F0 through G5.

We gratefully acknowledge NPOI observers D. Allen, L. Bright, B. Burrell, C. Denison, L. Foley, B. O’Neill, C. Sachs, S. Strosahl, D. Theiling, W. Wack, and R. Winner for their careful and efficient operation of the NPOI over the many epochs of data collection required for this paper. We also gratefully acknowledge the skillful instrument makers at the USNO and Lowell Observatory instrument shops, and thank the staff of the USNO Library for assistance with our many reference requests. Lastly, we thank Dr. Paul Shankland, Director of USNO Flagstaff Station, for his long-standing and continuous support of the NPOI Program.

The NPOI project is funded by the Oceanographer of the Navy and the Office of Naval Research. This research has made use of the SIMBAD literature database and the VizieR catalog access tool, both operated at CDS, Strasbourg, France, the Washington Double Star Catalog and associated catalogs, maintained at the U.S. Naval Observatory, Washington, DC, the NASA/IPAC Infrared Science Archive, operated by the Jet Propulsion Laboratory, California Institute of Technology, under contract with the National Aeronautics and Space Administration, and the JSTOR digital archive.

## REFERENCES

- Absil, O., Le Bouquin, J. -B., Berger, J. -P. et al. 2011, *A&A*, 535, A68
- Abt, H. A. 1965, *ApJS*, 11, 429
- Abt, H. A., & Morrell, N. I. 1995, *ApJS*, 99, 135
- Aitken, R. G. 1932, *New General Catalogue of Double Stars within 120° of the North Pole*, Carnegie Inst. Washington D. C. Publ., 417, 0
- Alonso, A., Salaris, M., Arribas, S. et al. 2000, *A&A*, 355, 1060
- Armstrong, J. T., Mozurkewich, D., Rickard, L. J et al. 1998, *ApJ*, 496, 550
- Avni, Y. 1976, *ApJ*, 210, 642
- Baines, E. K., McAlister, H. A., ten Brummelaar, T. A. et al. 2009, *ApJ*, 701, 154
- Baldwin, J. E., Beckett, M. G., Boysen, R. C. et al. 1996, *A&A*, 306, L13
- Balega, I. I., & Balega, Y. Y. 1988, *Sov. Astron. Lett.*, 14, 393
- Batten, A. H., Fletcher, J. M., & Mann, P. J. 1978, *Publ. Dominion Astrophys. Obs.*, 15, 121
- Benson, J. A., Mozurkewich, D., & Jefferies, S. M. 1998, *Proc. SPIE*, 3350, 493
- Benson, J. A., Hummel, C. A., & Mozurkewich, D. 2003, *Proc. SPIE*, 4838, 358
- Blackwell, D. E., Lynas-Gray, A. E., & Petford, A. D. 1991, *A&A*, 245, 567
- Blackwell, D. E., & Lynas-Gray, A. E. 1994, *A&A*, 282, 899
- Boden, A. F., Koresko, C. D., van Belle, G. T. et al. 1999, *ApJ*, 515, 356

- Bonneau, D., Blazit, A., Foy, R. et al. 1980, A&AS, 42, 185
- Bonneau, D., & Foy, R. 1980, A&A, 86, 295
- Bonneau, D., Clausse, J.-M., Delfosse, X. et al. 2006, A&A, 456, 789
- Booth, A. J. 1997, in IAU Symp. 189, eds. T. R. Bedding, A. J. Booth & J. Davis (Dordrecht: Kluwer), 147
- Bridle, A. H., & Schwab, F. R. 1999, in Synthesis Imaging in Radio Astronomy II, eds. G. B. Taylor, C. L. Carilli, and R. A. Perley, ASP Conf. Ser., 180, 371
- Brown, R. H. 1974, The Intensity Interferometer (London: Taylor & Francis Ltd.)
- Cannon, A. J., & Pickering, E. C. 1918, Henry Draper Catalogue and Extension 1 (HD, HDE), Harv. Ann. 91-100 (1918-1924)
- Clark, J. H. III, Ha, L., Mozurkewich, D. et al. 1998, Proc. SPIE, 3350, 497
- Cohen, M., Walker, R. G., Carter, B. et al. 1999, AJ, 117, 1864
- Cruzalèbes, P., Jorissen, A., Sacuto, S. et al. 2010, A&A, 515, A6
- Cutri, R. M., Skrutskie, M. F., Van Dyk, S. et al. 2003, The 2MASS All-Sky Catalog of Point Sources, Univ. of Massachusetts and Infrared Processing and Analysis Center (IPAC/California Institute of Technology)
- De Rosa, R. J., Patience, J., Zavala, R. T. et al. 2014, ASP Conf. Ser., 487, 251
- Di Benedetto, G. P. 2005, MNRAS, 357, 174
- Drilling, J. S., & Landolt, A. U. 1999, Allen’s Astrophysical Quantities, 4th Ed., edited by A. N. Cox (Springer-Verlag, New York), 388
- Drummond, J. D. 2014, AJ, 147, 65



- Ducati, J. R. 2002, Catalogue of Stellar Photometry in Johnson’s 11-Color System, Dept. of Astron., Univ. Wisconsin
- Duchêne, G., & Kraus, A. 2013, *Annu. Rev. Astron. Astrophys.*, 51, 269
- Dyer, S. D., & Christensen, D. A. 1999, *J. Opt. Soc. Am. A*, 16, 2275
- Edwards, T. W. 1976, *AJ*, 81, 245
- Eggleton, P. P., & Tokovinin, A. A. 2008, *MNRAS*, 389, 869
- ESA 1997, The Hipparcos and Tycho Catalogues, ESA SP-1200
- Farrington, C. D., ten Brummelaar, T. A., Mason, B. D. et al. 2010, *AJ*, 139, 2308
- Fricke, W., Schwan, H., Lederle, T. et al. 1988, *Veroeffentlichungen des Astronomischen Rechen-Instituts Heidelberg*, 31, 1
- Gallenne, A., Monnier, J. D., Mérand, A. et al. 2013, *A&A*, 552, A21
- Gallenne, A., Mérand, A., Kervella, P. et al. 2015, *A&A*, 579, A68
- Griffin, R. F. 2008, *The Observatory*, 128, 21
- Griffin, R. F. 2013, *The Observatory*, 133, 322
- Guyon, O. 2003, *Proc. SPIE*, 4838, 1440
- Hanbury Brown, R., Davis, J., & Allen, L. R. 1967a, *MNRAS*, 137, 375
- Hanbury Brown, R., Davis, J., & Allen, L. R. 1967b, *MNRAS*, 137, 393
- Hanbury Brown, R., Davis, J., Lake, R. J. W. et al. 1974, *MNRAS*, 167, 475
- Hartkopf, W. I. 2000, in *Principles of Long Baseline Stellar Interferometry*, ed. P. R. Lawson (Pasadena: JPL), 295

- Hartkopf, W. I., McAlister, H. A., Mason, B. D. et al. 1997, AJ, 114, 1639
- Hartkopf, W. I., Mason, B. D., & Worley, C. E. 2001a, Sixth Catalog of Orbits of Visual Binary Stars, *www.usno.navy.mil/USNO/astrometry/optical-IR-prod/wds/orb6*
- Hartkopf, W. I., Mason, B. D., Wycoff, G. L. et al. 2001b, Fourth Catalog of Interferometric Measurements of Binary Stars, *www.usno.navy.mil/USNO/astrometry/optical-IR-prod/wds/int4*
- Hartkopf, W. I., Mason, B. D., & Rafferty, T. 2008, AJ, 135, 1334
- Herschel, W. 1803, Philosophical Transactions of the Royal Society of London Series I, 93, 339
- Hindsley, R. B., Armstrong, J. T., Schmitt, H. R. et al. 2011, Applied Optics, 50, 2692
- Hoffleit, D., & Warren Jr., W. H. 1991, The Bright Star Catalogue, 5th Revised Ed. (Preliminary Version), Astronomical Data Center, NSSDC/ADC
- Horch, E. P., Meyer, R. D., & van Altena, W. F. 2004, AJ, 127, 1727
- Horch, E. P., van Altena, W. F., Cyr, W. M., Jr. et al. 2008, AJ, 136, 312
- Horch, E. P. et al. 2010, AJ, 139, 205
- Holmberg, J., Nordström, B., & Andersen, J. 2009, A&A, 501, 941
- Hummel, C. A., Armstrong, J. T., Quirrenbach, A. et al. 1994, AJ, 107, 1859
- Hummel, C. A., Armstrong, J. T., Buscher, D. F. et al. 1995, AJ, 110, 376
- Hummel, C. A., Mozurkewich, D., Armstrong, J. T. et al. 1998, AJ, 116, 2536
- Hummel, C. A., Carquillat, J.-M., Ginestet, N. et al. 2001, AJ, 121, 1623

- Hummel, C. A., Benson, J. A., Hutter, D. J. et al. 2003, AJ, 125, 2630
- Hummel, C. A., Rivinius, Th., Nieva, M.-F. et al. 2013, A&A, 554, A52
- Hutter, D. J., & Elias, N. M., II. 2002, Proc. SPIE, 4838, 1234
- Johnson, H. L. 1966, Annu. Rev. Astron. Astrophys., 4, 193
- Kamper, K. W., Legget, D., & McCarthy, D. W. Jr. 1989, AJ, 98, 686
- Konacki, M., Muterspaugh, M. W., Kulkarni, S. R. et al. 2010, ApJ, 719, 1293
- Kovtyukh, V., Szabados, L., Chekhonadskikh, F. et al. 2015, MNRAS, 488, 3567
- Lafrasse, S., Mella, G., Bonneau, G. et al. 2010, Proc. SPIE, 7734, 77344E
- Lawson, P. R., Lay, O. P., Johnston, K. J. et al. 2007, Terrestrial Planet Finder  
Interferometer Science Working Group Report, JPL Publication 07-1
- Lesh, J. R. 1968, ApJS, 17, 371
- Mason, B. D. 2008, Third Photometric Magnitude Difference Catalog,  
*www.usno.navy.mil/USNO/astrometry/optical – IR – prod/wds/dm3*
- Mason, B. D. 2011, IAU Inf. Circ. 175
- Mason, B. D., Henry, T. J., Hartkopf, W. I. et al. 1998, AJ, 116, 2975
- Mason, B. D., Wycoff, G. L., Hartkopf, W. I. et al. 2001, AJ, 122, 3466,  
*www.usno.navy.mil/USNO/astrometry/optical – IR – prod/wds/WDS*
- McAlister, H. A. 1992, Complementary Approaches to Double and Multiple Star  
Research, IAU Colloquium No. 135, edited by H. A. McAlister and W. I. Hartkopf  
(Astronomical Society of the Pacific, San Francisco), p. 527

- McAlister, H. A., Hartkopf, W. I., Hutter, D. J. et al. 1987, AJ, 92, 183
- McAlister, H. A., Mason, B. D., Hartkopf, W. I. et al. 1993, AJ, 106, 1639
- Morel, P., Morel, Ch., Provost, J. et al. 2000, A&A, 354, 636
- Mozurkewich, D. 1994, Proc. SPIE, 2200, 76
- Mozurkewich, D. 2000, in, Principles of Long Baseline Stellar Interferometry, ed. P. R. Lawson (Pasadena: JPL), 231
- Mozurkewich, D. 2005, Internal NPOI Technical Report
- Mozurkewich, D., Johnston, K. J., Simon, R. S. et al. 1991, AJ, 101, 2207
- Mozurkewich, D., Armstrong, J. T., Hindsley, R.B. et al. 2003, AJ, 126, 2502
- Muterspaugh, M. W., Hartkopf, W. I., Lane, B. F. et al. 2010a, AJ, 140, 1623
- Muterspaugh, M. W., Lane, B. F., Kulkarni, S. R. et al. 2010b, AJ, 140, 1657
- Neugebauer, G., Habing, H. J., van Duinen, R. et al. 1984, ApJ, 278, L1
- Neuhäuser, R., Mugrauer, M., Fukagawa, M. et al. 2007, A&A, 462, 777
- Nordgren, T. E., Germain, M. E., Benson, J. A. et al. 1999, AJ, 118, 3032
- Nordgren, T. E., Sudol, J. J., & Mozurkewich, D. 2001, AJ, 122, 2707
- Ochsenbein, F., Bauer, P., & Mareout, J. 2000, A&AS, 143, 23
- Pan, X., Shao, M., Colavita, M. M. et al. 1992, ApJ, 384, 624
- Parsons, S. B., & Ake, T. B. 1998, ApJS, 119, 83
- Parsons, S. B., Franz, O. G., & Wasserman, L. H. 2005, AJ, 129, 1700

- Patience, J., De Rosa, R., Prato, L. et al. 2012, APS, Annual Meeting of the Four Corners  
Section of the APS, abstract #E2.002
- Perryman, M. A. C., Lindegren, L., Kovalevsky, J. et al. 1997, A&A, 323, L49
- Pourbaix, D., Tokovinnin, A. A., Batten, A. H. et al. 2004, A&A, 424, 727
- Raghavan, D., McAlister, H. A., Henry, T. J. et al. 2010, ApJS, 190, 1
- Raghavan, D., Farrington, C. D., ten Brummelaar, T. A. et al. 2012, ApJ, 745, 24
- Ramírez, I., & Meléndez, J. 2005, ApJ, 626, 446
- Ren, S., & Fu, Y. 2013, AJ, 145, 81
- Richichi, A., Percheron, I., & Khristoforova, M. 2005, A&A, 431, 773
- Riddle, R. L. et al. 2015, ApJ, 799, 4
- Scardia, M., Prieur, J.-L., Sala, M. et al. 2005, MNRAS, 357, 1255
- Scardia, M., Prieur, J.-L., Pansecchi, L. et al. 2006, MNRAS, 367, 1170
- Scardia, M., Argyle, R. W., Prieur, J.-L. et al. 2007, Astron. Nach., 328, 146
- Schmidt-Kaler, Th. 1982, Landolt-Börnstein: Numerical Data and Functional Relationships  
in Science and Technology, edited by K. Schaifers and H. H. Voigt (Springer-Verlag,  
Berlin), VI/2b
- Schmitt, H. R., Pauls, T. A., Tycner, C. et al. 2009, ApJ, 691, 984
- Schoeller, M., Balega, I. I., Balega, Y. Y. et al. 1998, SvAL, 24, 283
- Shao, M. & Staelin, D. H. 1977, J. Opt. Soc. Am., 67, 81
- Shao, M., Colavita, M. M., Hines, B. E. et al. 1988, A&A, 193, 357

- Skrutskie, M. F., Cutri, R. M., Stiening, R. et al. 2006, AJ, 131, 1163
- Söderhjelm, S. 1999, A&A, 341, 121
- Straižys, V. 1992, Multicolor Stellar Photometry (Tucson: Pachart Publishing House)
- Thompson, A. R., Moran, J. M., & Swenson, G. W., Jr. 2001, Interferometry and Synthesis in Radio Astronomy, 2nd Ed. (New York: Wiley)
- Tokovinin, A. A. 1997, A&AS, 124, 75, [www.ctio.noao.edu/atokovinin/stars/intro.html](http://www.ctio.noao.edu/atokovinin/stars/intro.html)
- Traub, W. A. 2000, in Principles of Long Baseline Stellar Interferometry, ed. P. R. Lawson (Pasadena: JPL), 31
- Turnbull, M. C. 2004, Ph.D. dissertation, Univ. Arizona, Pub. Number: AAT 3145140.DAI-B 65/09, p. 4624
- Tycner, C., Hutter, D. J., & Zavala, R. T. 2010, Proc. SPIE, 7734, 773439-1
- van Belle, G. T., van Belle, G., Creech-Eakman, M. J. et al. 2008, ApJS, 176, 276
- van Belle, G., T., & von Braun, K. 2009, ApJ, 694, 1085
- Van Hamme, W. 1993, AJ, 106, 2096
- van Leeuwen, F. 2007, A&A, 474, 653
- Wall, J. V. 1996, QJRAS, 37, 519
- Wenger, M., Ochsenbein, F., Egert, D. et al. 2000, A&AS, 143, 9
- White, N. M., & Feierman, B. H. 1987, AJ, 94, 751
- Zavala, R. T., Adelman, S. J., Hummel, C. A. et al. 2007 ApJ, 655, 1046
- Zavala, R. T., Hummel, C. A., Boboltz, D. A. et al. 2010 ApJ, 715, L44



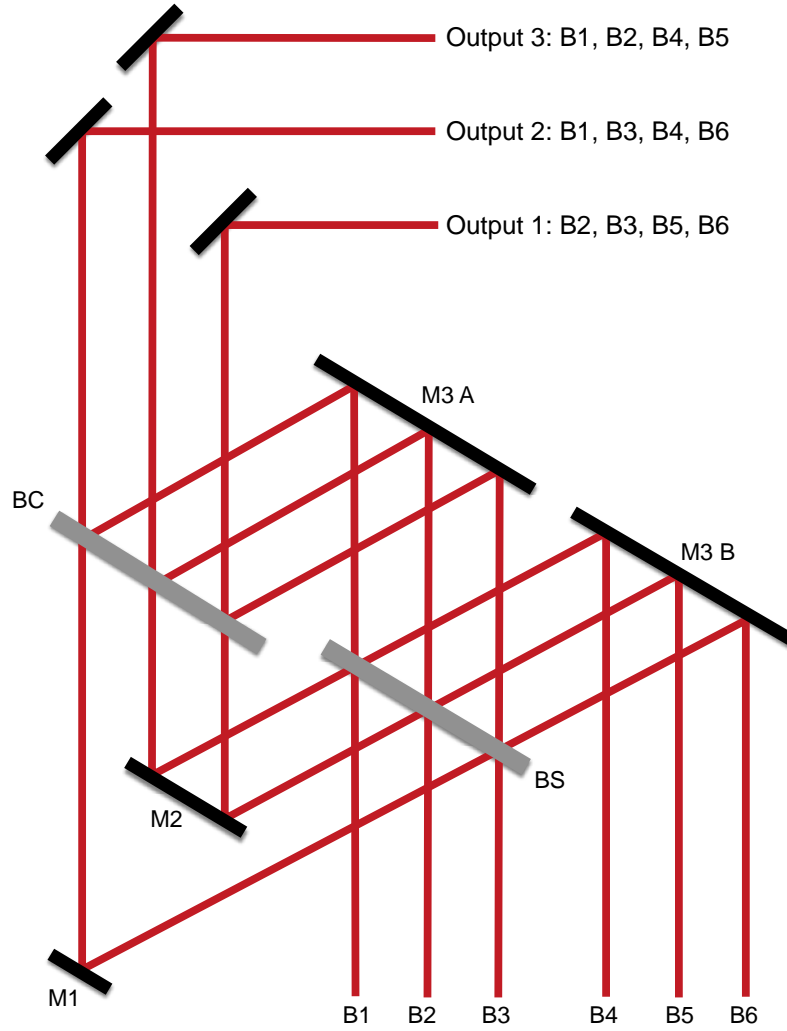


Fig. 1.— A schematic of the NPOI beam combiner. B1 through B6 are the incoming beams, BS and BC are beam splitters. Outputs 1 and 3, and the corresponding spectrometers, were used for all of the reported observations. The three complementary output beams from the other side of BC, which are discarded, are not shown.



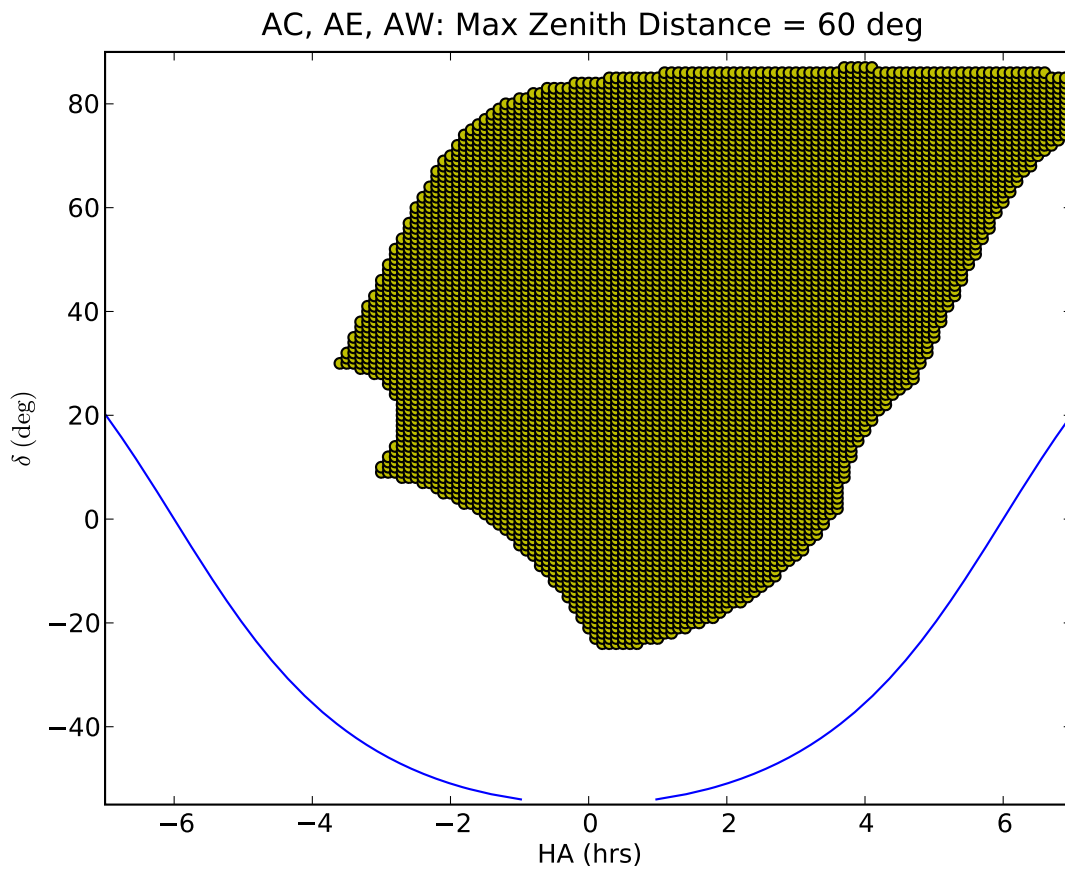


Fig. 2.— Sky coverage plot for the NPOI bright star survey observations utilizing the Center (AC), East (AE), and West (AW) stations of the astrometric array. The blue, solid curve represents the horizon, and the crosshatched area represents the observable sky.

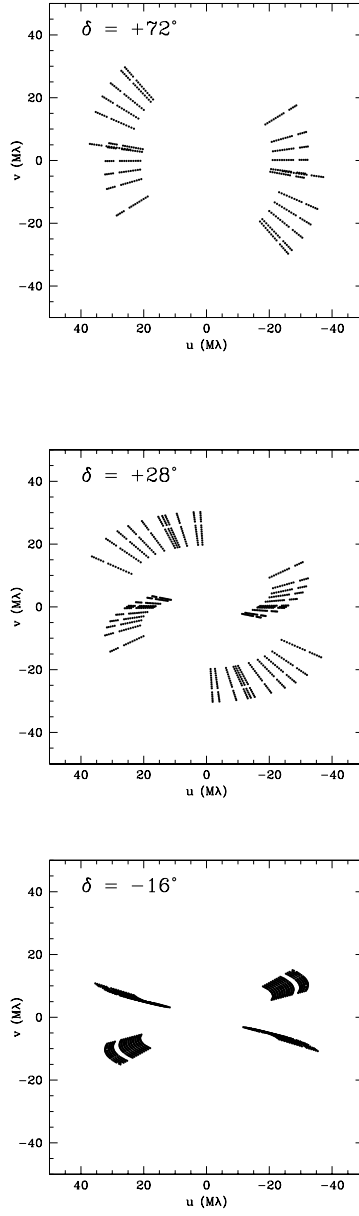


Fig. 3.— Example  $uv$  coverage plots for the NPOI bright star survey observations on the AC-AE and AC-AW baselines at three different declinations. The declinations shown are for the northernmost ( $\chi$  Dra), a midrange ( $\beta$  Gem), and southernmost ( $\eta$  Crv) stars from Table 1. The  $uv$  points represent actual interferometric observations of these stars. The  $u$  and  $v$  spatial frequency axes are in mega-wavelengths. Each baseline produces data from 16 spectral/spatial channels and thus results in a radial ray in the  $uv$ -diagram for each observation.

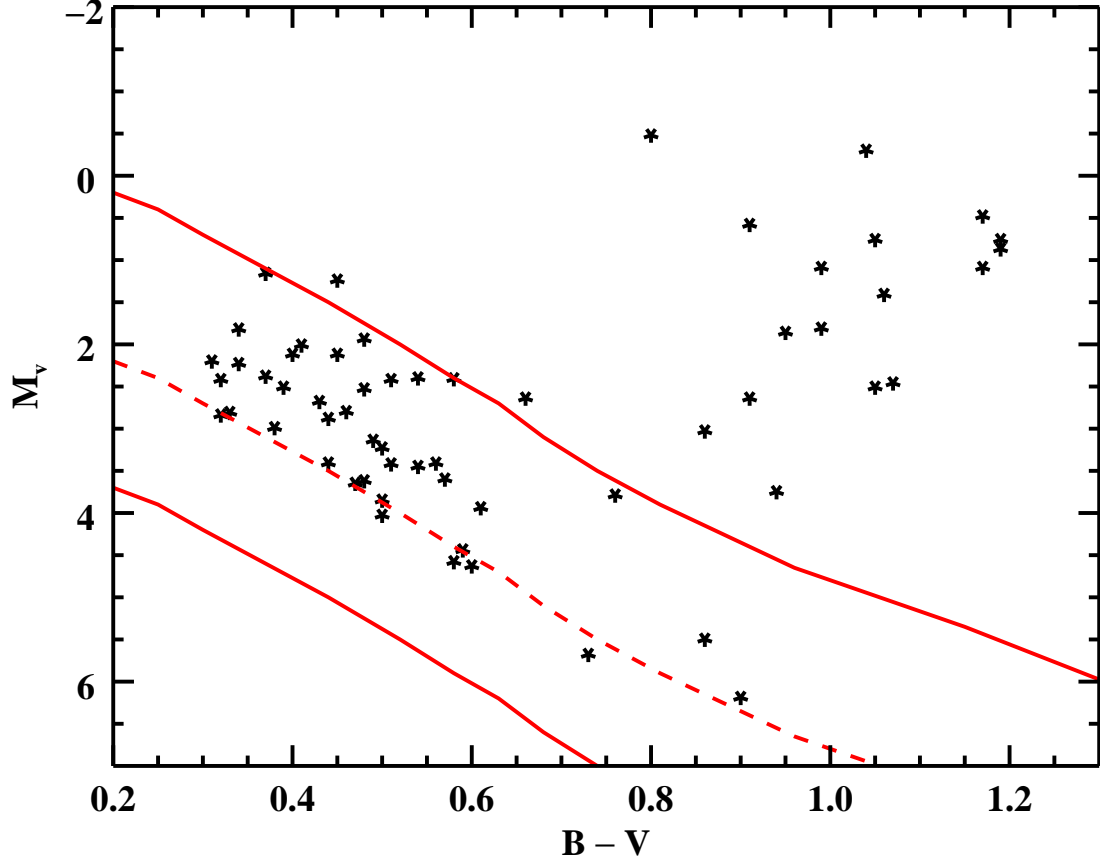


Fig. 4.— Color-Magnitude diagram of the stars in the program list (§ 3). The dashed red line is the Main Sequence (Schmidt-Kaler 1982), while the solid red lines at -2 and +1.5 magnitudes with respect to this curve represent nominal limits for Main Sequence stars for the purposes of the adopted program star list.

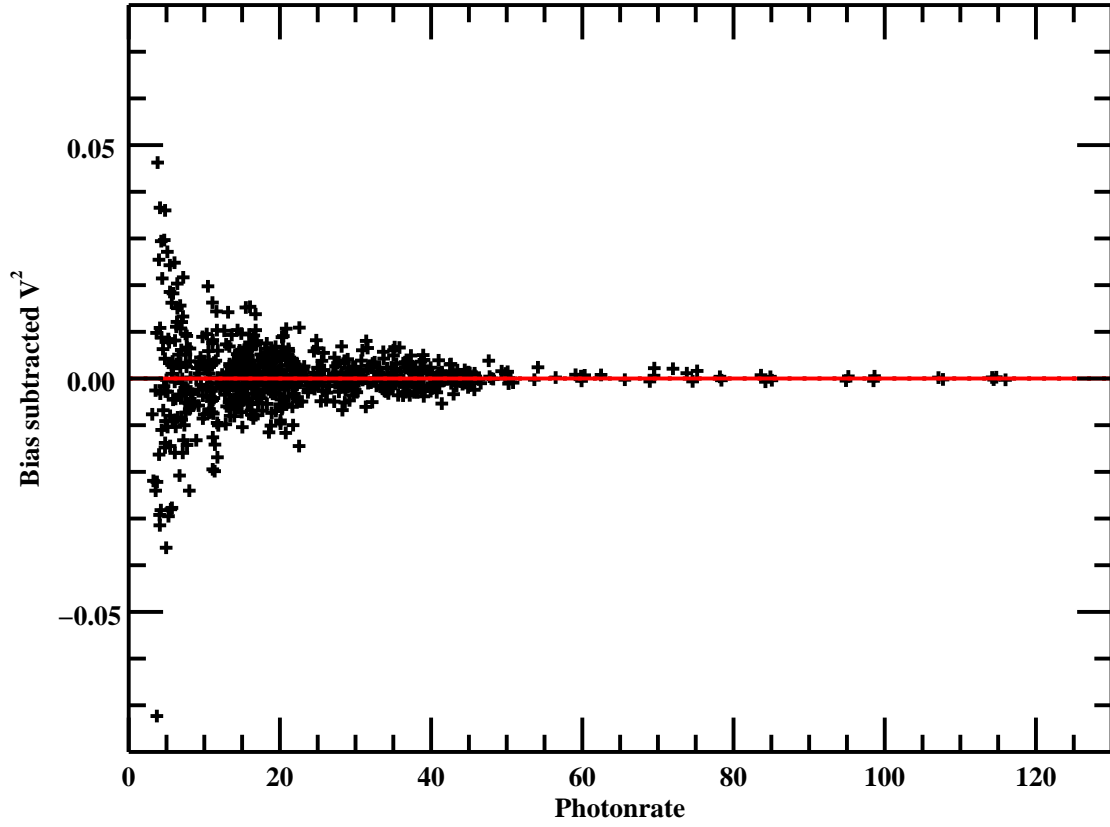


Fig. 5.— The incoherent  $V^2$  *vs* scan averaged photon rate as measured after the bias subtraction has been performed for the NPOI spectrometer 3, for observations made on 2004 May 10 UT.

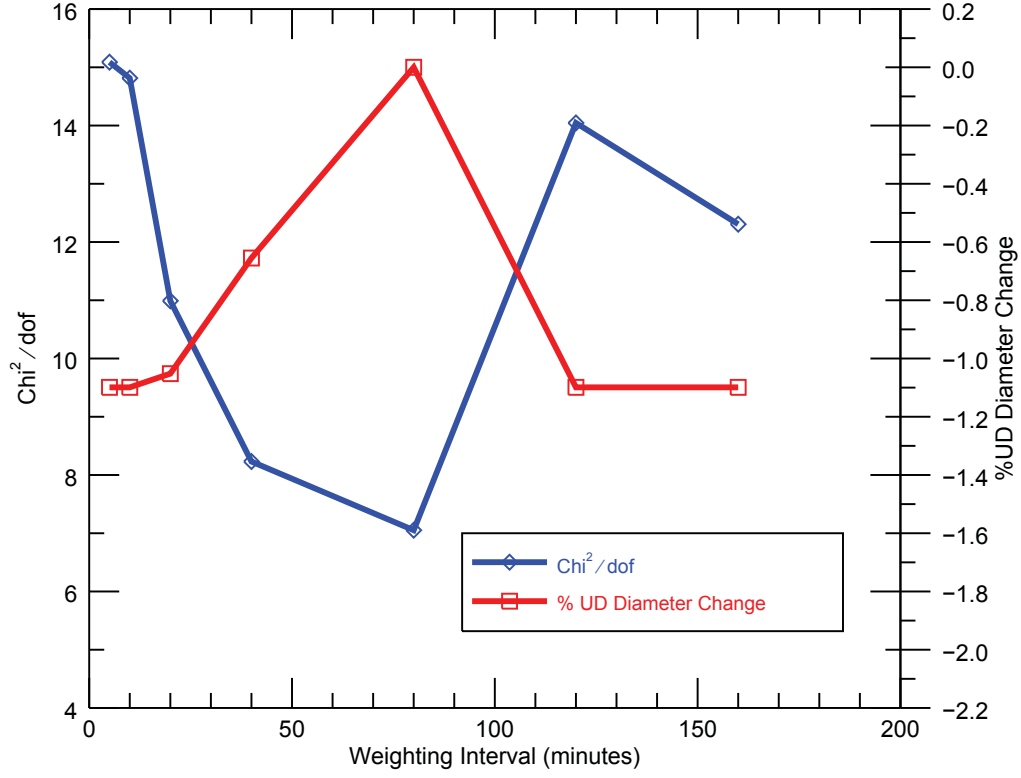


Fig. 6.— The goodness of fit of the diameter model (blue curve) and the resulting percentage change in the fitted angular diameter (red curve) are both functions of the time weighting of the calibrator star observations in the calibration of the program star interferometric visibilities. Data plotted are for  $\beta$  Ophiuchi on 2004 May 03 UT.

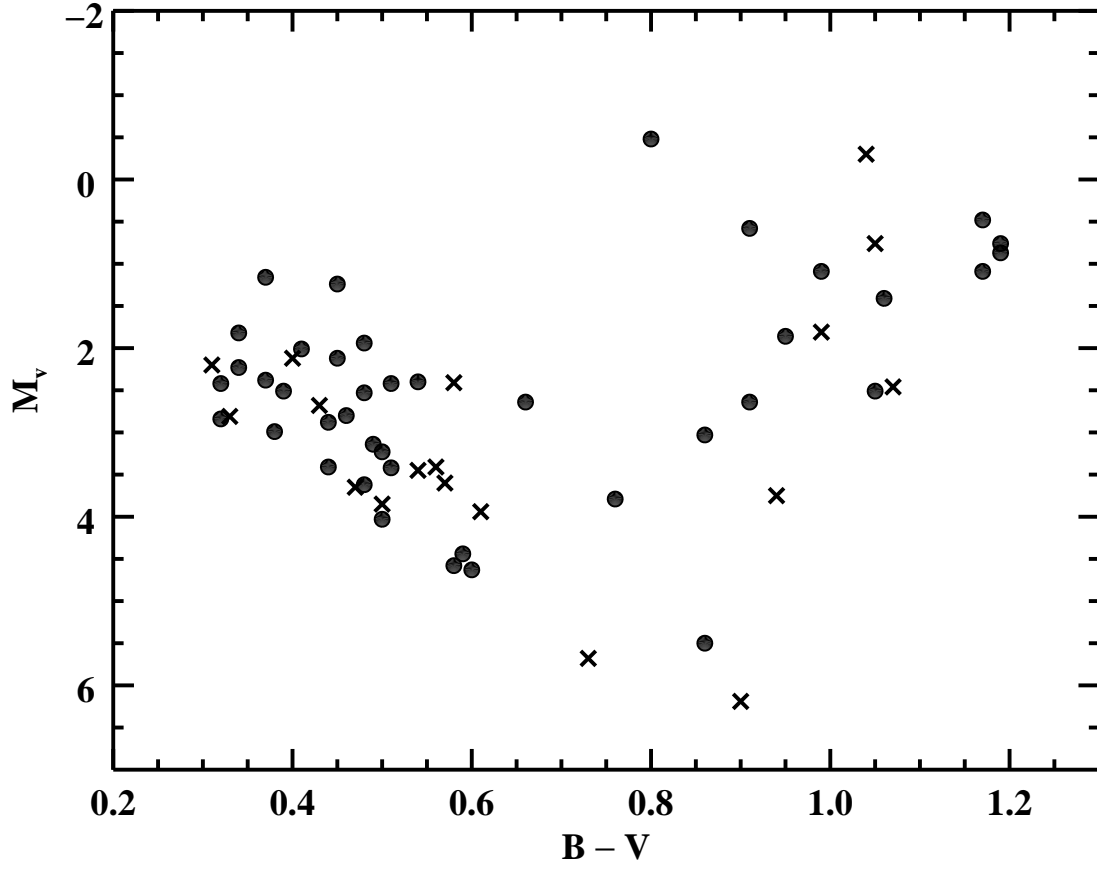


Fig. 7.— Color-Magnitude diagram of the stars in the program star list showing sources observed to date (filled circles) and not yet observed (crosses).

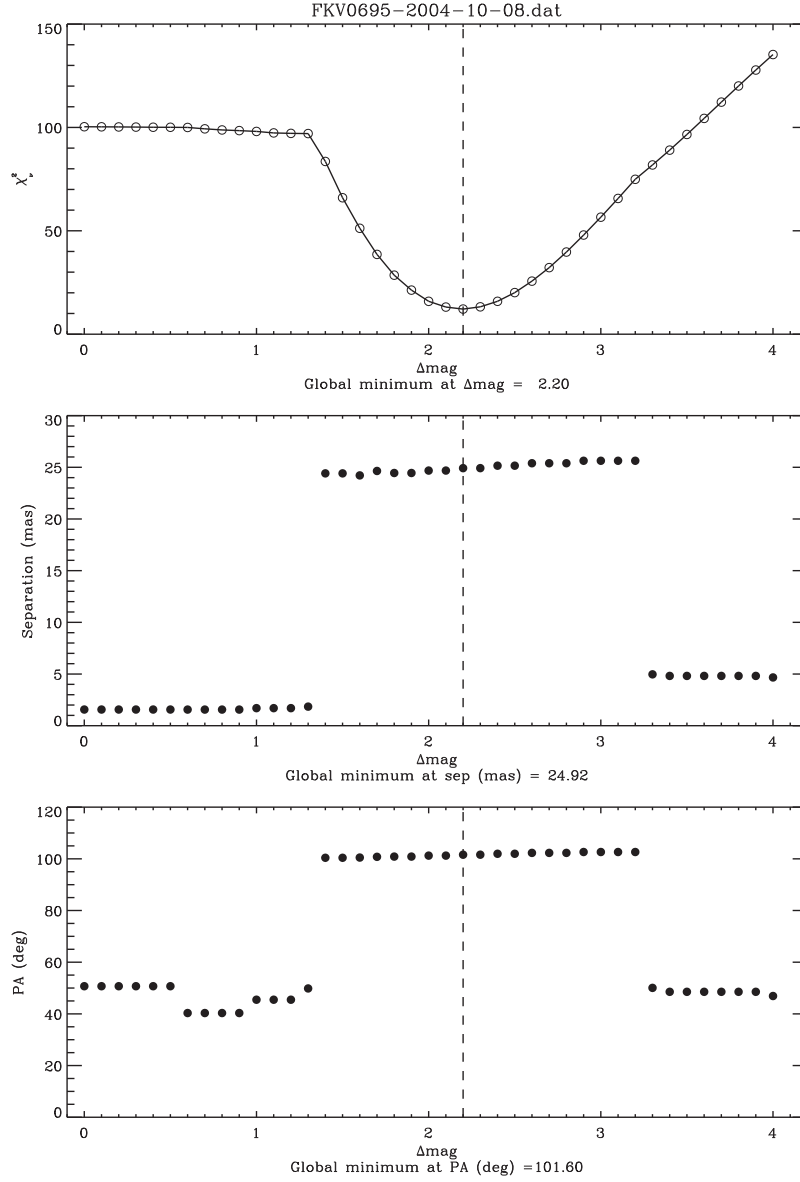


Fig. 8.— Output of the GRIDFIT program for observations of  $\chi$  Dra on 2004 October 8 UT. The top panel shows the minimum value of the reduced  $\chi^2$  for grid searches over separation and position angle at successive, fixed component magnitude differences ( $\Delta m$ ), in 0.1 magnitude increments, over the range 0 to 4 magnitudes. The second and third panels display the corresponding values of component separation and position angle for the best-fit model at each  $\Delta m$  value. The dashed vertical lines correspond to the global  $\chi^2$  minimum.

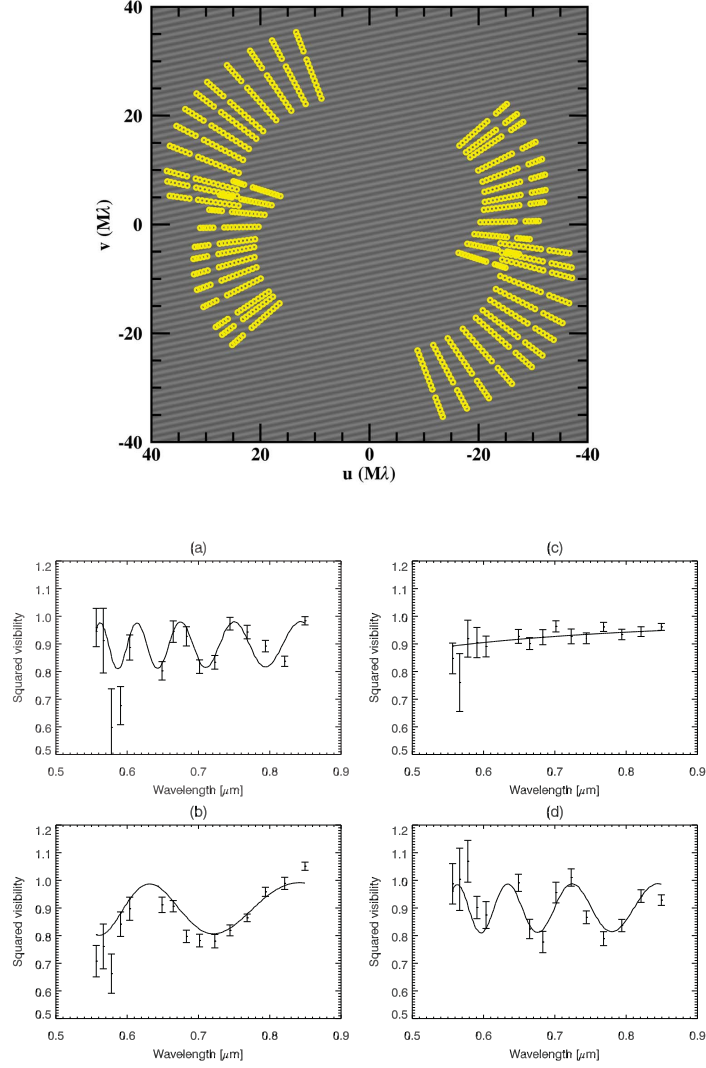


Fig. 9.— Changes in interferometer response with baseline projection: *Upper Panel* :  $uv$  plot for the 12 observations (yellow circles) of 59 Cyg on 2004 July 30 UT on the AC-AE (lower-left, upper right) and AC-AW (upper left, lower right) baselines, superimposed on the Fourier transform of the best-fit binary model for that date (Tables 6 & 11). The time sequence of the observations on each baseline proceeds in clockwise order. *Lower Panel* : Plots *a* through *d* display, for the 2nd, 5th, 7th, and 11th observation on the AC-AE baseline, respectively, the calibrated  $V^2$  vs wavelength with the best fit model for that date ( $\rho = 173.65$  mas,  $\theta = 11^\circ 62$ ,  $\Delta m_{700} = 2.83$ ) overplotted at the time of each observation (solid lines).



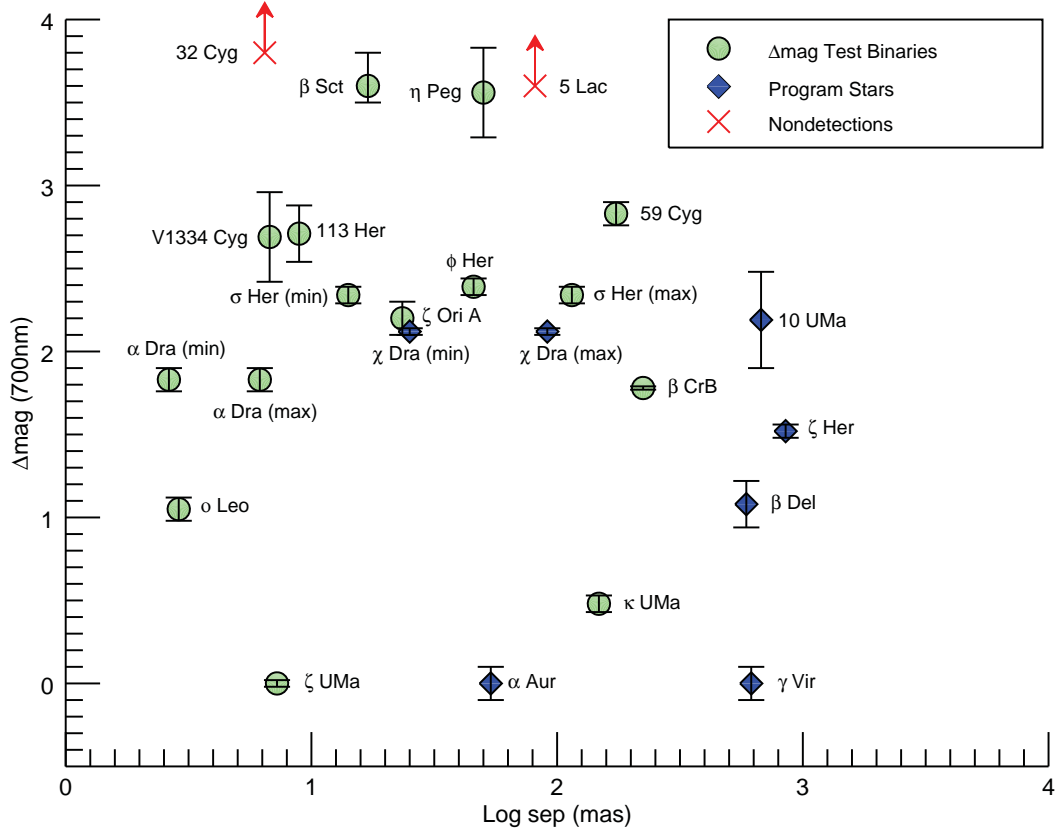


Fig. 10.— Primary-secondary magnitude difference  $\langle \Delta m_{700} \rangle$  plotted against the log of the mean component separation in milliarcseconds for binaries observed by the NPOI.  $\Delta m$  test binaries (Tables 6, 9 & 11) are shown as filled circles, program stars (Tables 12 & 13) are shown as filled diamonds, and estimated lower limits for nondetections (Table 11, with  $\Delta m_{550}$  values plotted) are shown as crosses with arrows.

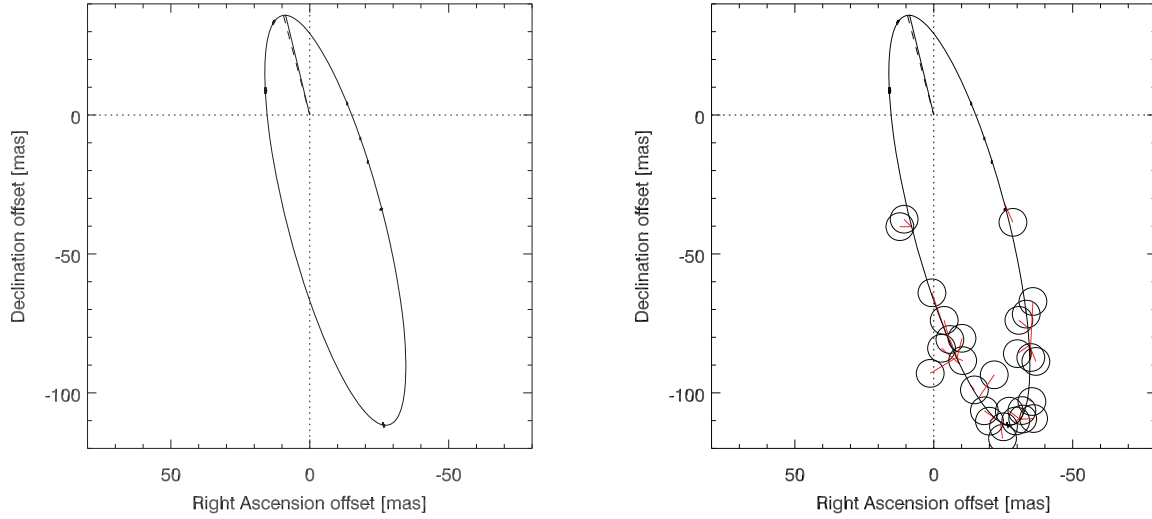


Fig. 11.— Orbit of  $\sigma$  Her AB: *Left Panel* : Plot of the fitted relative positions at each of the 16 epochs of observation (Table 9), with error ellipses plotted to scale. The apparent orbit corresponding to the best-fit orbital solution to these points (Table 10) is overplotted. *Right Panel* : Same as left panel, but with archival measurements from the INT4 overplotted. Red line segments indicate the offset of each INT4 measurement with respect to the position predicted by the new NPOI orbit at the epoch of each observation. Assumed error circles of radius 5 mas are also plotted for INT4 entries that lack error estimates.

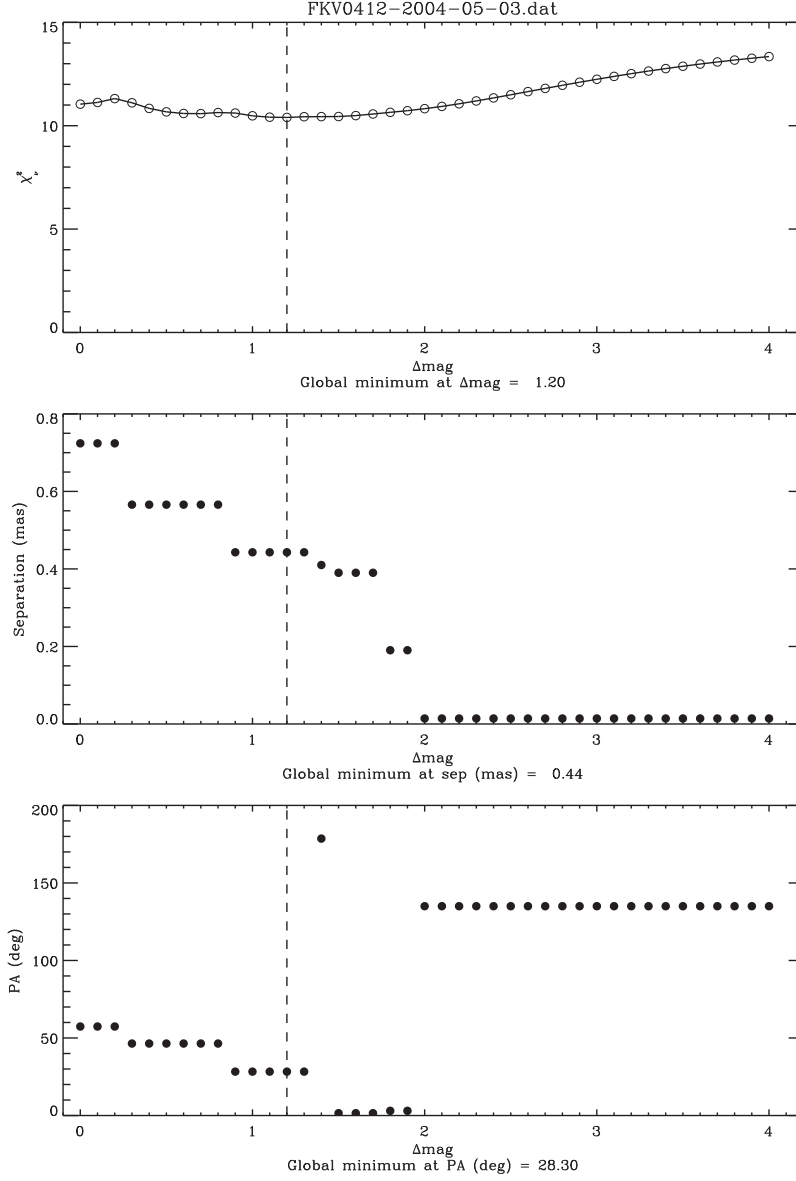


Fig. 12.— Output of the GRIDFIT program for observations of 46 LMi on 2004 May 3 UT. The format of the plot is the same as in Figure 8. The top panel illustrates an example of a GRIDFIT search resulting in no statistically significant  $\chi^2_\nu(\text{min})$  for grid searches over separation and position angle over the range 0 to 4 magnitudes.

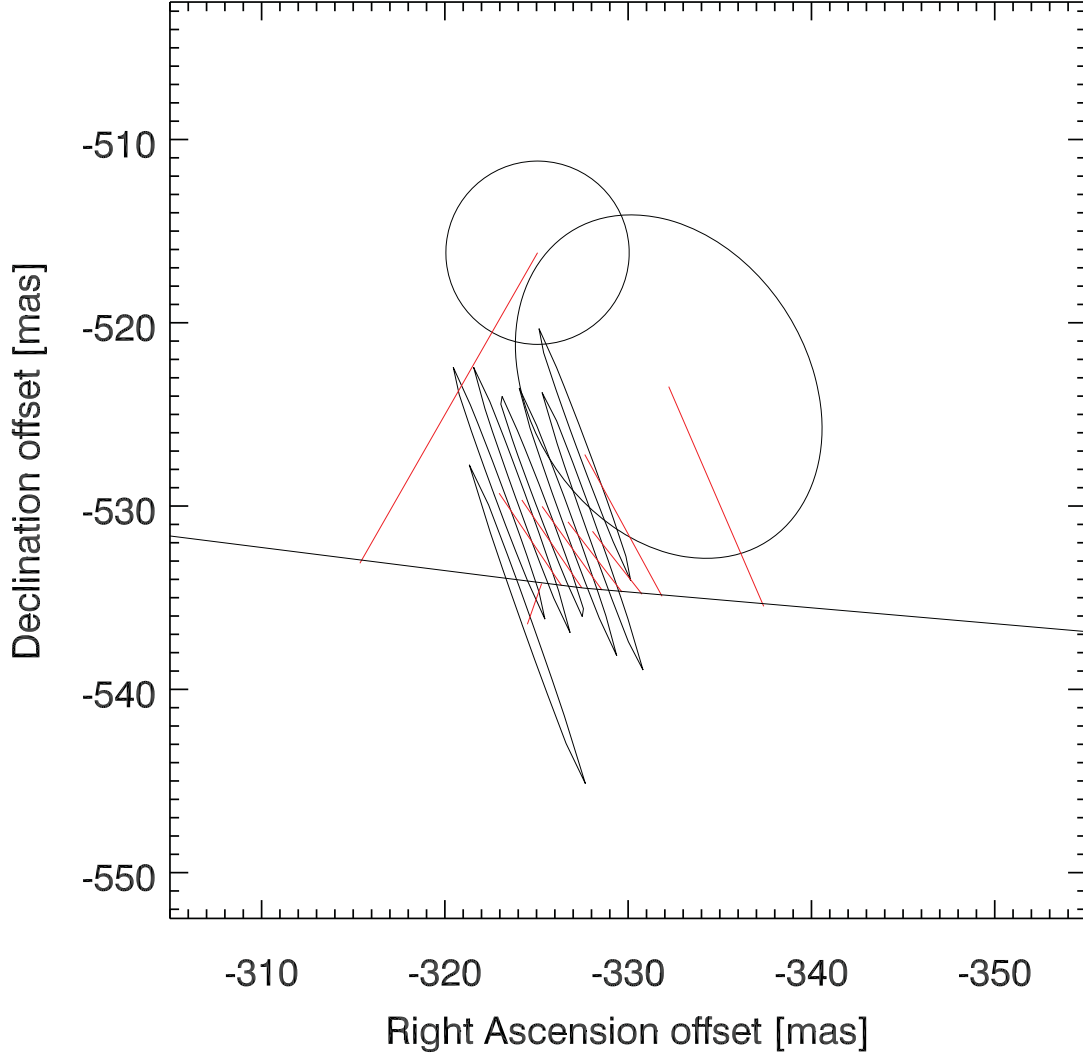


Fig. 13.— Orbit of  $\gamma$  Vir AB: Plot of the fitted relative positions at each of the 7 epochs of NPOI observation (Table 12; average position:  $\rho = 622.64$  mas,  $\theta = 211^\circ 53$ ), with (narrow) error ellipses plotted to scale. A small section of the apparent orbit corresponding to the orbital elements of Scardia et al. (2007) is overplotted in black. Archival measurements from the INT4 (Hartkopf et al. 2008; Scardia et al. 2005) are also overplotted, with error ellipses. Red line segments indicate the offset of each NPOI and INT4 measurement with respect to the position predicted by the Scardia et al. (2007) orbit at the epoch of each observation.

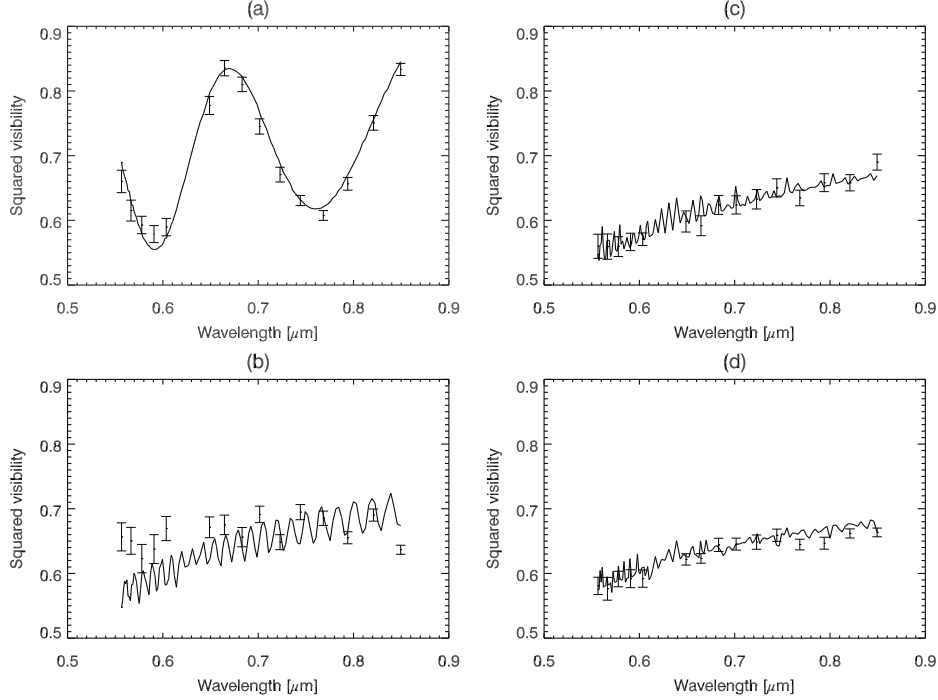


Fig. 14.— Observations and modeling of the very wide binary system  $\zeta$  Her: Using data obtained on 2004 May 13 UT, plots *a* through *d* display, for the 1st, 2nd, 4th, and 6th observation on the AC-AE baseline, respectively, the calibrated  $V^2$  vs wavelength with the best fit model for that date ( $\rho = 859.06$  mas,  $\theta = 235^\circ 98$ ,  $\Delta m_{700} = 1.52$ ; Tables 12 & 13) overplotted (solid lines). The differences in the oscillation period with wavelength between the plots are analogous to those seen in Figure 9, but are more extreme due to the much wider component separation of  $\zeta$  Her. The differences in the amplitude of the  $V^2$  oscillations between the plots are primarily due to the varying effects of bandwidth smearing as a function of baseline projection.

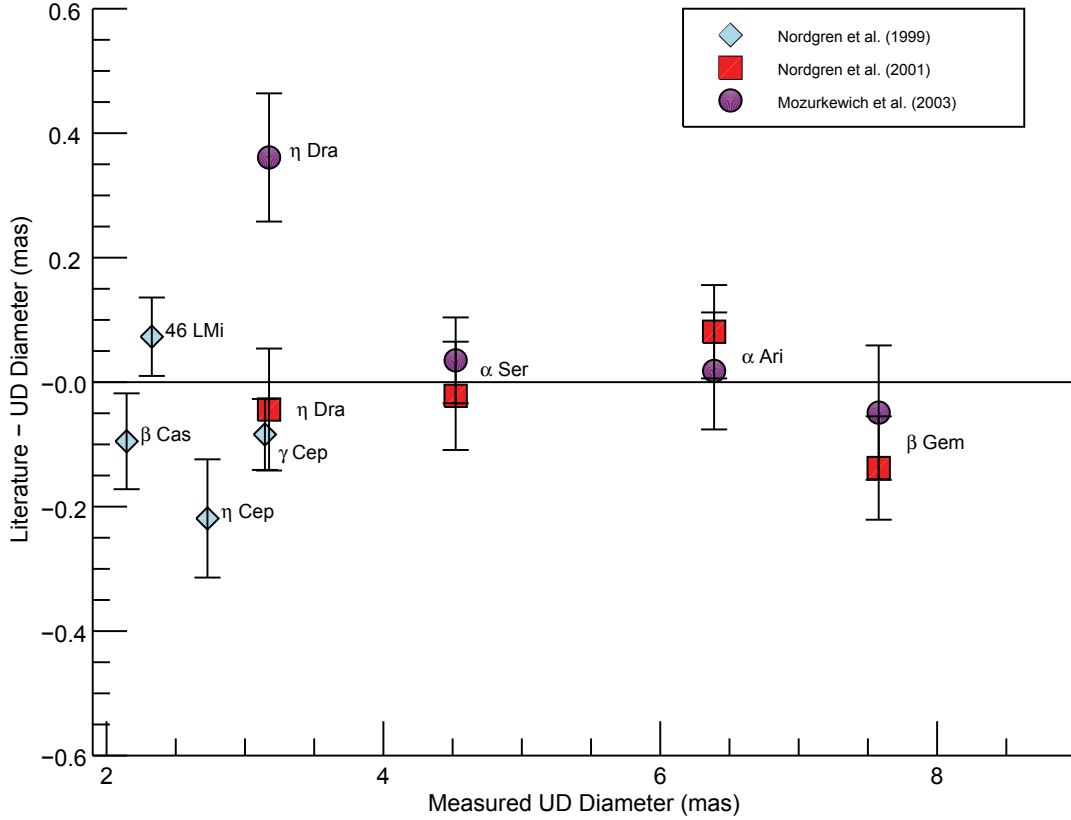


Fig. 15.— *Direct Measures*: Comparison of measured uniform disk angular diameters from this study (“UD Diameter”; Table 14, Col. 3) with previous measurements made using the NPOI (Nordgren et al. 1999, 2001) and the Mark III interferometer (Mozurkewich et al. 2003). The difference (literature - UD Diameter) in milliarcseconds is plotted against the measured UD Diameter. Plotted errors are the quadratic combination of the Table 14 and literature values.

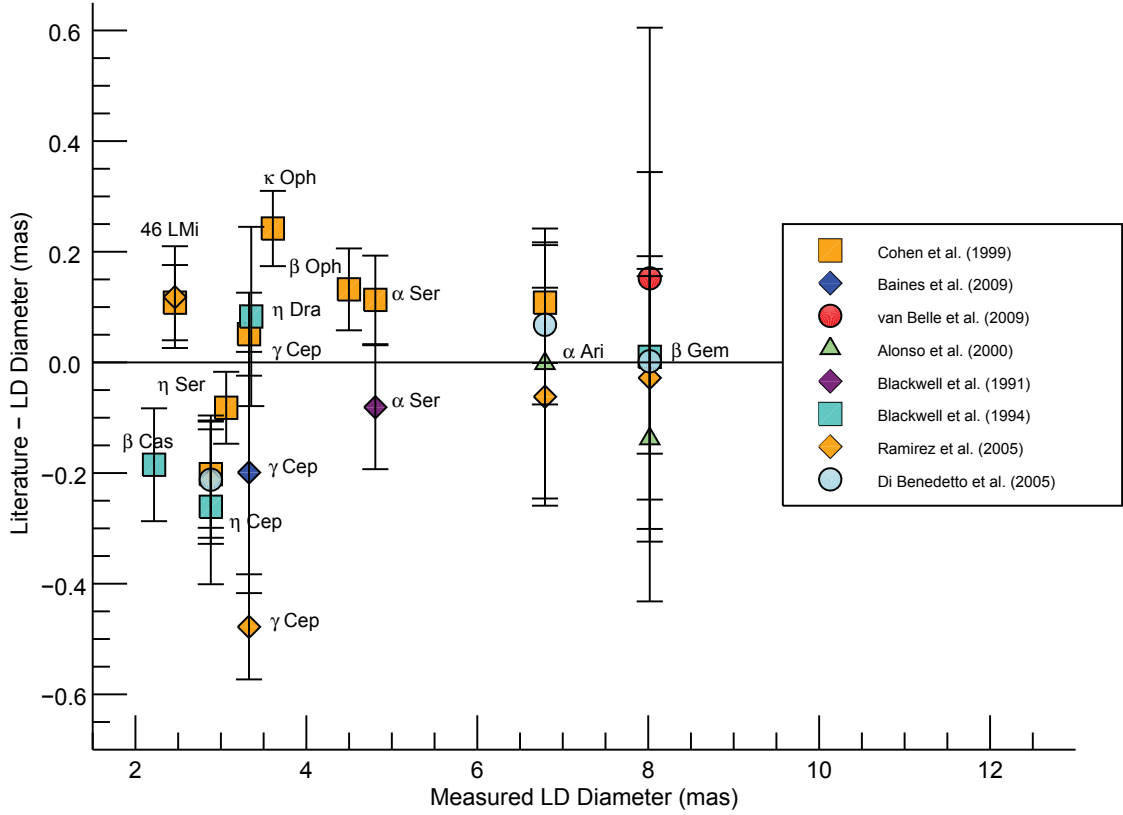


Fig. 16.— *Indirect Measures*: Comparison of limb darkened angular diameters from this study (“LD Diameter”; Table 14, Col. 6) with *estimates* derived from radiometric methods (Cohen et al. 1999), SED fits (Baines et al. 2009; van Belle & von Braun 2009), the infrared flux method (Alonso et al. 2000; Blackwell et al. 1991; Blackwell & Lynas-Gray 1994; Ramírez & Meléndez 2005), and the infrared surface brightness method (Di Benedetto 2005). The difference (literature - LD Diameter) in milliarcseconds is plotted against the measured LD Diameter. The plotted errors were calculated as per Figure 15.

Table 1. Program Stars

HIP	HR	FK5	Other Name	$m_V$ (mag)	$B-V$ (mag)	$\pi$ (mas)	Distance (pc)	$M_V$ (mag)	Spectral Type
(1)	(2)	(3)	(4)	(5)	(6)	(7)	(8)	(9)	(10)
746	21	2	$\beta$ Cas	2.27	0.37	59.89	16.70	1.16	F2III-IV
3419	188	22	$\beta$ Cet	2.04	1.04	34.04	29.38	-0.30	G9.5IIICH-1
3821	219	...	$\eta$ Cas	3.45	0.58	167.99	5.95	4.58	F9V+dM0
7513	458	1045	$v$ And	4.10	0.54	74.25	13.47	3.45	F8V
8102	509	59	$\tau$ Cet	3.49	0.73	274.17	3.65	5.68	G8V
8796	544	64	$\alpha$ Tri	3.41	0.48	50.87	19.66	1.94	F6IV
9884	617	74	$\alpha$ Ari	2.01	1.17	49.48	20.21	0.48	K2-IIICa-1
12777	799	93	$\theta$ Per	4.10	0.50	89.03	11.23	3.85	F8V
12828	813	98	$\mu$ Cet	4.26	0.31	38.71	25.83	2.20	F0IV
14632	937	112	$\iota$ Per	4.05	0.61	94.93	10.53	3.94	G0V
16537	1084	127	$\epsilon$ Eri	3.73	0.90	310.75	3.22	6.19	K2V
16852	1101	1101	10 Tau	4.29	0.57	72.89	13.72	3.60	F9IV-V
17378	1136	135	$\delta$ Eri	3.53	0.94	110.58	9.04	3.75	K0+IV
22449	1543	1134	1 Ori	3.18	0.47	124.60	8.03	3.65	F6V
24608	1708	193	$\alpha$ Aur	0.08	0.80	77.29	12.94	-0.48	G5IIIe+G0III
28103	2085	226	$\eta$ Lep	3.70	0.33	66.47	15.04	2.81	F1III
31592	2429	2510	7 CMa	3.95	1.07	50.41	19.84	2.46	K1III
32362	2484	256	$\xi$ Gem	3.34	0.45	57.02	17.54	2.12	F5III
35550	2777	279	$\delta$ Gem A	3.51	0.34	55.45	18.03	2.23	F2IV
36366	2852	286	$\rho$ Gem	4.17	0.32	54.06	18.50	2.84	F0V
37279	2943	291	$\alpha$ CMi A	0.40	0.43	285.93	3.50	2.68	F5IV-V
37826	2990	295	$\beta$ Gem	1.16	0.99	96.74	10.34	1.09	K0IIIb
44248	3579	339	10 UMa	3.96	0.44	60.86	16.43	2.88	F5V
46733	3757	355	23 UMa	3.65	0.34	43.20	23.15	1.82	F0IV
46853	3775	358	$\theta$ UMa	3.18	0.48	74.15	13.49	2.53	F6IV
53229	4247	412	46 LMi	3.79	1.06	33.40	29.94	1.41	K0+III-IV
55642	4399	...	$\iota$ Leo	3.93	0.41	41.26	24.24	2.01	F4IV
57757	4540	445	$\beta$ Vir	3.59	0.56	91.74	10.90	3.41	F9V
61174	4775	...	$\eta$ Crv	4.29	0.38	54.92	18.21	2.99	F2III-IV



Table 1—Continued

HIP	HR	FK5	Other Name	$m_V$ (mag)	$B-V$ (mag)	$\pi$ (mas)	Distance (pc)	$M_V$ (mag)	Spectral Type
(1)	(2)	(3)	(4)	(5)	(6)	(7)	(8)	(9)	(10)
61317	4785	470	$\beta$ CVn	4.25	0.60	119.46	8.37	4.63	G0V
61941	4825/6	...	$\gamma$ Vir	2.74	0.37	84.53	11.83	2.38	F0V+F0V
64394	4983	492	$\beta$ Com	4.24	0.59	109.23	9.15	4.44	F9.5V
67927	5235	513	$\eta$ Boo	2.68	0.58	88.17	11.34	2.41	G0IV
69701	5338	525	$\iota$ Vir	4.07	0.51	46.74	21.39	2.42	F6III
70497	5404	531	$\theta$ Boo	4.04	0.50	68.63	14.57	3.23	F7V
71957	5487	545	$\mu$ Vir	3.87	0.39	53.54	18.68	2.51	F2III
77070	5854	582	$\alpha$ Ser	2.63	1.19	44.54	22.45	0.87	K2IIIbCN1
78072	5933	591	$\gamma$ Ser	3.85	0.48	89.92	11.12	3.62	F6V
78527	5986	598	$\theta$ Dra	4.00	0.54	47.79	20.92	2.40	F8IV
80331	6132	...	$\eta$ Dra	2.73	0.91	37.18	26.90	0.58	G8-IIIab
81693	6212	...	$\zeta$ Her	2.80	0.66	92.63	10.80	2.64	F9IV+G7V <sup>a</sup>
83000	6299	633	$\kappa$ Oph	3.19	1.17	37.99	26.32	1.09	K2III
86742	6603	665	$\beta$ Oph	2.77	1.19	39.78	25.14	0.76	K2III
86974	6623	667	$\mu$ Her	3.42	0.76	119.05	8.40	3.79	G5IV
88601	6752	...	70 Oph	4.03	0.86	196.62	5.09	5.50	K0V
89937	6927	695	$\chi$ Dra	3.57	0.50	124.11	8.06	4.03	F7V
89962	6869	688	$\eta$ Ser	3.25	0.95	52.81	18.94	1.86	K0III-IV
92043	7061	703	110 Her	4.20	0.46	52.37	19.09	2.80	F6V
95501	7377	730	$\delta$ Aql	3.35	0.32	65.05	15.37	2.42	F3IV
98036	7602	749	$\beta$ Aql	3.72	0.86	72.95	13.71	3.03	G8IV
101769	7882	...	$\beta$ Del	3.62	0.45	33.49	29.86	1.24	F5IV
102422	7957	783	$\eta$ Cep	3.42	0.91	69.73	14.34	2.64	K0IV
102488	7949	780	$\epsilon$ Cyg	2.48	1.05	45.26	22.09	0.76	K0-III
104887	8130	...	$\tau$ Cyg	3.72	0.40	47.80	20.92	2.12	F2IV
109176	8430	831	$\iota$ Peg	3.76	0.44	85.06	11.76	3.41	F5V
112447	8665	...	$\xi$ Peg	4.19	0.49	61.54	16.25	3.14	F6III-IV
116584	8961	890	$\lambda$ And	3.87	0.99	38.74	25.81	1.81	G8III-IV
116727	8974	893	$\gamma$ Cep	3.21	1.05	72.50	13.79	2.51	K1III-IV

Table 1—Continued

HIP	HR	FK5	Other Name	$m_V$ (mag)	$B-V$ (mag)	$\pi$ (mas)	Distance (pc)	$M_V$ (mag)	Spectral Type
(1)	(2)	(3)	(4)	(5)	(6)	(7)	(8)	(9)	(10)
116771	8969	892	$\iota$ Psc	4.12	0.51	72.51	13.79	3.42	F7V

Note. — Cols. (1), (7), and (8): *Hipparcos* number, parallax, and distance from the *Hipparcos Catalogue* (ESA 1997). Cols. (2), (3), and (4): HR number (Hoffleit & Warren 1991), FK5 number (Fricke et al. 1988), and other name (Bayer or Flamsteed designation) from the *SIMBAD* database (Wenger et al. 2000), and references therein. Cols. (5), (6), and (9): Apparent  $m_V$  magnitude,  $B-V$  color index, and absolute  $M_V$  magnitude from TPF-I SWG spreadsheet (Lawson et al. 2007), and references therein. Col. (10): Spectral type from the *The Bright Star Catalogue*, 5th Rev. Ed. (Hoffleit & Warren 1991), unless otherwise noted.

<sup>a</sup>Edwards (1976)

Table 2. Calibrator Stars

HIP	HR	FK5	Other Name	$m_V$ (mag)	$V - K$ (mag)	Spectral Type	Adopted
							$\theta_{LD}$ (mas)
(1)	(2)	(3)	(4)	(5)	(6)	(7)	(8)
2920	153	17	$\zeta$ Cas	3.66	-0.59	B2IV	0.432
8886	542	63	$\epsilon$ Cas	3.38	-0.58	B3III	0.493
9598	580	70	50 Cas	3.98	0.06	A2V	0.565
10670	664	79	$\gamma$ Tri	4.01	0.05	A1Vnn	0.555
23767	1641	185	$\eta$ Aur	3.17	-0.69	B3V	0.507
26311	1903	210	$\epsilon$ Ori	1.70	-0.57	B0Ia	0.876 <sup>a</sup>
33018	2540	261	$\theta$ Gem	3.60	0.44	A3III	0.797 <sup>b</sup>
35350	2763	277	$\lambda$ Gem	3.58	0.04	A3V	0.673
48319	3888	368	$\nu$ UMa	3.80	0.65	F2IV	0.889
49583	3975	379	$\eta$ Leo	3.52	0.22	A0Ib	0.774
49593	3974	2812	21 LMi	4.48	0.48	A7V	0.584
54879	4359	423	$\theta$ Leo	3.34	0.26	A2V	0.861
60965	4757	465	$\delta$ Crv	2.95	-0.05	B9.5V	0.845
61281	4787	472	$\kappa$ Dra	3.87	0.05	B6IIIpe	0.587
63125	4915	485	$\alpha^2$ CVn	2.90	-0.25	A0pSiEuHg	0.765
66249	5107	501	$\zeta$ Vir	3.37	0.15	A3V	0.834 <sup>b</sup>
67301	5191	509	$\eta$ UMa	1.86	-0.41	B3V	1.114
72220	5511	547	109 Vir	3.72	0.07	A0V	0.643
75097	5735	569	$\gamma$ UMi	3.05	0.35	A3II-III	1.039
77233	5867	583	$\beta$ Ser	3.67	0.12	A2IV	0.679
79992	6092	608	$\tau$ Her	3.89	-0.40	B5IV	0.440
84379	6410	641	$\delta$ Her	3.14	0.33	A3IV	0.989
87108	6629	668	$\gamma$ Oph	3.75	0.13	A0Vnp	0.656
92043	7061	703	110 Her	4.19	1.00	F6V	0.974 <sup>b</sup>
92161	7069	1491	111 Her	4.36	0.28	A5III	0.510 <sup>b</sup>
93805	7236	717	$\lambda$ Aql	3.44	-0.12	B9Vn	0.644
95081	7371	3547	$\pi$ Dra	4.59	0.14	A2III s	0.449
96468	7447	...	$\iota$ Aql	4.36	-0.12	B5III	0.422

Table 2—Continued

HIP	HR	FK5	Other Name	$m_V$ (mag)	$V - K$ (mag)	Spectral Type	Adopted
							$\theta_{LD}$ (mas)
(1)	(2)	(3)	(4)	(5)	(6)	(7)	(8)
99655	7740	758	33 Cyg	4.30	0.22	A3IV-Vn	0.541
105138	8146	1559	$\nu$ Cyg	4.43	-0.05	B2Vne	0.420
109410	8454	835	$\pi$ Peg	4.29	1.17	F5III	0.945 <sup>b</sup>
111169	8585	848	$\alpha$ Lac	3.77	-0.08	A1V	0.569
113889	8773	1602	$\beta$ Psc	4.53	-0.22	B6Ve	0.367

Note. — Cols.(1) through (4) per Table 1. Cols. (5) and (7):  $m_V$  magnitude and spectral type from *The Bright Star Catalogue*, 5th Rev. Ed. (Hoffleit & Warren 1991). Col. (6):  $V - K$  color index calculated from Col. (5) value and  $K$  magnitude from the *2MASS* catalog (Cutri et al. 2003). Col. (8): Adopted limb darkened angular diameter (§ 4.1).

<sup>a</sup>Mozurkewich et al. (1991), corrected to limb darkened diameter (§ 4.1).

<sup>b</sup>Blackwell et al. (1991)

Table 3. Program Stars - Observation Log

Object FK5/HR (1)	Other Name (2)	UT Date (yyyy-mm-dd) (3)	No. of Observations (4)	No. of Visibilities (5)	Calibrator FK5/HR (6)
FK5 2	$\beta$ Cas	2004-09-23	9	279	FK5 63
		2004-09-24	8	248	FK5 63
		2004-09-27	9	279	FK5 63
HR 219	$\eta$ Cas	2004-09-30	1	31	FK5 17
		2004-10-01	7	217	FK5 17
		2004-10-05	4	108	FK5 17
FK5 64	$\alpha$ Tri	2004-10-01	7	217	FK5 79
		2004-10-05	6	186	FK5 79
FK5 74	$\alpha$ Ari	2004-10-01	7	217	FK5 79
		2004-10-05	4	124	FK5 79
FK5 193	$\alpha$ Aur	2004-03-20	2	62	FK5 185
		2004-03-21	3	93	FK5 185
		2004-03-23	1	31	FK5 185
FK5 256	$\xi$ Gem	2004-03-10	1	31	FK5 277
		2004-03-11	1	31	FK5 277
		2004-03-12	1	31	FK5 277
		2004-03-14	4	124	FK5 277
		2004-03-15	3	93	FK5 277
		2004-03-17	6	170	FK5 277
		2004-03-18	4	124	FK5 277
		2004-03-19	6	186	FK5 277
FK5 279	$\delta$ Gem A	2004-03-10	1	31	FK5 277
		2004-03-11	1	31	FK5 277

Table 3—Continued

Object FK5/HR (1)	Other Name (2)	UT Date (yyyy-mm-dd) (3)	No. of Observations (4)	No. of Visibilities (5)	Calibrator FK5/HR (6)
		2004-03-12	2	62	FK5 277
		2004-03-14	5	155	FK5 277
		2004-03-15	4	124	FK5 277
		2004-03-17	7	217	FK5 277
		2004-03-18	5	155	FK5 277
		2004-03-19	8	248	FK5 277
FK5 286	$\rho$ Gem	2004-05-04	7	217	FK5 261
		2004-05-05	7	217	FK5 261
		2004-05-06	9	279	FK5 261
FK5 295	$\beta$ Gem	2004-03-10	1	31	FK5 277
		2004-03-11	1	31	FK5 277
		2004-03-12	1	31	FK5 277
		2004-03-14	4	124	FK5 277
		2004-03-15	4	124	FK5 277
		2004-03-17	11	341	FK5 277
		2004-03-18	5	155	FK5 277
		2004-03-19	9	279	FK5 277
FK5 339	10 UMa	2004-03-11	4	124	FK5 368
		2004-03-14	8	248	FK5 368
		2004-03-15	9	279	FK5 368
		2004-05-28	10	310	FK5 368
		2004-05-30	17	527	FK5 368
		2004-05-31	20	620	FK5 368
FK5 355	23 UMa	2004-03-10	2	62	FK5 368
		2004-03-11	3	93	FK5 368

Table 3—Continued

Object FK5/HR (1)	Other Name (2)	UT Date (yyyy-mm-dd) (3)	No. of Observations (4)	No. of Visibilities (5)	Calibrator FK5/HR (6)
		2004-03-12	1	31	FK5 368
		2004-03-14	11	341	FK5 368
		2004-03-15	11	341	FK5 368
FK5 358	$\theta$ UMa	2004-03-10	2	62	FK5 368
		2004-03-11	3	93	FK5 368
		2004-03-12	1	31	FK5 368
		2004-03-14	10	310	FK5 368
		2004-03-15	10	310	FK5 368
FK5 412	46 LMi	2004-05-01	21	636	HR 3974
		2004-05-03	19	589	HR 3974
HR 4399	$\iota$ Leo	2004-03-17	10	310	FK5 423
		2004-03-18	9	279	FK5 423
HR 4775	$\eta$ Crv	2004-05-07	7	217	FK5 465
		2004-05-09	27	837	FK5 465
		2004-05-10	22	682	FK5 465
FK5 470	$\beta$ CVn	2004-05-04	5	155	FK5 485
		2004-05-05	5	155	FK5 485
		2004-05-06	6	186	FK5 485
		2004-05-07	4	124	FK5 485
		2004-05-09	9	279	FK5 485
		2004-05-10	5	80	FK5 485
HR 4826 <sup>a</sup>	$\gamma$ Vir	2004-03-17	5	155	FK5 501
		2004-03-18	5	155	FK5 501

Table 3—Continued

Object FK5/HR (1)	Other Name (2)	UT Date (yyyy-mm-dd) (3)	No. of Observations (4)	No. of Visibilities (5)	Calibrator FK5/HR (6)
		2004-03-19	9	279	FK5 501
		2004-03-20	14	434	FK5 501
		2004-03-21	14	434	FK5 501
		2004-03-22	8	248	FK5 501
		2004-03-23	15	465	FK5 501
FK5 492	$\beta$ Com	2004-05-04	5	155	FK5 485
		2004-05-05	5	155	FK5 485
		2004-05-06	6	186	FK5 485
		2004-05-07	5	155	FK5 485
		2004-05-09	8	248	FK5 485
		2004-05-10	5	155	FK5 485
FK5 525	$\iota$ Vir	2004-05-04	4	124	FK5 547
		2004-05-05	4	124	FK5 547
		2004-05-06	5	155	FK5 547
		2004-05-07	2	62	FK5 547
		2004-05-09	2	62	FK5 547
		2004-05-10	1	31	FK5 547
		2004-05-13	4	124	FK5 547
		2004-05-14	5	155	FK5 547
		2004-05-15	2	62	FK5 547
		2004-05-18	5	155	FK5 547
		2004-05-19	22	682	FK5 547
		2004-05-20	20	620	FK5 547
FK5 531	$\theta$ Boo	2004-05-13	11	341	FK5 509
		2004-05-14	12	372	FK5 509



Table 3—Continued

Object FK5/HR (1)	Other Name (2)	UT Date (yyyy-mm-dd) (3)	No. of Observations (4)	No. of Visibilities (5)	Calibrator FK5/HR (6)
FK5 545	$\mu$ Vir	2004-03-17	3	93	FK5 501
		2004-03-18	4	124	FK5 501
		2004-03-19	6	186	FK5 501
		2004-03-20	7	217	FK5 501
		2004-03-21	6	186	FK5 501
		2004-03-22	8	248	FK5 501
		2004-03-23	7	217	FK5 501
FK5 582	$\alpha$ Ser	2004-03-14	6	186	FK5 583
		2004-03-17	3	93	FK5 583
		2004-03-18	5	155	FK5 583
		2004-03-19	7	217	FK5 583
		2004-03-20	7	187	FK5 583
		2004-03-21	6	186	FK5 583
		2004-03-22	10	280	FK5 583
		2004-03-23	8	248	FK5 583
FK5 591	$\gamma$ Ser	2004-03-14	6	186	FK5 583
		2004-03-17	3	93	FK5 583
		2004-03-18	6	186	FK5 583
		2004-03-19	7	217	FK5 583
		2004-03-20	9	279	FK5 583
		2004-03-21	6	186	FK5 583
		2004-03-22	10	310	FK5 583
		2004-03-23	8	248	FK5 583
FK5 598	$\theta$ Dra	2004-05-13	8	248	FK5 569
		2004-05-14	8	248	FK5 569
		2004-05-15	3	93	FK5 569

Table 3—Continued

Object FK5/HR (1)	Other Name (2)	UT Date (yyyy-mm-dd) (3)	No. of Observations (4)	No. of Visibilities (5)	Calibrator FK5/HR (6)
		2004-05-16	3	93	FK5 569
		2004-05-18	11	341	FK5 569
HR 6132	$\eta$ Dra	2004-05-13	8	248	FK5 569
		2004-05-14	8	218	FK5 569
		2004-05-16	3	93	FK5 569
		2004-05-18	11	326	FK5 569
HR 6212	$\zeta$ Her	2004-05-07	5	155	FK5 641
		2004-05-13	7	217	FK5 641
		2004-05-14	8	248	FK5 641
		2004-05-28	10	310	FK5 641
		2004-05-30	10	295	FK5 641
		2004-05-31	11	341	FK5 641
		2004-06-02	14	434	FK5 641
FK5 633	$\kappa$ Oph	2004-04-30	3	93	FK5 668
		2004-05-01	11	341	FK5 668
		2004-05-03	12	372	FK5 668
		2004-05-04	8	248	FK5 668
		2004-05-05	7	217	FK5 668
		2004-05-06	8	248	FK5 668
FK5 665	$\beta$ Oph	2004-04-30	2	62	FK5 668
		2004-05-01	7	217	FK5 668
		2004-05-03	7	217	FK5 668
		2004-05-04	7	217	FK5 668
		2004-05-05	6	186	FK5 668
		2004-05-06	6	186	FK5 668

Table 3—Continued

Object FK5/HR (1)	Other Name (2)	UT Date (yyyy-mm-dd) (3)	No. of Observations (4)	No. of Visibilities (5)	Calibrator FK5/HR (6)
		2004-05-19	7	217	FK5 668
		2004-05-20	7	217	FK5 668
		2004-05-21	6	186	FK5 668
		2004-05-23	5	155	FK5 668
		2004-05-24	6	186	FK5 668
FK5 667	$\mu$ Her	2004-05-07	5	155	FK5 641
		2004-05-10	3	93	FK5 641
		2004-05-13	7	217	FK5 641
		2004-05-14	8	248	FK5 641
		2004-05-16	3	93	FK5 641
		2004-05-18	10	310	FK5 641
HR 6752	70 Oph	2004-05-01	5	155	FK5 668
		2004-05-03	4	108	FK5 668
		2004-05-19	7	217	FK5 668
		2004-05-20	7	217	FK5 668
		2004-05-21	6	186	FK5 668
		2004-05-23	5	155	FK5 668
		2004-05-24	8	248	FK5 668
FK5 695	$\chi$ Dra	2004-05-21	6	186	HR 7371
		2004-05-25	1	31	HR 7371
		2004-10-08	5	155	HR 7371
FK5 688	$\eta$ Ser	2004-04-30	2	62	FK5 668
		2004-05-01	2	62	FK5 668
		2004-05-03	4	124	FK5 668
		2004-05-19	7	217	FK5 668

Table 3—Continued

Object FK5/HR (1)	Other Name (2)	UT Date (yyyy-mm-dd) (3)	No. of Observations (4)	No. of Visibilities (5)	Calibrator FK5/HR (6)
		2004-05-20	7	217	FK5 668
		2004-05-21	5	155	FK5 668
		2004-05-23	1	31	FK5 668
		2004-05-24	1	31	FK5 668
FK5 703	110 Her	2004-09-23	6	186	FK5 1491
		2004-09-24	4	124	FK5 1491
		2004-09-27	7	217	FK5 1491
		2004-09-28	9	279	FK5 1491
FK5 730	$\delta$ Aql	2004-09-23	6	186	FK5 1491
		2004-09-24	4	124	HR 7447
		2004-09-27	7	202	HR 7447
		2004-09-28	8	248	HR 7447
FK5 749	$\beta$ Aql	2004-09-23	6	186	FK5 1491
		2004-09-24	4	124	HR 7447
		2004-09-27	7	217	HR 7447
		2004-09-28	8	248	HR 7447
HR 7882	$\beta$ Del	2004-09-30	5	155	FK5 835
		2004-10-01	5	139	FK5 835
		2004-10-05	4	124	FK5 835
FK5 783	$\eta$ Cep	2004-09-30	5	155	FK5 835
		2004-10-01	6	186	FK5 835
		2004-10-05	6	186	FK5 835
FK5 831	$\iota$ Peg	2004-09-30	5	155	FK5 835

Table 3—Continued

Object FK5/HR (1)	Other Name (2)	UT Date (yyyy-mm-dd) (3)	No. of Observations (4)	No. of Visibilities (5)	Calibrator FK5/HR (6)
		2004-10-05	5	155	FK5 835
HR 8665	$\xi$ Peg	2004-09-23	5	155	FK5 1602
		2004-09-24	5	155	FK5 1602
		2004-09-27	4	124	FK5 1602
		2004-09-28	11	341	FK5 1602
FK5 893	$\gamma$ Cep	2004-09-23	8	248	FK5 70
		2004-09-24	8	248	FK5 70
		2004-09-27	7	202	FK5 70
		2004-09-28	23	713	FK5 70
FK5 892	$\iota$ Psc	2004-09-23	6	186	FK5 1602
		2004-09-24	6	186	FK5 1602
		2004-09-27	5	155	FK5 1602
		2004-09-28	14	434	FK5 1602

Note. — Cols. (1) and (6): FK5 (Fricke et al. 1988) or HR number (Hoffleit & Warren 1991), as per NPOI scheduling and archiving software. Col. (2): Per Table 1. Col. (3): UT date of NPOI observations. Col. (4): Total number of interferometric observations using AC-AE and AC-AW baselines. Col. (5): Number of  $V^2$  measurements made over available spectral channels, over all recorded beam combiner outputs (less edits).

<sup>a</sup>HR 4826 =  $\gamma$  Vir B, but both A and B components of  $\gamma$  Vir = HIP 61941 observed.

Table 4.  $\Delta m$  Test Binaries

HR	FK5	HIP	WDS	Other Name	$m_V$ Magnitude	Spectral Type
(1)	(2)	(3)	(4)	(5)	(6)	(7)
1948	...	...	J05407–0157Aa,Ab	$\zeta$ Ori A	2.05	O9.5Iab+B1IV <sup>a</sup>
3594	341	44471	J09036+4709AB	$\kappa$ UMa	3.60	A1Vn
3852	365	47508	J09412+0954Aa,Ab	o Leo	3.52	F9III+A5m <sup>b</sup>
5054	497	...	J13239+5456Aa,Ab	$\zeta$ UMa A	2.27	A2V+A2V <sup>c</sup>
5291	521	68756	...	$\alpha$ Dra	3.65	A0III
5747	572	75695	J15278+2906AB	$\beta$ CrB	3.68	F0p
6023	601	79101	J16088+4456AB	$\phi$ Her	4.26	B9VspHgMn+A8V <sup>d</sup>
6168	621	81126	J16341+4226AB	$\sigma$ Her	4.20	B9V
7063	1489	92175	...	$\beta$ Sct	4.22	G4IIa+B9V <sup>e</sup>
7133	3508	92818	J18547+2239Aa,Ab	113 Her	4.59	G4III+A6V
7751	...	99848	J20155+4743A	32 Cyg	3.98	K3Ib+B3V
8047	1551	103632	J20598+4731Aa,Ab	59 Cyg	4.74	B1.5Vnne <sup>f</sup>
8157	...	105269	J21194+3814Aa,Ab <sup>g</sup>	V1334 Cyg	5.83	F1II+B7.0V <sup>h</sup>
8572	3799	111022	J22295+4742AB	5 Lac	4.36	M0II+B8V
8650	857	112158	J22430+3013Aa,Ab	$\eta$ Peg	2.94	G2II-III+A5V <sup>c</sup>

Note. — Cols. (1) and (2): HR (Hoffleit & Warren 1991) and FK5 (Fricke et al. 1988) numbers, as per the NPOI scheduling and archiving software, or from the *SIMBAD* database (Wenger et al. 2000). Cols. (3), (4), and (5): *Hipparcos* number, WDS number, and other name (Bayer or Flamsteed designation), unless otherwise noted, are from the *SIMBAD* database, and references therein. Cols. (6) and (7):  $m_V$  magnitude and spectral type from *The Bright Star Catalogue*, 5th Rev. Ed. (Hoffleit & Warren 1991), unless otherwise noted.

<sup>a</sup>Hummel et al. (2013)

<sup>b</sup>Hummel et al. (2001)

<sup>c</sup>Hummel et al. (1998)

<sup>d</sup>Spectral type of secondary: Zavala et al. (2007)

<sup>e</sup>Parsons et al. (2005)

<sup>f</sup>Lesh (1968)

<sup>g</sup>Mason et al. (2001)

<sup>h</sup>Kovtyukh et al. (2015)

Table 5.  $\Delta m$  Test Binaries - Observation Log

Object FK5/HR (1)	Other Name (2)	UT Date (yyyy-mm-dd) (3)	No. of Observations (4)	No. of Visibilities (5)	Calibrator FK5/HR (6)
HR 1948	$\zeta$ Ori A	2004-03-11	4	124	FK5 210
		2004-03-12	3	93	FK5 210
FK5 341	$\kappa$ UMa	2004-03-11	3	93	FK5 368
		2004-03-14	8	248	FK5 368
		2004-03-15	10	310	FK5 368
FK5 365	$\omicron$ Leo	2004-03-17	10	310	FK5 379
		2004-03-18	5	155	FK5 379
		2004-03-19	4	124	FK5 379
FK5 497	$\zeta$ UMa A	2004-05-21	18	526	FK5 509
		2004-05-23	22	682	FK5 509
		2004-05-24	13	403	FK5 509
FK5 521	$\alpha$ Dra	2013-03-05	14	434	FK5 472
		2013-05-24	7	217	FK5 472
		2013-05-26	7	217	FK5 472
		2013-05-27	27	837	FK5 472
FK5 572	$\beta$ CrB	2004-05-07	5	155	FK5 583
		2004-05-09	6	186	FK5 583
		2004-05-10	4	124	FK5 583
FK5 601	$\phi$ Her	2004-04-30	2	62	FK5 608
		2004-05-01	10	310	FK5 608
		2004-05-03	11	341	FK5 608
		2004-05-04	8	248	FK5 608
		2004-05-05	7	217	FK5 608



Table 5—Continued

Object FK5/HR (1)	Other Name (2)	UT Date (yyyy-mm-dd) (3)	No. of Observations (4)	No. of Visibilities (5)	Calibrator FK5/HR (6)
		2004-05-06	8	248	FK5 608
		2004-07-23	13	403	FK5 608
		2004-07-30	14	434	FK5 608
		2004-07-31	7	217	FK5 608
FK5 621 <sup>a</sup>	$\sigma$ Her	...	...	...	...
FK5 1489	$\beta$ Sct	2004-08-06	4	124	FK5 717
		2004-08-08	6	186	FK5 717
		2004-08-09	8	255	FK5 717
		2004-08-11	8	248	FK5 717
		2004-08-22	5	155	FK5 717
		2004-08-23	8	248	FK5 717
		2004-08-26	5	155	FK5 717
		2004-08-27	8	248	FK5 717
HR 7133	113 Her	2004-07-07 <sup>b</sup>	11	341	FK5 703
		2004-07-08 <sup>b</sup>	8	248	FK5 703
		2004-07-09 <sup>b</sup>	12	372	FK5 703
HR 7751	32 Cyg	2004-07-21	10	310	FK5 758
		2004-07-22	3	93	FK5 758
		2004-07-30	12	372	FK5 758
		2004-08-01	5	140	FK5 758
		2004-08-02	5	155	FK5 758
FK5 1551	59 Cyg	2004-07-21	10	310	FK5 758
		2004-07-22	3	93	FK5 758
		2004-07-30	12	372	FK5 758

Table 5—Continued

Object FK5/HR (1)	Other Name (2)	UT Date (yyyy-mm-dd) (3)	No. of Observations (4)	No. of Visibilities (5)	Calibrator FK5/HR (6)
		2004-08-01	5	155	FK5 758
		2004-08-02	4	124	FK5 758
HR 8157	V1334 Cyg	2009-11-25	15	287	FK5 1559
		2009-12-01	14	260	FK5 1559
		2009-12-18 <sup>c</sup>	6	148	FK5 1559
HR 8572	5 Lac	2004-07-21	8	248	FK5 848
		2004-07-22	2	62	FK5 848
		2004-07-30	11	341	FK5 848
		2004-07-31	12	357	FK5 848
		2004-08-01	6	186	FK5 848
		2004-08-02	3	93	FK5 848
FK5 857	$\eta$ Peg	2004-08-06	7	217	FK5 835
		2004-08-08	15	465	FK5 835
		2004-08-11	14	325	FK5 835
		2004-08-12	2	62	FK5 835
		2004-08-26	18	558	FK5 835
		2004-08-27	22	682	FK5 835

Note. — Cols. (1) and (6): FK5 (Fricke et al. 1988) or HR number (Hoffleit & Warren 1991), as per the NPOI scheduling and archiving software. Col. (2): Per Table 4. Col. (3): UT date of NPOI observations. Col. (4): Total number of interferometric observations using AC-AE and AC-AW baselines, unless otherwise noted. Col. (5): Number of  $V^2$  measurements made over available spectral channels, over all recorded beam combiner outputs (less edits).

<sup>a</sup>See Table 8

<sup>b</sup>AC-AE and AE-AN baselines used. AE-AN baseline = 34.9 m, with AN station at  $330^\circ$  with respect to AE.

<sup>c</sup>AC-AE, AE-AN, AN-AC, and AC-AW baselines used. AN-AC baseline = 22.8 m, with AC station at  $180^\circ$  with respect to AN. Closure data available between the first three baselines.

Table 6.  $\Delta m$  Test Binaries - Binary Model Fits

Object	Other	UT Date		$\rho$	$\theta$	$\sigma_{maj}$	$\sigma_{min}$	$\phi$
FK5/HR	Name	(yyyy-mm-dd)	MJD	(mas)	(deg)	(mas)	(mas)	(deg)
(1)	(2)	(3)	(4)	(5)	(6)	(7)	(8)	(9)
HR 1948 <sup>a</sup>	$\zeta$ Ori A	2004-03-11	53075.32	23.5	332.2	0.49	0.28	178
		2004-03-12	53076.30	23.6	332.5	0.48	0.29	6
FK5 341	$\kappa$ UMa	2004-03-11	53075.32	145.92	306.58	0.58	0.27	130.6
		2004-03-14	53078.31	146.25	306.51	0.54	0.27	145.4
		2004-03-15	53079.33	146.37	306.53	0.48	0.29	137.1
FK5 365	$\sigma$ Leo	2004-03-17	53081.34	3.50	219.72	0.65	0.27	163.4
		2004-03-18	53082.37	2.75	247.22	0.63	0.27	164.7
		2004-03-19	53083.35	2.33	289.01	0.63	0.28	166.1
FK5 497	$\zeta$ UMa A	2004-05-21	53146.35	7.04	353.49	0.53	0.27	159.6
		2004-05-23	53148.35	7.24	21.39	0.58	0.25	158.8
		2004-05-24	53149.34	7.67	33.73	0.59	0.26	145.2
FK5 521 <sup>b</sup>	$\alpha$ Dra	2013-03-05	56356.33	6.23	256.05	0.59	0.26	8.3
		2013-05-24	56436.32	2.61	242.50	0.65	0.25	129.3
		2013-05-26	56438.32	4.11	244.73	0.64	0.25	133.9
		2013-05-27	56439.31	4.50	247.53	0.47	0.26	152.0
FK5 572	$\beta$ CrB	2004-05-07	53132.26	224.72	161.71	0.53	0.29	154.5
		2004-05-09	53134.26	224.77	161.66	0.57	0.31	140.7
		2004-05-10	53135.29	225.37	161.63	0.56	0.32	135.2
FK5 601 <sup>c</sup>	$\phi$ Her	2004-04-30	53125.30	44.16	156.39	0.92	0.44	169.8
		2004-05-01	53126.28	43.77	156.12	0.84	0.46	160.8
		2004-05-03	53128.29	44.11	156.74	0.87	0.45	160.2
		2004-05-04	53129.27	44.19	157.19	0.84	0.47	155.0
		2004-05-05	53130.30	44.28	157.45	0.83	0.46	159.4

Table 6—Continued

Object	Other	UT Date		$\rho$	$\theta$	$\sigma_{maj}$	$\sigma_{min}$	$\phi$
FK5/HR	Name	(yyyy-mm-dd)	MJD	(mas)	(deg)	(mas)	(mas)	(deg)
(1)	(2)	(3)	(4)	(5)	(6)	(7)	(8)	(9)
		2004-05-06	53131.28	44.31	157.65	0.83	0.46	159.4
		2004-07-23	53209.30	48.72	177.01	0.98	0.41	152.4
		2004-07-30	53216.30	48.87	178.74	0.96	0.43	149.5
		2004-07-31	53217.33	49.22	178.79	1.06	0.42	132.5
FK5 621 <sup>d</sup>	$\sigma$ Her	...	...	...	...	...	...	...
FK5 1489	$\beta$ Sct	2004-08-06	53223.30	16.02	162.35	0.70	0.31	0.0
		2004-08-08	53225.31	17.19	163.85	0.70	0.34	0.0
		2004-08-09	53226.29	16.74	161.02	0.72	0.31	0.0
		2004-08-11	53228.30	16.06	159.84	0.71	0.31	0.0
		2004-08-22	53239.31	16.19	161.99	0.73	0.33	0.0
		2004-08-23	53240.29	18.99	163.39	0.70	0.30	0.0
		2004-08-26	53243.29	16.29	156.77	0.68	0.33	0.0
		2004-08-27	53244.30	16.83	162.31	0.71	0.31	0.0
HR 7133	113 Her	2004-07-07	53193.34	8.75	270.16	0.75	0.16	46.7
		2004-07-08	53194.32	9.24	271.06	0.59	0.16	58.7
		2004-07-09	53195.30	8.78	271.39	0.64	0.17	46.8
FK5 1551	59 Cyg	2004-07-21	53207.34	173.41	11.65	0.96	0.53	165.2
		2004-07-22	53208.32	174.98	11.74	1.13	0.51	175.8
		2004-07-30	53216.30	173.65	11.62	0.96	0.56	160.9
		2004-08-01	53218.31	173.40	11.35	1.28	0.56	130.7
		2004-08-02	53219.34	176.57	11.77	1.12	0.53	173.2
HR 8157	V1334 Cyg	2009-11-25	55160.31	7.38	188.99	0.64	0.30	0.0
		2009-12-01	55166.28	6.69	188.51	0.63	0.31	0.0
		2009-12-18	55183.31	6.19	187.46	0.44	0.26	0.0

Table 6—Continued

Object	Other	UT Date		$\rho$	$\theta$	$\sigma_{maj}$	$\sigma_{min}$	$\phi$
FK5/HR	Name	(yyyy-mm-dd)	MJD	(mas)	(deg)	(mas)	(mas)	(deg)
(1)	(2)	(3)	(4)	(5)	(6)	(7)	(8)	(9)
FK5 857	$\eta$ Peg	2004-08-06	53223.35	49.02	193.21	0.56	0.28	176.7
		2004-08-08	53225.35	49.82	193.15	0.55	0.27	165.3
		2004-08-11	53228.34	49.58	193.87	0.52	0.28	170.0
		2004-08-12	53229.32	49.45	194.63	0.59	0.29	5.0
		2004-08-26	53243.37	51.17	195.85	0.49	0.28	159.9
		2004-08-27	53244.35	50.96	196.13	0.47	0.30	160.8

Note. — Col. (1): FK5 (Fricke et al. 1988) or HR number (Hoffleit & Warren 1991), as per NPOI scheduling and archiving software. Col. (2): per Table 4. Col. (3): UT date of NPOI observations. Col. (4): Modified Julian Date (MJD) of NPOI observations. Col. (5): Fitted binary separation. Col. (6): Fitted binary position angle. Col. (7): Semimajor axis of error ellipse. Col. (8): Semiminor axis of error ellipse. Col. (9): Position angle of error ellipse.

<sup>a</sup>Fitted values from Hummel et al. (2013)

<sup>b</sup>Models fitted only to data from AC-AE and AC-AW baselines

<sup>c</sup>Fitted values from Zavala et al. (2007)

<sup>d</sup>See Table 9

Table 7.  $\sigma$  Her - Calibrator Stars

HIP	HR	FK5	Other Name	$m_V$ (mag)	$V - K$ (mag)	Spectral Type	Adopted $\theta_{LD}$
							(mas)
(1)	(2)	(3)	(4)	(5)	(6)	(7)	(8)
48319	3888	368	$\nu$ UMa	3.80	0.65	F2IV	0.89
49583	3975	379	$\eta$ Leo	3.49	0.19	A0Ib	0.75
50372	4033	383	$\lambda$ UMa	3.40	-0.02	A2IV	0.71
54879	4359	423	$\theta$ Leo	3.34	0.26	A2V	0.86
55434	4386	427	$\sigma$ Leo	4.06	-0.08	B9.5Vs	0.49
61281	4787	472	$\kappa$ Dra	3.87	0.05	B6IIIpe	0.59
63125	4915	485	$\alpha^2$ CVn	2.90	-0.24	A0pSiEuHg	0.76
64844	5017	494	20 CVn	4.73	0.72	F3III	0.60
65721	5072	1349	70 Vir	5.00	1.50	G4V	0.98
66249	5107	501	$\zeta$ Vir	3.40	0.18	A3V	0.83
...	5478	...	$\zeta$ Boo	4.50	0.80	A2III	0.70
74785	5685	564	$\beta$ Lib	2.61	-0.30	B8V	0.84
78933	5993	...	o Sco	3.96	-0.05	B1V	0.50
79992	6092	608	$\tau$ Her	3.89	-0.39	B5IV	0.44
80170	6095	609	$\gamma$ Her	3.75	0.81	A9III	0.94
84379	6410	641	$\delta$ Her	3.14	0.33	A3IV	0.99
87108	6629	668	$\gamma$ Oph	3.75	0.13	A0Vnp	0.65
88794	6779	681	o Her	3.83	-0.12	B9.5V	0.53
93747	7235	716	$\zeta$ Aql	2.99	0.11	A0Vn	0.92
93805	7236	717	$\lambda$ Aql	3.44	-0.12	B9Vn	0.64
95853	7420	733	$\iota^2$ Cyg	3.79	0.19	A5Vn	0.67
101421	7852	768	$\epsilon$ Del	4.03	-0.35	B6III	0.42
101589	7871	...	$\zeta$ Del	4.68	0.32	A3V	0.48
105102	8143	1558	$\sigma$ Cyg	4.23	0.55	B9Iab	0.60
111169	8585	848	$\alpha$ Lac	3.77	-0.08	A1V	0.57

Note. — Cols. (1) through (4): per Table 1. Col. (5): From the *Hipparcos Catalogue* (ESA 1997), or the *HD Catalogue* (Cannon & Pickering 1918). Col. (6):  $V - K$  color index calculated from Col. (5) value and  $K$  magnitude from the *2MASS* catalog (Cutri et al. 2003). Col. (7): Spectral type from *The Bright Star Catalogue*, 5th Rev. Ed. (Hoffleit & Warren 1991). Col. (8): Adopted limb darkened angular diameter (§ 4.1).



Table 8.  $\sigma$  Her - Observation Log

UT Date (yyyy-mm-dd) (1)	No. of Observations (2)	No. of Visibilities (3)	Calibrators FK5/HR (4)
1997-05-29 <sup>a</sup>	8	674	FK5 423, FK5 494, FK5 609, FK5 641 FK5 668, FK5 768
1997-05-30 <sup>a</sup>	8	680	FK5 423, FK5 494, FK5 609, FK5 641 FK5 668, FK5 768
1997-05-31 <sup>a</sup>	3	255	FK5 501, FK5 641, FK5 668, FK5 768
1998-03-20 <sup>a</sup>	6	570	FK5 472, FK5 641, FK5 681
1998-05-23 <sup>a</sup>	16	1520	FK5 383, FK5 641, FK5 716, FK5 1558
1998-07-04 <sup>a</sup>	9	852	FK5 485, FK5 641, FK5 717, FK5 733 FK5 848
1998-10-07 <sup>a</sup>	4	380	FK5 641, FK5 733, FK5 848
2001-05-10 <sup>b</sup>	6	491	HR 5993, HR 7871, FK5 379, FK5 427 FK5 501, FK5 564, FK5 608, FK5 716 FK5 768, FK5 1349
2001-05-22 <sup>a</sup>	11	972	FK5 368, FK5 383, FK5 501, FK5 608 FK5 609, FK5 641
2004-05-28	10	310	HR 5478, FK5 368, FK5 608, FK5 641
2004-05-29	13	403	HR 5478, FK5 368, FK5 608, FK5 641
2004-05-30	12	372	HR 5478, FK5 368, FK5 608, FK5 641
2004-05-31	11	341	HR 5478, FK5 368, FK5 608, FK5 641
2004-06-01	1	31	HR 5478, FK5 368, FK5 608, FK5 641
2004-06-02	14	434	HR 5478, FK5 608, FK5 641
2004-06-03	16	496	HR 5478, FK5 608, FK5 641

Note. — Col. (1): UT date of NPOI observations. Col. (2): Total number of interferometric observations on AC-AE and AC-AW baselines, unless otherwise noted. Col. (3): Number of  $V^2$  measurements made over available spectral channels, over all recorded beam combiner outputs (less edits). Col. (4): per Table 7.

<sup>a</sup>AC-AE, AC-AW, and AE-AW baselines used. AE-AW baseline = 37.5 m, with AW sta-

tion at  $266^\circ$  with respect to AE. Data collected using earlier three-station beam combiner, producing 32 spectral channel data, covering 450 nm - 860 nm, on each of three spectrometer outputs (less one defective channel, for a total of 95  $V^2$  measurements per observation).

<sup>b</sup>AC-AE, AC-E02, and AE-E02 baselines used. AC-E02 baseline = 9.6 m, with E02 station at  $39^\circ$  with respect to AC. AE-E02 baseline = 15.9 m, with E02 station at  $314^\circ$  with respect to AE. Data collected using earlier three-station beam combiner, producing 32 spectral channel data, covering 450 nm - 860 nm, on each of three spectrometer outputs (less one defective channel, for a total of 95  $V^2$  measurements per observation).

Table 9.  $\sigma$  Her - Binary Model Fits

UT Date (yyyy-mm-dd)	MJD	$\rho$ (mas)	$\theta$ (deg)	$\sigma_{\text{maj}}$ (mas)	$\sigma_{\text{min}}$ (mas)	$\phi$ (deg)	O- $C_\rho$ (mas)	O- $C_\theta$ (deg)
(1)	(2)	(3)	(4)	(5)	(6)	(7)	(8)	(9)
1997-05-29	50597.36	35.67	21.71	0.45	0.17	171.3	0.45	-0.7
1997-05-30	50598.34	35.57	21.75	0.46	0.17	173.0	0.28	-0.5
1997-05-31	50599.41	36.02	20.85	0.58	0.18	145.9	0.65	-1.3
1998-03-20	50892.47	14.06	286.96	0.60	0.16	7.5	0.02	-2.0
1998-05-23	50956.32	20.07	244.99	0.50	0.16	171.7	0.08	-0.5
1998-07-04	50998.19	26.83	231.05	0.57	0.17	175.1	0.12	-0.6
1998-10-07	51093.11	42.53	217.17	0.60	0.21	124.3	-0.49	-0.1
2001-05-10	52039.41	115.13	193.45	0.56	0.16	165.5	0.40	0.1
2001-05-22	52051.44	114.20	193.32	0.48	0.17	157.7	-0.38	0.1
2004-05-28	53153.39	17.91	62.67	0.52	0.28	146.4	-0.06	-0.4
2004-05-29	53154.42	18.04	62.13	0.51	0.27	150.1	-0.03	-0.4
2004-05-30	53155.40	18.11	61.33	0.53	0.28	143.8	-0.05	-0.7
2004-05-31	53156.38	18.27	61.06	0.51	0.28	152.0	0.01	-0.4
2004-06-01	53157.27	18.35	60.57	0.56	0.26	178.6	-0.02	-0.4
2004-06-02	53158.34	18.46	59.77	0.48	0.28	158.7	-0.00	-0.7
2004-06-03	53159.37	18.54	59.38	0.48	0.28	159.5	-0.03	-0.5

Note. — Col. (1): UT date of NPOI observations. Col. (2): MJD of NPOI observations. Col. (3): Fitted binary separation. Col. (4): Fitted binary position angle. Col. (5): Semimajor axis of error ellipse. Col. (6): Semiminor axis of error ellipse. Col. (7): Position angle of error ellipse. Col.(8): Difference between fitted binary separation and prediction from new NPOI orbit (§ 5.1.1, Figure 11). Col.(9): Difference between fitted binary position angle and prediction from new NPOI orbit (§ 5.1.1, Figure 11).

Table 10.  $\sigma$  Her - Orbital Elements

Parameter	Value
$a$ (mas)	$76.21 \pm 0.27^a$
$e$	$0.5135 \pm 0.0028$
$i$ (deg)	$105.25 \pm 0.51$
$\omega$ (deg)	$184.97 \pm 0.40$
$\Omega$ (deg) (J2000.0)	$14.95 \pm 0.47$
$P$ (days)	$2706.19 \pm 4.89$
$T$ (JD - 244E4)	$10665.4 \pm 2.68$
$\chi_\nu^2$	1.34

<sup>a</sup>Possible systematic error 0.5 mas  
(§ 2.1.4)

Table 11.  $\Delta m$  Test Binaries - Mean Separations and  $\Delta m$  Fits

Object	Other	$\langle \rho \rangle$	$\sigma_\rho$	$\log \langle \rho \rangle$	$\langle \Delta m_{700} \rangle$	$\sigma_{\Delta m}$
FK5/HR	Name	(mas)	(mas)	mas	(mag)	(mag)
(1)	(2)	(3)	(4)	(5)	(6)	(7)
HR 1948	$\zeta$ Ori A	23.55	0.07	1.37	2.20 <sup>a</sup>	0.1 <sup>a</sup>
FK5 341	$\kappa$ UMa	146.18	0.23	2.17	0.48	0.05
FK5 365	$\phi$ Leo	2.86	0.59	0.46	1.05	0.07
FK5 497	$\zeta$ UMa A	7.32	0.32	0.86	0.00 <sup>b</sup>	0.02 <sup>b</sup>
FK5 521	$\alpha$ Dra (min)	2.61	...	0.42	1.83	0.07
	$\alpha$ Dra (max)	6.23	...	0.79	1.83	0.07
FK5 572	$\beta$ CrB	224.95	0.36	2.35	1.78	0.01
FK5 601	$\phi$ Her	45.74	2.41	1.66	2.39 <sup>c</sup>	0.05 <sup>c</sup>
FK5 621	$\sigma$ Her (min)	14.06	...	1.15	2.34	0.05
	$\sigma$ Her (max)	115.13	...	2.06	2.34	0.05
FK5 1489	$\beta$ Sct	16.79	0.98	1.23	3.6	+0.2/-0.1
HR 7133	113 Her	8.92	0.28	0.95	2.71	0.17
HR 7751	32 Cyg	6.46 <sup>d</sup>	...	0.81	3.8 <sup>e</sup>	...
FK5 1551	59 Cyg	174.40	1.38	2.24	2.83	0.07
HR 8157	V1334 Cyg	6.75	0.60	0.83	2.69	0.27
HR 8572	5 Lac	82.0 <sup>f</sup>	...	1.91	3.6 <sup>e</sup>	...
FK5 857	$\eta$ Peg	50.00	0.87	1.70	3.56	0.27

Note. — Col. (1): FK5 (Fricke et al. 1988) or HR number (Hoffleit & Warren 1991), as per NPOI scheduling and archiving software. Col. (2): per Table 4. Col. (3): Mean of nightly separation measurements (except for  $\alpha$  Dra and  $\sigma$  Her). Col. (4): Standard deviation of the nightly separation measurements. Col. (5): log of Col. (3) value. Col. (6): Average of the nightly fitted component magnitude difference at 700 nm, unless otherwise noted. Col. (7): Standard deviation of the nightly  $\Delta m_{700}$  fits.

<sup>a</sup>Values from Hummel et al. (2013)

<sup>b</sup>Values from Hummel et al. (1998)

<sup>c</sup>Values from Zavala et al. (2007)

<sup>d</sup>Not detected; estimated using orbital elements of Ren & Fu (2013) and references therein, see text

<sup>e</sup>Not detected;  $\Delta m_V$  value from Parsons & Ake (1998), see text

<sup>f</sup>Not detected; value from Hartkopf et al. (1997), see text

Table 12. Binary Program Stars - Binary Model Fits

Object	Other	UT Date		$\rho$	$\theta$	$\sigma_{maj}$	$\sigma_{min}$	$\phi$
FK5/HR	Name	(yyyy-mm-dd)	MJD	(mas)	(deg)	(mas)	(mas)	(deg)
(1)	(2)	(3)	(4)	(5)	(6)	(7)	(8)	(9)
FK5 193	$\alpha$ Aur	2004-03-20	53084.28	52.81	244.16	0.85	0.28	0.0
		2004-03-21	53085.31	53.46	241.20	0.88	0.29	0.0
		2004-03-23	53087.27	52.72	235.94	15.57	0.20	0.0
FK5 339	10 UMa	2004-03-11	53075.32	687.37	1.91	0.72	0.28	13.9
		2004-03-14	53078.31	681.96	2.08	0.69	0.29	9.2
		2004-03-15	53079.33	686.93	2.03	0.71	0.28	12.6
		2004-05-28	53153.30	677.94	359.86	3.40	0.16	25.7
		2004-05-30	53155.31	671.77	359.81	1.87	0.32	26.9
		2004-05-31	53156.34	672.57	359.72	1.82	0.29	27.4
HR 4825/6 <sup>a</sup>	$\gamma$ Vir	2004-03-17	53081.30	620.70	211.86	7.44	0.28	20.4
		2004-03-18	53082.28	624.49	211.69	8.23	0.28	19.6
		2004-03-19	53083.30	623.35	211.61	7.78	0.27	20.0
		2004-03-20	53084.28	621.89	211.54	6.75	0.28	20.8
		2004-03-21	53085.31	621.01	211.47	7.71	0.27	19.9
		2004-03-22	53086.29	620.05	211.39	7.38	0.28	20.3
		2004-03-23	53087.27	626.96	211.17	9.52	0.27	19.6
HR 6212	$\zeta$ Her	2004-05-07	53132.26	862.03	236.02	1.94	0.28	14.3
		2004-05-13	53138.32	859.06	235.98	1.27	0.27	17.6
		2004-05-14	53139.30	859.32	235.87	1.20	0.27	19.0
		2004-05-28	53153.26	860.45	235.90	1.59	0.29	10.3
		2004-05-30	53155.31	857.66	236.26	1.82	0.29	8.7
		2004-05-31	53156.29	860.61	235.82	1.57	0.30	9.0
		2004-06-02	53158.30	861.06	235.90	1.33	0.28	15.4
FK5 695	$\chi$ Dra	2004-05-21	53146.30	76.27	196.89	0.64	0.24	0.0

Table 12—Continued

Object	Other	UT Date		$\rho$	$\theta$	$\sigma_{maj}$	$\sigma_{min}$	$\phi$
FK5/HR	Name	(yyyy-mm-dd)	MJD	(mas)	(deg)	(mas)	(mas)	(deg)
(1)	(2)	(3)	(4)	(5)	(6)	(7)	(8)	(9)
		2004-05-25	53150.27	90.47	193.28	0.74	0.25	0.0
		2004-10-08	53286.30	25.14	281.46	0.75	0.25	0.0
HR 7882	$\beta$ Del	2004-09-30	53278.32	582.44	358.20	0.41	0.20	164.7
		2004-10-01	53279.35	582.19	358.22	0.41	0.20	165.7
		2004-10-05	53283.36	582.94	358.28	0.42	0.21	163.5

Note. — Col. (1): FK5 (Fricke et al. 1988) or HR number (Hoffleit & Warren 1991), as per NPOI scheduling and archiving software. Col. (2): per Table 1. Col. (3): UT date of NPOI observations. Col. (4): MJD of NPOI observations. Col. (5): Fitted binary separation. Col. (6): Fitted binary position angle. Col. (7): Semimajor axis of error ellipse. Col. (8): Semiminor axis of error ellipse. Col. (9): Position angle of error ellipse.

<sup>a</sup> $\gamma$  Vir AB fitted.



Table 13. Binary Program Stars - Mean Separations and  $\Delta m$  Fits

Object	Other	$\langle \rho \rangle$	$\sigma_\rho$	$\log \langle \rho \rangle$	$\langle \Delta m_{700} \rangle$	$\sigma_{\Delta m}$
FK5/HR	Name	(mas)	(mas)	mas	(mag)	(mag)
(1)	(2)	(3)	(4)	(5)	(6)	(7)
FK5 193	$\alpha$ Aur	53.66	0.97	1.73	0.00	0.1
FK5 339	10 UMa	679.76	6.83	2.83	2.19	0.29
HR 4825/6 <sup>a</sup>	$\gamma$ Vir	622.64	2.46	2.79	0.00	0.10
HR 6212	$\zeta$ Her	860.03	1.45	2.93	1.52	0.04
FK5 695	$\chi$ Dra (min)	25.14	...	1.40	2.12	0.02
...	$\chi$ Dra (max)	90.47	...	1.96	2.12	0.02
HR 7882	$\beta$ Del	582.52	0.38	2.77	1.08	0.14

Note. — Col. (1): FK5 (Fricke et al. 1988) or HR number (Hoffleit & Warren 1991), as per NPOI scheduling and archiving software. Col. (2): per Table 1. Col. (3): Mean of nightly separation measurements from Table 12 (except for  $\chi$  Dra). Col. (4): Standard deviation of the nightly separation measurements. Col. (5): log of Col. (3) value. Col. (6): Average of the nightly fitted component magnitude difference at 700 nm. Col. (7): Standard deviation of the nightly  $\Delta m_{700}$  fits.

<sup>a</sup> $\gamma$  Vir AB fitted.

Table 14. Single Program Stars - Angular Diameter Fits

Object	Other	$\theta_{UD}$	$\sigma_{UD}$		$\theta_{LD}$	$\sigma_{LD}$
FK5/HR	Name	(mas)	(mas)	LDC	(mas)	(mas)
(1)	(2)	(3)	(4)	(5)	(6)	(7)
FK5 2	$\beta$ Cas	2.145	0.055	1.034	2.218	0.058
FK5 74	$\alpha$ Ari	6.389	0.024	1.063	6.792	0.043
FK5 295	$\beta$ Gem	7.578	0.015	1.058	8.018	0.043
FK5 412	46 LMi	2.327	0.050	1.058	2.462	0.054
FK5 582	$\alpha$ Ser	4.522	0.024	1.063	4.807	0.035
HR 6132	$\eta$ Dra	3.174	0.071	1.057	3.355	0.077
FK5 633	$\kappa$ Oph	3.394	0.035	1.063	3.608	0.041
FK5 665	$\beta$ Oph	4.231	0.021	1.063	4.498	0.032
FK5 688	$\eta$ Ser	2.894	0.043	1.058	3.062	0.048
FK5 783	$\eta$ Cep	2.729	0.082	1.056	2.882	0.088
FK5 893	$\gamma$ Cep	3.144	0.037	1.059	3.329	0.042

Note. — Col. (1): FK5 (Fricke et al. 1988) or HR number (Hoffleit & Warren 1991), as per NPOI scheduling and archiving software. Col. (2): per Table 1. Col. (3): Uniform disk angular diameter. Col. (4): Error in uniform disk angular diameter. Col. (5): Limb darkening correction factor. Col. (6): Limb darkened angular diameter. Col. (7): Error in limb darkened angular diameter.